Isern, A.R., Anselmetti, F.S., Blum, P., et al., 2002
Proceedings of the Ocean Drilling Program, Initial Reports Volume 194

9. Site 1198[1]

Shipboard Scientific Party[2]

INTRODUCTION

Site 1198 (proposed Site CS-05A) is in 319 m of water at the crossing of regional lines MAR07 (shotpoint [SP] 2262) (Fig. F1) and MAR54 (SP 900). This site lies ~10 km northeast of the modern south-central Great Barrier Reef and 13.5 km northwest of Site 1196 (Fig. F2). Two holes were drilled at Site 1198. Hole 1198A penetrated 251.5 meters below seafloor (mbsf), and Hole 1198B penetrated 522.6 mbsf.

Site 1198 is in front of the current-exposed northern margin of the Southern Marion Platform (SMP) at a distance of ~5 km from the platform escarpment. Because of their periplatform setting, sediments at Site 1198 were expected to contain a platform as well as an open marine sedimentary signal. The primary objective of this site was to recover the proximal sequences adjacent to the southern carbonate platform and to provide an age for the initiation and drowning of this platform. In addition, the Megasequence D sediment drift, which overlies the unconformity marking the end of platform growth, will provide information on the Pliocene–Holocene paleoceanography of the Marion Plateau region. A further objective was to investigate the role of fluid flow in this proximal carbonate platform setting.

OPERATIONS

Operations at Site 1198 (proposed site CS-05A) began when a beacon was dropped precisely on site coordinates at 1636 hr on 7 February 2001. Because the strong current moved the beacon before it landed on the seafloor, the vessel was offset 150 m to the southeast of the original coordinates to compensate for the displacement. The precision depth recorder indicated a water depth of 322.2 m.

F1. Seismic line MAR07, p. 27.

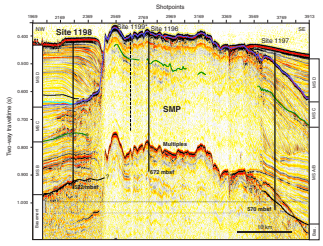

F2. Bathymetry map, p. 28.

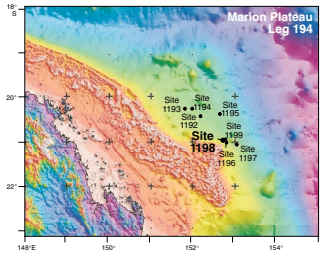

[1] Examples of how to reference the whole or part of this volume.
[2] Shipboard Scientific Party addresses.

Hole 1198A

Hole 1198A was spudded with the advanced piston corer (APC) at 2030 hr on 7 February (Table T2, p. 87, in the "Leg Summary" chapter; Tables T1, T2). The water depth determined from the drill string measurement and the recovered mudline was 319.4 m. Coring advanced to the APC refusal depth at 203.0 mbsf, and average recovery for this interval was 102.2%. Cores were oriented starting with Core 194-1198A-3H. Downhole temperature measurements were attempted at 33.5, 62.0, 90.5, 119.0, 147.5, 176.0, and 203.0 mbsf.

Subsequent coring with the extended core barrel (XCB) deepened the hole to 251.5 m. The first XCB core had 29% recovery, and the subsequent four cores had zero recovery. Based on the experience at Site 1197 with XCB coring in the corresponding seismic stratigraphic interval (Megasequence C), the hole was abandoned in favor of a new hole to be cored with the rotary core barrel (RCB).

T1. Coring summary, p. 56.

T2. Expanded coring summary, p. 57.

Hole 1198B

The vessel was offset 20 m east of Hole 1198A. Hole 1198B was spudded with the RCB at 2125 hr on 8 February. After drilling ahead with a center bit to 195.7 mbsf, coring resumed and deepened the hole 4 m into acoustic basement to a total depth of 522.6 mbsf. During the process, the drill string became stuck after cutting Core 194-1198B-6R (243.6 to 253.3 mbsf) and had to be worked free by pulling up to 220 kilopounds (kips). During the working of the stuck drill pipe, circulation was maintained, with a maximum pump pressure of 800 psi and a mud pump output of 450 gal/min or 90 strokes/min. To reduce the potential for further hole problems, coring was interrupted twice to make a wiper trip from 385.1 to 183.0 mbsf and from 397.6 to 385.1 mbsf, and the annulus was flushed frequently with sepiolite flushes.

Average recovery for the interval 195.7–359.1 mbsf (Cores 194-1198B-1R through 17R) was 9.98 m, or 6.1%. Recovery for the interval 359.1–522.6 mbsf (Cores 194-1198B-18R through 34R) was 65.2%. The average recovery for the entire hole was 35.7%.

After the last core was recovered, the hole was flushed and displaced with sepiolite, the bit was released on bottom, and the bit was pulled back to 91.8 mbsf in preparation for logging.

Only one pass with the triple combination tool (triple combo) was made in the upper portion of the open hole. The tool was unable to descend below 235.5 mbsf because of a narrowing hole diameter caused by the collapse of the upper part of the hole (presumably the interval poorly recovered in the cores). While attempts were made to move the tool past the tight spot, the hole diameter narrowed down to ~4 in and trapped the triple combo tool string. After the tool was worked free, the hole was logged up from 231 mbsf to the seafloor. Above 192 mbsf the hole was found to be dramatically enlarged, reflected by a maximum opening of the caliper to >17 in. It was decided not to make any further logging runs because of the deteriorating hole condition.

The logging equipment was rigged down, and the drilling assembly was tripped to the surface. The beacon failed to release from the tether. The vessel departed at 0430 hr on 11 February, ending operations at Site 1198 and returning to Site 1196.

LITHOSTRATIGRAPHY AND SEDIMENTOLOGY

Site 1198 was drilled through a sequence of hemipelagic drift deposits into underlying talus and slope sediments of the Southern Marion Platform (SMP). Below, Site 1198 penetrated hemipelagic sediments, a thin veneer of deep euphotic carbonates, and basaltic basement. The ~517-m-thick sediment sequence was divided into five lithologic units according to variations in sedimentary structures and texture, grain size, terrigenous vs. carbonate content, degree of lithification, and biotic assemblages (Fig. F3; Table T3).

Unit I is a 200.6-m-thick upper Pliocene to Pleistocene sequence of alternating mudstone to skeletal grainstone intervals deposited in a hemipelagic environment with varying input of terrigenous constituents. At 200.6 mbsf, a 10- to 25-cm-thick layer of brown phosphate nodules corresponds to a hardground that marks the top of Unit II (200.6–397.6 mbsf). Unit II comprises two intervals of fine-grained skeletal packstone to grainstone rich in neritic constituents, deposited in a periplatform environment (Subunits IIA and IIC). Between these subunits, the 96-m-thick Subunit IIB consists of coarse-grained skeletal grainstone to rudstone with abundant larger benthic foraminifers deposited at the base of the SMP escarpment, 5 km to the southeast. The boundary between Units II and III at 397.6 mbsf corresponds to a sharp contact between silt-sized packstone with neritic debris, underlying variously colored mudstone to packstone deposits without neritic components. Unit IV consists of skeletal floatstone to rudstone with larger benthic foraminifers and rhodoliths, interpreted to be deposited in a deep euphotic environment. Acoustic basement (Unit V; below 513.2 mbsf) is characterized by an olivine basalt.

Sediments recovered at Site 1198 are unconsolidated in the upper 60 mbsf, become more consolidated to 200.6 mbsf, and are semilithified for the remainder of the drilled interval.

Core recovery at this site is good above 200 mbsf, very poor within the semilithified, friable sediments of Subunits IIA and IIB, moderate in Subunit IIC, and good below 397 mbsf (Units III–V) (Fig. F3). The poorly recovered interval corresponds to the seismic Megasequence C (see "Seismic Stratigraphy," p. 22).

F3. Lithologic summary, p. 29.

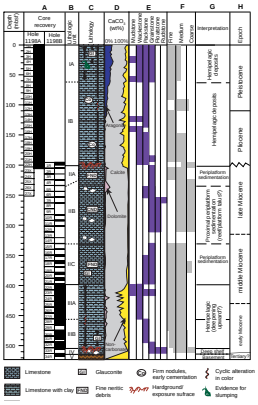

T3. Lithologic units and subunits, p. 63.

Lithologic Units

In this chapter, noncarbonate content, as determined by X-ray diffraction (XRD) analysis, is inferred to reflect clay content. This assumption is based on the fact that little coarse-grained siliciclastic material was observed in low-calcium carbonate intervals.

Unit I (0–200.6 mbsf; Pleistocene–Late Pliocene)

Unit I is a light gray to olive-gray, moderately to well-sorted succession characterized by alternations of wackestone to grainstone. Pyrite is present to common throughout this unit. This large package of sediments is divided into two subunits on the basis of sedimentary structures, texture, grain size, calcium carbonate content, degree of lithification, and biotic assemblages.

Subunit IA (0–62.0 mbsf)

Subunit IA shows a large variability in sediment texture, gradually alternating from unconsolidated dark greenish gray skeletal wackestone

to light gray grainstone, both with minor amounts of clay. These changes are well reflected in calcium carbonate data (Fig. F3, column C) (also see "Geochemistry," p. 15). The biota found within this unit comprises a broad range of species, dominated by planktonic foraminifers with minor amounts of small benthic foraminifers, pteropods, echinoderm fragments, and scaphopods. Smear slide analysis showed the presence of common silt-sized skeletal components dominated by mollusk fragments. Synsedimentary slump structures are located in the upper 60 m of Hole 1198A (see Fig. F4). Within the upper ~30 m, glauconite is rare to present, mostly infilling foraminiferal tests. At the base of this subunit, a thin layer of light greenish mudstone marks the boundary with Subunit IB. Additionally, XRD analyses show the appearance of aragonite above 117 mbsf, with a continuously increasing trend upcore, showing values of ~30 wt% at the seafloor.

F4. Close-up photograph of synsedimentary soft sediment deformation, p. 30.

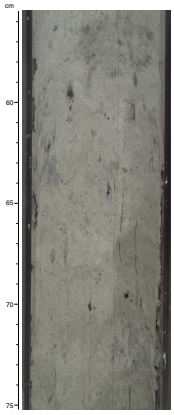

Subunit IB (62.0–200.6 mbsf)

In Subunit IB, the lithology changes to a succession of well-sorted, light greenish gray, firmly consolidated skeletal packstone dominated by planktonic foraminifers (62–138 mbsf). Slight variations in grain size and clay content result in changes from lighter to darker color. Clay content varies between ~10% and ~20%. Below 138 mbsf the clay content increases steadily to the base of Unit I, with a maximum content of ~30% (Fig. F3), resulting in an overall downcore color change from olive-gray to pale olive. In the lower part of Subunit IB, the texture of the sediment is more variable, ranging from skeletal wackestone to packstone. Within Subunit IB, a few layers containing small carbonate concretions (Cores 194-1198A-9H, 12H, 18H, and 21H) indicate early cementation. Furthermore, the abundance of dark brownish, fine to medium sand-sized phosphatic grains (up to 1–5 mm) increases within the lowermost 3.5 m of Unit I.

Unit II (200.6–397.6 mbsf; Miocene)

The boundary between Units I and II coincides with the Megasequence C/D boundary (see "Seismic Stratigraphy," p. 22) and is marked by a 10- to 25-cm-thick layer consisting mostly of olive to dark olive phosphatic nodules (see Fig. F5) up to 6 cm in diameter. The texture within each nodule is skeletal packstone dominated by planktonic foraminifers and minor amounts of small benthic foraminifers.

F5. Close-up photograph of boundary between periplatform sediment and a layer of phosphatic nodules, p. 31.

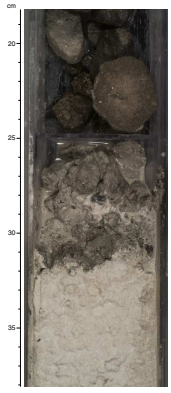

Unit II is a poorly recovered sequence of periplatform sediments that was divided into three subunits: an upper (Subunit IIA) and lower (Subunit IIC) succession of mostly fine to very fine grained skeletal neritic detritus and an interbedded coarser unit (Subunit IIB) rich in larger benthic foraminifers.

Subunit IIA (200.6–225.0 mbsf; late Miocene)

Subunit IIA consists of silt- to fine sand-sized, well- to moderately sorted, white to pale brownish skeletal packstone to grainstone. Planktonic foraminifers still predominate, but larger benthic foraminifers and other neritic skeletal components, such as mollusks, bryozoans, echinoid spines, and shell fragments also occur. At the base of Subunit IIA, a small 1.5-cm-thick lamination consisting of imbricated larger benthic foraminifers is observed. Mineralogical analyses indicate up to 20 wt% dolomite within this section (see Fig. F3 and "Geochemistry," p. 15).

Subunit IIB (225.0–330.3 mbsf; Late Middle Miocene–Late Miocene)

Subunit IIB is characterized by white to pale yellowish, medium to coarse sand-sized, moderately to well-sorted skeletal grainstone/floatstone to rudstone. Within the sediment, larger benthic foraminifers (e.g., *Lepidocyclina* sp., *Operculina* sp., and *Amphistegina* sp.) are abundant. In addition, fragmented neritic skeletal grains are common, such as rhodoliths, red algae, sponges, echinoderms, and bryozoans (see Fig. F6). Small benthic and planktonic foraminifers are also present. These sediments are weakly cemented and friable. Within Cores 194-1198B-7R through 12R, repetitive changes from skeletal floatstone/grainstone to grainstone and wackestone were observed. The base of this subunit coincides roughly with the seismic Megasequence B/C boundary at 330.3 mbsf (see "Seismic Stratigraphy," p. 22).

Subunit IIC (330.3–397.6 mbsf)

The top 30 m of Subunit IIC consists of brownish white fine-grained skeletal packstone to grainstone, which gradually changes downcore into light gray to light olive-gray silt-sized packstone to grainstone with minor clay. The most striking characteristic defining this subunit is the presence of fine skeletal grains dominating the sediment texture. Planktonic and small benthic foraminifers are abundant to dominant, making up the coarse fraction with fine sand- to silt-sized neritic skeletal grains present, mainly as abraded larger benthic foraminifers, bryozoans, red algae, and mollusks (Fig. F7).

Unit III (397.6–503.6 mbsf; Middle[?]–Early Miocene)

The transition between Units II and III is marked by the appearance of firm, nonlithified layers of mudstone to wackestone with clay in Cores 194-1198B-22R to 23R (397–417 mbsf; see Table T3). This interval is also marked by a sudden downcore decrease in calcium carbonate content and the disappearance of fine neritic grains. In addition, distinct changes in seismic velocity and grain density occur (see "Core Physical Properties" p. 19).

Unit III is a light gray to dark olive, moderately to well-sorted interval with alternations of silt to sand-sized wackestone to grainstone. Within this unit, clay shows an overall increase from 5% to 10% at the bottom to 50% in the top (Fig. F3). Pyrite is rare. Discernible small-scale, rhythmic changes of texture and color also occur. Unit II is divided into two subunits.

Subunit IIIA (397.6–447.1 mbsf)

Subunit IIIA consists of silt- to fine sand-sized, well to moderately sorted, lithified skeletal wackestone to packstone with clay. Color ranges from light to dark greenish gray. Planktonic and small benthic foraminifers are the most abundant skeletal components, but mollusks and larger benthic foraminifer fragments also occur. Rare faint, wavy laminations and crude bedding structures were observed in the upper 30 m. Small-scale (up to 20 cm) fining-upward sequences occur at the base of wackestone intervals in Cores 194-1198B-23R through 27R (407–455 mbsf), which distinguish this subunit from Subunit IIIB. High-amplitude changes in the ratio of calcium carbonate to noncarbonate and magnetic susceptibility are another characteristic feature of this subunit (see "Geochemistry," p. 15, and "Paleomagnetism," p. 12).

F6. Close-up photograph of coarse-grained periplatform sediment facies, p. 32.

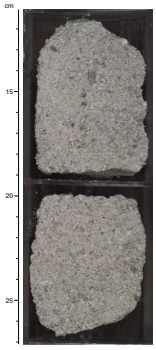

F7. Photomicrograph of fine-grained periplatform sediment facies, p. 33.

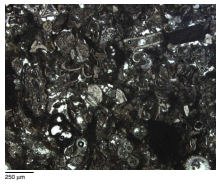

Subunit IIIB (447.1–503.6 mbsf)

Subunit IIIB is characterized by alternations of silt-sized, moderately to well-sorted, greenish gray to olive-gray colored packstone and grainstone with clay. Facies changes appear either gradational or bioturbated. Clay content is generally lower than in Subunit IIIA. In the lowermost 7.5 m of Subunit IIIB, small (up to 5-cm-thick) laminated intervals occur. The base of this unit exhibits a sharp, discontinuous contact to underlying Unit IV (Fig. F8).

Unit IV (503.6–513.2 mbsf; Early Miocene)

The top of this interval is encrusted with alternations of submillimeter-scaled layers of phosphate and pyrite indicating a hardground surface (Fig. F9). Below this hardground, the uppermost 50 cm of Unit IV consists of a light yellowish brown to white lithified skeletal floatstone with large rhodoliths and larger benthic foraminifers. Below this floatstone occurs a lithified skeletal floatstone to rudstone dominated by larger benthic foraminifers (mostly *Lepidocyclina* spp. and *Cycloclypeus* sp. common) and large platy-shaped rhodoliths (Fig. F10). The upper meter of this lithology is stained brownish red. Rhodoliths and larger benthic foraminifers are oriented horizontally within a light greenish gray clay- to silt-sized matrix with a laminated texture. Minor skeletal components include bryozoans, planktonic foraminifers, and coralline algae. The lamination disappears toward the base of this unit, when smaller, more robust foraminifers (*Amphistegina* sp.) and more spheroidal rhodoliths appear. Toward the bottom of Unit IV, glauconite grains are present.

Unit V (513.2–? mbsf; Pre-Miocene)

Olivine basalt was recovered below a sharp contact with the overlying carbonate-rich Unit IV. This lithology represents acoustic basement as seen on seismic data (see "Seismic Stratigraphy," p. 22). The groundmass of the rock consists of a darkish green matrix of plagioclase phenocrysts. Some mineral-infilled veins are present. The rock is heavily altered as indicated by the presence of zeolites. Quartz crystals found in this rock do not show undulatory extinction, indicating that they have not been deformed.

Discussion

Based on benthic foraminifer faunal assemblages, the sediments recovered at Site 1198 were deposited on the talus or proximal slope adjacent to the SMP in a water depth of >200 m (upper bathyal) ("Biostratigraphy and Paleoenvironments," p. 8). The only exception is the few meters of sediment above basement (see below), which was deposited in a deep euphotic environment (~50–150 m).

Pre-Miocene (Unit V)

The age and origin of the olivine basalt acoustic basement is uncertain, but is interpreted as synrift basaltic flows.

F8. Close-up photograph of Unit III/IV boundary, p. 34.

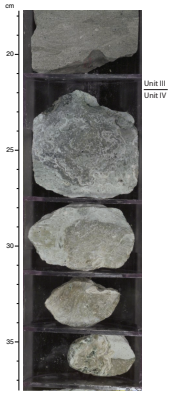

F9. Photomicrograph of thin section close-up of laminae of pyrite and phosphate, p. 35.

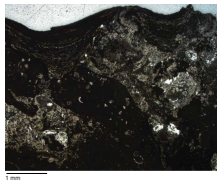

F10. Close-up photograph of deep euphotic shelf facies, p. 36.

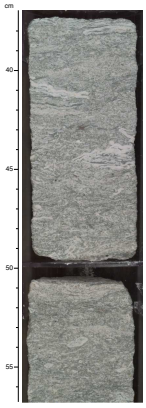

Early Miocene (~18.2–18.8 Ma; Unit IV)

Abrupt flooding of the basement is indicated by a short interval containing spheroidal rhodoliths and robust foraminifers of the genus *Amphistegina,* followed by a few-meters-thick series of skeletal floatstone to rudstone, mainly composed of larger benthic foraminifers (*Lepidocyclina* sp.) and rhodoliths. This skeletal assemblage is indicative of deep euphotic water depths of ~50–150 m (Tsuji, 1993) (see **"Biostratigraphy and Paleoenvironments,"** p. 8), and it may have been deposited on the flanks of a carbonate buildup, located northwest of Site 1198, as seen in the seismic data (see **"Seismic Stratigraphy,"** p. 22). Reddish to brownish color toward the top of this unit might show some influence of subaerial weathering, indicating probable shallowing of the depositional environment. The top of Unit IV is marked by a phosphatic hardground, suggesting a hiatus between Units IV and III.

Early–Middle Miocene (~18.5–15.5 Ma; Unit III)

The base of Unit III is characterized by hemipelagic limestones with clays and a high calcium carbonate content with silt- to fine sand-sized (skeletal?) grains. Upsection, the clay content increases, and small fining-upward sequences occur more frequently. In the same interval, the amplitude of the carbonate vs. noncarbonate increases upsection. A similar trend of increasing clay content was observed for the interval spanning the early to middle Miocene at Site 1194 (Subunits VB to IVB) (see Fig. **F3**). This trend is interpreted as a deepening-upward trend in a hemipelagic setting. The fining-upward trend further suggests a reduction of carbonate and deposition in a more distal platform environment. In addition, the observed high-amplitudinal, high-frequency changes in the ratio of calcium carbonate vs. noncarbonate deposition, as observed in the upper part of Subunit IIIA, may have been controlled by sea level changes.

Middle Miocene (15.5–12 Ma; Subunit IIC)

Above 400 mbsf (equivalent to <15 Ma [Zones N9–N15]; see **"Biostratigraphy and Paleoenvironments,"** p. 8), a prominent increase to higher calcium carbonate content distinguishes Unit III from Unit II. The boundary between Subunits IIB and IIC, defined lithologically and geochemically, coincides with the Megasequence B/C boundary at ~320 mbsf (see **"Seismic Stratigraphy,"** p. 22). The carbonate-rich sedimentary package of Subunit IIC, which may have been deposited during the major late middle Miocene sea level drop that seismically and biostratigraphically correlates with the carbonate package built on the slope of the Northern Marion Platform (NMP) (Unit III at Site 1194) (see **"Seismic Stratigraphy,"** p. 27, and **"Lithostratigraphy and Sedimentology,"** p. 6, in the "Site 1193" chapter, and **"Seismic Stratigraphy,"** p. 27, and **"Lithostratigraphy and Sedimentology,"** p. 3, in the "Site 1194" chapter.) At Site 1198, the source for the neritic material deposited in Unit II was likely to be the SMP.

Late Miocene (~11–7.7 Ma; Subunits IIB and IIA)

Late Miocene platform growth at Site 1198 is represented by Subunits IIB and IIA, which consist of a talus to proximal slope facies deposited adjacent to the SMP. Subunit IIB sediments (Cores 194-1198B-7R

through 12R) were probably shed across the nondepositional escarpment 5 km east of Site 1198 and then mixed with pelagic constituents. Eventually, during the late Miocene, the SMP platform drowned as documented at Site 1198 by the end of neritic-derived deposition at the top of Subunit IIA. Once neritic carbonate shedding ceased, a phosphatic hardground with rounded phosphatic nodules formed, representing a nondepositional period of ~4 Ma (see "Age Model," p. 14). During the onset of hemipelagic deposition of Unit I, this hardground became reworked as shown by fine to medium sand-sized phosphatic grains (up to 1–5 mm in size) in the lowermost 3.5 m of Unit I.

Pliocene to Pleistocene (3 Ma–Holocene; Unit I)

During the Pliocene and Pleistocene, a 200-m-thick hemipelagic mudstone to grainstone unit was deposited in an upper bathyal environment. Bedding geometries seen on seismic data (see "Seismic Stratigraphy," p. 22) indicate that Unit I sediments are drift deposits. The appearance of aragonite at about 117 mbsf, with a continuously increasing trend upcore, can be either a primary input or a diagenetic signal. Within the upper 70 m of Site 1198, soft sediment deformation indicates the presence of slumps, which also can be traced on the seismic section (see "Seismic Stratigraphy," p. 22).

BIOSTRATIGRAPHY AND PALEOENVIRONMENTS

Shipboard analyses of calcareous nannofossils and planktonic foraminifers reveal a late Pleistocene to early Miocene age for the 523-m-thick sequence cored at Site 1198 (Table T4). See "Age Model," p. 14, for age vs. depth and sedimentation rate plots. Microscopic analysis of sand-sized (>63 µm) biogenic sediment constituents provided data for paleoenvironmental interpretations (Table T5). Core catcher samples were the basis for the biostratigraphic analyses, and additional samples were taken where necessary.

T4. Biostratigraphic datums, p. 64.

T5. Summary of paleoenvironmental interpretations, p. 65.

Calcareous Nannofossils

Hole 1198A

Calcareous nannofossils are abundant and well preserved in all the samples examined from this hole except in the last two core catcher samples, which yielded poorly preserved early Pliocene nannofossils. Sample 194-1198A-1H-2, 80 cm, contains few *Emiliania huxleyi* and abundant *Gephyrocapsa* >4 µm among other Pleistocene taxa. This suggests that oxygen isotope Stages 1–4, if present, lie above this sample. The first occurrence (FO) of *E. huxleyi,* which is known to correlate with oxygen isotope Stage 8 (at ~0.26 Ma), is located between Samples 194-1198A-1H-CC and 2H-2, 80 cm. The last occurrence (LO) of *Pseudoemiliania lacunosa,* which correlates with oxygen isotope Stage 12 at 0.46 Ma, is placed between Samples 194-1198A-2H-CC and 3H-CC. *Calcidiscus macintyrei* was first encountered in Sample 1194-1198A-1H-CC, indicating that the sample is older than 1.7 Ma. The Pliocene/Pleistocene boundary is generally drawn just below the LO of *C. macintyrei.*

Few *Discoaster brouweri* were found in Sample 194-1198A-14H-CC. The LO of *D. brouweri* (2.0 Ma) is placed between this and Sample 194-1198A-13H-CC. *Discoaster pentaradiatus* and *Discoaster surculus* were first

found in Sample 194-1198A-18H-CC and *Discoaster tamalis* in Sample 194-1198A-19H-CC, indicating an age older than 2.6 and 2.8 Ma, respectively, for the two samples. The LO of *Reticulofenestra pseudoumbilicus* (3.7 Ma) is placed between Samples 194-1198A-21H-CC and 22H-3, 85–87 cm. This datum can be used to approximate the early/late Pliocene boundary.

Hole 1198B

Samples 194-1198B-2R-CC through 16R-CC contained generally rare and poorly preserved nannofossils with several samples being barren of nannofossils, leading to relatively poor biostratigraphic resolution for this interval. The LO of *Reticulofenestra umbilicus* (>7 µm) (9.0 Ma) is placed between Samples 194-1198B-8R-CC and 10R-CC based on absence of the species in the former sample and its presence in the latter sample. Similarly, the LO of *Cyclicargolithus floridanus* is placed between Samples 194-1198B-13R-CC and 16R-CC based on absence of the species in the former sample and its presence in the latter sample. Because Sample 194-1198B-14R-CC is barren of nannofossils and recovery for Core 194-1198B-15R was 0%, there is a relatively large error bar in the current placement of the datum. The LO of *Sphenolithus heteromorphus* (13.6 Ma) is located between Samples 194-1198B-18R-CC and 19R-CC. The FO of this index fossil (18.2 Ma) is tentatively placed between Samples 194-1198B-31R-CC and 33R-2, 10 cm, based on the presence of the species in the former sample and its absence in the latter sample. *Sphenolithus belemnos,* which has a range of 18.5–19.3 Ma, was not found in Core 194-1198B-33R. Thus, an age of 18.2–18.5 Ma is tentatively assigned to Core 194-1198B-33R.

Planktonic Foraminifers

Hole 1198A

Samples 194-1198A-1H-CC through 20H-CC revealed a late Pleistocene (Zone N23) to late Pliocene (Zones N20–N21) sequence reaching to a depth of 185.8 mbsf. Samples 194-1198A-21H-CC and 22H-CC were determined to be early Pliocene in age.

Samples 194-1198A-1H-CC through 5H-CC comprise foraminifers of the late middle Pleistocene Zone Pt 1b, based on the presence of *Globigerionoides ruber* (pink) and the absence of *Globorotalia tosaensis*. Sample 194-1198A-1H-CC contains the "pink" morphotype of *G. ruber,* whose LO datum is ~0.12 Ma in the Pacific (although it does vary), thus defining the youngest possible age for the sample. The LO datum of *G. tosaensis,* which marks the base of Zone Pt 1b was placed between Samples 194-1198A-5H-CC and 6H-CC. The LO datum of *Globigerinoides fistulosus* is placed between Samples 194-1198A-11H-CC and 12H-CC. The LO and FO datums of both *Globigerinoides extremus* and *Globorotalia truncatulinoides* are positioned between Samples 194-1198A-15H-3, 85–87 cm, and 15H-CC. Samples 194-1198A-6H-CC through 15H-CC therefore represent the early Pleistocene Zone Pt 1a, probably with some overlap into the Pliocene PL6 Zone (synonymous with the Zone N21/N22 boundary) (Fig. F8, p. 47, in the "Explanatory Notes" chapter). The precise placement of this boundary in Hole 1198A is marred by downhole contamination and appears to be smeared out.

Foraminifers in Samples 194-1198A-21H-CC through 23H-CC are only moderately preserved and are difficult to precisely identify. Sample

194-1198A-21H-CC contains an assemblage that includes *G. extremus, Dentoglobigerina altispira,* and *Globorotalia pseudomiocenica,* whereas *Sphaeroidinellopsis seminulina* and *Globorotalia margaritae* are absent. This sample is assigned to the time interval defined by Zones N21 and N20 (PL4–PL5). Sample 194-1198A-22H-CC may be placed in Zone N19 based on the absence of *Globorotalia plesiotumida* and *Globigerina nepenthes*. *G. plesiotumida* and *Sphaeroidinella dehiscens* are present in Samples 194-1198A-23X-CC and 23X-1, 0–25 cm, which can therefore be constrained to an age at the Zone N18/N19 boundary.

Hole 1198B

Samples 194-1198B-1R-CC through 16R-CC indicate a late to possibly middle Miocene sequence in Hole 1198B. The preservation quality of foraminifers is moderate to poor, with many samples containing recrystallized specimens and/or few age-diagnostic taxa.

The FO of *G. extremus* is placed between Samples 194-1198B-3R-CC (214.8 mbsf) and 6R-CC (243.7 mbsf), indicating that the Zone N17/N16 boundary occurs between these two samples. The *G. plesiotumida* FO datum is observed between Samples 194-1198B-11R-CC and 13R-CC; thus, the Zone N15/N16 boundary can be placed here. This boundary approximates the middle/late Miocene boundary. The last reliable datum recorded was the FO of *Orbulina* spp. between Samples 194-1198B-19R-CC and 20R-CC. This datum defines an early middle Miocene age for these samples. Core 2194-1198B-6R through Sample 194-1198B-32R-CC contains no age-diagnostic planktonic foraminifers and thus could not be assigned to any zone.

Benthic Foraminifers

Hole 1198A

All samples from Hole 1198A, (194-1198A-1H-CC [4.95 mbsf] through 23H-CC [195.02 mbsf]) contain planktonic foraminiferal tests and test debris, as well as a generally common diverse assemblage of benthic foraminifers characteristic of upper bathyal water depths. Most samples also contain at least a small amount of reworked material.

Samples 194-1198A-1H-CC (4.95 mbsf) through 6H-CC (52.24 mbsf), which span lithologic Subunit IA (see **"Lithostratigraphy and Sedimentology,"** p. 3), include a minor coarse component of outer neritic/upper bathyal hard-substrate macrofauna. Pteropods are also common to abundant in this interval. Samples 194-1198A-17H-CC (63.37 mbsf) through 21H-CC (195.02 mbsf) from lithologic Subunit IB (see **"Lithostratigraphy and Sedimentology,"** p. 3) differ from those of Subunit IA, as they lack any significant coarse component.

Samples 194-1198A-22X-CC (202.96 mbsf) and 23X-CC (205.79 mbsf) from the top of lithologic Subunit IIA (see **"Lithostratigraphy and Sedimentology,"** p. 3) are bimodal in size distribution, representing two very different sources. Medium to fine sand fractions as well as the samples overall are dominated by planktonic foraminiferal tests. Coarse sand fractions are characterized by a diverse assemblage of larger benthic foraminifers, with debris from bryozoan and other neritic macrofauna. Reworked clasts are also common.

Hole 1198B

Samples 194-1198B-1R-CC (199.43 mbsf) and 2R-CC (205.6 mbsf) from the top of lithologic Subunit IIA (see "Lithostratigraphy and Sedimentology," p. 3), are dominated by medium to fine sand-sized planktonic foraminiferal tests with a significant coarse sand-sized fraction containing a diverse assemblage of larger benthic foraminifers, with debris from bryozoan and other neritic macrofauna as well as reworked clasts. Samples 194-1198B-3R-CC (214.8 mbsf) and 4R-CC (224.93 mbsf), which are also from lithologic Subunit IIA, are bimodal in grain size but with much less planktonic influence. Instead, the fine fraction is dominated by silt and fine sand of probable neritic origin.

Samples 194-1198B-5R-CC (234.27 mbsf) through 15R-1, 24–26 cm (330.5 mbsf), from lithologic Subunit IIB (see "Lithostratigraphy and Sedimentology," p. 3), are dominated by neritic material. A diverse assemblage of larger benthic foraminifers, particularly *Lepidocyclina* spp., are abundant in all samples and often are the dominant constituent. Rhodoliths, red algal fragments, coral, and bryozoans are also important components. Planktonic foraminifers and typical upper bathyal benthic foraminiferal taxa such as *Cibicidoides* and nodosarids are also found in most samples in this subunit (see Table T5). Samples from lithologic Subunit IIC (i.e., 194-1198B-16R-CC [340.3 mbsf] through 21R-CC [391–44 mbsf]) contain sediments from both planktonic and neritic sources, although compared to Subunit IIB, the planktonic foraminifers are more abundant and the neritic debris is generally much finer grained.

Fine neritic debris dominates the sediments of lithologic Unit III (Samples 194-1198B-22R-CC [407.48 mbsf] through 33R-CC [501.23 mbsf]) (see "Lithostratigraphy and Sedimentology," p. 3). Planktonic foraminifers and outer neritic/upper bathyal benthic foraminifers become increasingly difficult to recognize with depth through this interval.

A short interval of skeletal floatstone to rudstone, topped by a phosphatic hardground (lithologic Unit IV; see "Lithostratigraphy and Sedimentology," p. 3), is represented only by Sample 194-1198B-33R-2, 114–116 cm (505.97 mbsf). This small unit is characterized by a foraminiferal boundstone consisting of large, very thin larger benthic foraminifers, *Lepidocyclina* (*Eulepidina*) sp., bound together by thin red algal crusts (Fig. F11). This unit overlies lithologic Unit V, which is olivine basalt (see "Lithostratigraphy and Sedimentology," p. 3).

F11. Photomicrograph showing foraminiferal boundstone with thin larger benthic foraminifers bound together by thin red algal crusts, p. 37.

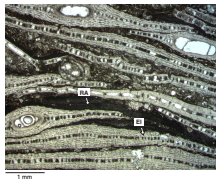

Interpretation

Major biogenic constituents of Unit IV include thin red algal crusts and very large, flat larger benthic foraminifers, both of which indicate very deep euphotic environments, possibly as deep as 100–150 m (Tsuji, 1993). The flooding of the basaltic basement rocks is possibly recorded in a thin interval of sediments that immediately overlie the basalts. These sediments are characterized by more robust rhodoliths, as well as smaller sizes and more robust morphologies among the larger benthic foraminifers. These factors are indicative of shallower paleowater at the base of Unit IV than on top.

Planktonic foraminifers, as well as benthic foraminifers characteristic of outer neritic to upper bathyal paleowater depths, occur through most of lithologic Units I through III (Table T5). Although sea level fluctuations undoubtedly affected both the source and supply of sediments,

paleowater depth may have had less influence on sedimentation through this interval than the source and rate of supply of hemipelagic clays and periplatform carbonates as a result of the proximity of the site to the Australian continental shelf, upcurrent platforms, and the nearby SMP. Unit III exhibits significant amounts of very fine neritic carbonate sediment and is interpreted to represent a distal periplatform depositional setting. Input of medium to coarse periplatform carbonates increases upsection through Subunit IIC, becoming the dominant component in Subunit IIB. A hardground on top of Subunit IIA marks an abrupt end to the deposition of neritic carbonates and probably nearby shedding and production.

Unit II provides enigmatic biostratigraphic data of potentially profound significance relative to the age ranges of the larger benthic foraminifers. Seismic data indicate that sediments at least in the upper part of this unit were shed from the SMP (see **"Seismic Stratigraphy,"** p. 22). Planktonic foraminifers and nannofossils indicate a late Miocene age for this unit (Table **T4**). Yet the dominant component of the coarser neritic sediments in this unit is a diverse assemblage of larger benthic foraminifers, including, and often dominated by *Lepidocyclina* spp. These foraminifers were long considered to be predominantly of early Miocene age in northern Australia (e.g., Chaproniere 1981, 1984). Betzler and Chaproniere (1993) and Chaproniere and Betzler (1993) considered that all *Lepidocyclina* found in northeastern Australia and Queensland Plateau sediments younger than Zone N12 (12.1 Ma) were reworked. Betzler (1997) later showed that on the Queensland Plateau, *Lepidocyclina* has an extended age range into the late Miocene. Allan et al. (2000) also found strontium isotopic evidence that the *Lepidocyclina* lineage continued into Zone N16 (8.3–10.9 Ma) in the late Miocene in the western Pacific, at least in New Guinea. The predominance, sorting, and excellent preservation of *Lepidocyclina* in periplatform sediments in Subunit IIA, which both planktonic foraminifers and nannofossils indicate to be no older than Zone N17 (6.0–8.3 Ma), provide strong evidence that these foraminifers did indeed survive well into the late Miocene.

Neritic sediments abruptly diminish above the phosphatic nodules that mark the boundary between lithologic Units II and I. In Subunit IB, sand-sized sediments are overwhelmingly planktonic in origin, even in the small reworked component. Substantial variations in the predominant sizes of the planktonic foraminiferal tests are apparent in this interval, which may be indicative of changes in current velocities and therefore sediment winnowing. Subunit IA is also of predominantly pelagic origin, but it contains a minor but conspicuous macrofaunal component, apparently transported either downslope from the nearby drowned SMP or from a more distant source by strong currents. The benthic foraminifers, some of which are likely from the same sources as the macrofaunal debris, are particularly common and diverse throughout Unit I.

PALEOMAGNETISM

The natural remanent magnetization (NRM) of archive halves or whole rounds of APC cores and RCB core sections from Site 1198 were measured at 5-cm intervals with the pass-through cryogenic magnetometer. Many sections were not measured in their entirety because they contained fragments that were small and thus could have rolled

over in the core barrel during the coring and recovery process. The NRM and 5- and 30-mT alternating-field (AF) demagnetization values were measured except when time constraints precluded the complete treatment.

Representative discrete samples were collected and measured from Holes 1198A and 1198B. These were used to aid the interpretation of the long-core records of magnetization by providing additional measurements of polarity and basic magnetic characterization.

Results

Long Core Measurements and Magnetostratigraphy

As at other Leg 194 sites, the sediments at Site 1198 had poor recovery in seismic Megasequence C and weak magnetization in Megasequences B and D. In addition, problems were encountered in measuring whole-round core sections in the 1–2 m heave conditions experienced at Site 1198. Apparently, the increased mass associated with whole-round sections in the magnetometer, coupled with the accelerations due to the ship's heave, stressed the plastic trackway, which affects the detection system of the magnetometer. This resulted in low-quality data in some of the cores. Inclinations of 0° ± 10° were excluded from the record (Fig. F12). This arbitrary cutoff is used because the mechanical problem in the magnetometer is known to produce near zero inclination. The cutoff is low enough that its elimination does not impair the recognition of true magnetozone boundaries.

The expanded Pleistocene section mitigates the effect of the difficulties and some magnetostratigraphy was obtained with the aid of the biostratigraphic datums (see "Biostratigraphy and Paleoenvironments," p. 8). In the magnetostratigraphy columns, alongside the inclination records, the hatched intervals in Figure F12 indicate indeterminate polarities. The reversed polarity at ~5 mbsf is probably a record of one of the excursions, or events, in the Brunhes Chron. The next good reversed interval is between 52 and 57 mbsf. Assigning this to the onset of Chron C1 is consistent with the biostratigraphic data, but with the coincidence of a core-top anomaly even this assignment is questionable. Down to a depth of 205 mbsf, only few intervals show a well-defined polarity. An exception is the normal interval from 140 to 148 mbsf, which, based on biostratigraphic datums, can be interpreted as the Olduvai Subchron (C2n). Finally, around 200 mbsf, there appears to be a partial record of the Gauss Chron (C2An).

Recovery was so poor in Megasequence C and the top of Megasequence B (200–400 mbsf) that no magnetostratigraphy was attempted. Recovery improved between 400 mbsf and the bottom of the hole, but the record has a strong residual normal overprint in the interval of good recovery between 400 and 500 mbsf that could not be demagnetized to separate the characteristic magnetization (Fig. F13).

The interval immediately above the basement basalt has a strong reversed magnetization, as does the basalt at the bottom of the hole. The basalt has a strong signal compared with the sediments, which, however, only amounts to one-tenth of the mean intensity for subaerial and submarine basalts given by Prévot and Grommé (1975). A stable primary magnetization appears to have been isolated by AF demagnetization.

F12. Long-core measurements, Hole 1198A, p. 38.

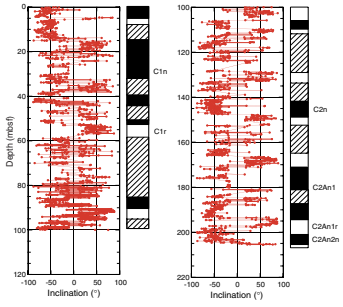

F13. Long-core measurements, Hole 1198B, p. 39.

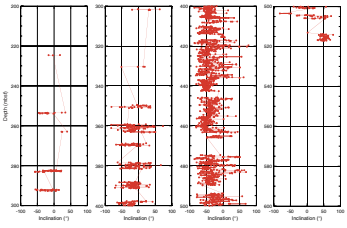

Discrete Samples

Representative discrete samples were subjected to standard rock magnetic analysis (see "Paleomagnetism," p. 15, in the "Explanatory Notes" chapter), and principal component analysis was carried out on samples with a sufficiently strong intensity of magnetization.

Figure F14 illustrates the remanent magnetism characteristics of two samples. Sample 194-1198A-7H-4, 110–112 cm, is weakly magnetized and representative of the skeletal wackestone/grainstone from Megasequence D. The dominant magnetic phase appears to be magnetite, but a minor higher coercivity contribution, possibly a sulfide, is indicated. The anhysteretic remanent magnetization (ARM) is approximately one order of magnitude smaller than the isothermal remanent magnetization (IRM), which is consistent with a detrital origin for the magnetite. The NRM is weak and at the limit of the sensitivity of the magnetometer. In contrast, Sample 194-1198B-34R-1, 66–68 cm, from the basement basalt, contains magnetite as the dominant magnetic phase. A strong NRM, about two orders of magnitude smaller than the IRM, is consistent with a primary thermoremanent magnetization that was acquired as the rock initially cooled.

The downhole variation of rock magnetism parameters is shown in Figure F15. In lithologic Unit I, the ratio of IRM (100 mT:1T) departs from 1, attesting to the presence of a harder phase in addition to the magnetite. Given the presence of pyrite, some of the magnetite may have been destroyed and partially replaced by sulfides, among which greigite could account for the slightly harder phase. IRM, ARM, and NRM are all weak in Unit I, as is to be expected from the difficulty experienced in measuring the NRM on long cores. The ratio of normalized ARM:IRM is low, suggesting that the grain size includes a coarser fraction. No representative samples from lithologic Unit II are available. The deep shelfal facies of lithologic Unit III has a strong hard component that is probably hematite, whereas the basalt is dominated by magnetite and shows a high intensity of magnetization.

AGE MODEL

At Site 1198, 13 calcareous nannofossil and 8 planktonic foraminifer datums were established for the 523-m-thick lower Miocene to Pleistocene sequence (Fig. F16; Table T6) (see "Biostratigraphy and Paleoenvironments," p. 8). Mechanical problems and poor recovery prevented the construction of a magnetostratigraphy (see "Paleomagnetism," p. 12). The age model is therefore based on the biostratigraphy.

As at other Leg 194 sites, recovery of Megasequence D at Site 1198 (0–201 mbsf) was excellent and biostratigraphic resolution good. The interval sedimentation rates range from 9 to 110 m/m.y. (average 53 m/m.y.) and are the highest rates for this Pliocene–Pleistocene sequence among all Leg 194 sites. A major hiatus separates Megasequence C from Megasequence D at 203 mbsf and lasted from 7.6 to 3.8 Ma (±0.5 m.y.). As at Site 1197, recovery of Megasequence C and the upper part of the underlying sequences is very poor and microfossils are rare and poorly preserved. The error bars associated with the biostratigraphic datums are accordingly large (Fig. F16). Miocene interval sedimentation rates range from 15 to 48 m/m.y. (average 28 m/m.y.).

Age picks for lithologic and seismic unit boundaries are summarized in Table T7.

F14. Remanent magnetism characteristics, p. 40.

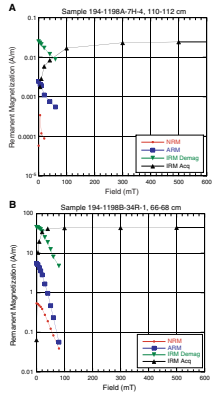

F15. Downcore variation of intensity of NRM, ARM, and IRM, p. 41.

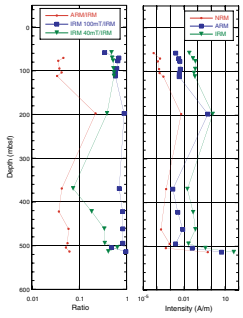

F16. Age-depth model and sedimentation rates, p. 42.

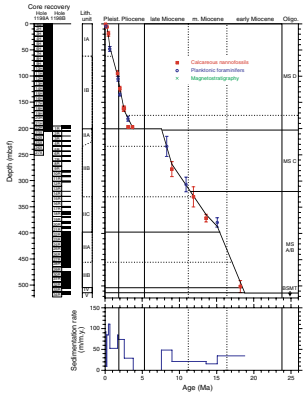

T6. Age-depth control points, p. 67.

T7. Age picks, p. 68.

GEOCHEMISTRY

Volatile Hydrocarbons

Concentrations of volatile hydrocarbon gases were measured from every core using the standard Ocean Drilling Program (ODP) headspace sampling technique and gas chromatographic analysis. Methane only occurred in very minor concentrations (1.7–6.6 ppmv) (Table T8).

The low gas content at Site 1198 is likely a function of appreciable pore water SO_4^{2-} concentrations limiting methanogenesis and the lack of mature organic matter that could provide a thermogenic component to the gas fraction.

T8. Headspace gas composition, p. 69.

Interstitial Water Chemistry

Pore waters were extracted from 40 samples at Site 1198 (Fig. F17; Table T9). Twenty-three samples were taken approximately every 10 m in Hole 1195A, from 2.90 to 204.40 mbsf through lithologic Unit I (see "Lithostratigraphy and Sedimentology," p. 3). In Hole 1198B, one sample was taken from a depth of 196.60 mbsf at the base of lithologic Unit I. From 197 to 350 mbsf, poor recovery of the unconsolidated sediments of lithologic Subunits IIA and IIB precluded pore water sampling. Sampling resumed in Hole 1198B at 350 mbsf, with samples taken at ~10 m intervals to a depth of 504.98 mbsf. Below 460 mbsf, it was not possible to extract sufficient water to complete the entire suite of shipboard chemical analyses. Results from Holes 1198A and 1198B are discussed together (Fig. F17; Table T9).

F17. Dissolved constituents, p. 43.

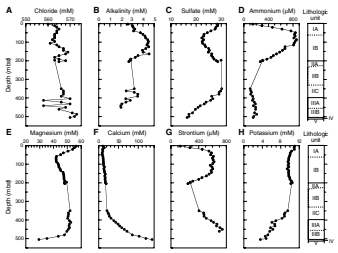

T9. Interstitial water chemistry, p. 70.

Chloride concentration increases from 560 to 565 mM over the upper 30 mbsf, and then remains between 564 and 561 mM to a depth of 115 mbsf (Fig. F17A). In the interval from ~100 to ~160 mbsf, chloride concentration increases to 569 mM; the concentration then falls to 563 mM at 180 mbsf. In the lower 20 m of lithologic Unit I, the concentration varies between 563 and 568 mM. Below the interval of no recovery, chloride remains ~567 mM from 350 to 390 mbsf. From 390 mbsf to the bottom of the cored interval, the concentration varies considerably, from 558 to 570 mM (Fig. F17A).

Alkalinity values rise steadily from typical bottom-water values of ~2.5 mM in the shallowest sample to ~4.5 mM at 100 mbsf (Fig. F17B). Values fall back to ~2.5 mM over the next 100 mbsf. This pattern observed in pore water alkalinity in the upper 200 mbsf is a pattern repeated in several other pore water constituents. In lithologic Subunit IIC and Unit III, alkalinity varies within narrow limits, from 2 to 2.5 mM.

Sulfate concentrations fall from 28.6 to ~22 mM over the interval from 2.9 to ~80 mbsf, remain constant to 115 mbsf, and then rise again to 28.6 mM at 200 mbsf (Fig. F17C). At the top of lithologic Subunit IIC at 350 mbsf, the sulfate concentration is 29.9 mM. From 350 to 505 mbsf, sulfate decreases linearly from 29.9 to 16.42 mM.

Ammonium concentration rises from 145 to ~850 µM in the upper 60 m of Hole 1198A (Fig. F17D). The concentration remains relatively constant to a depth of 115 mbsf then decreases to 246 µM at the base of lithologic Unit I. At the top of lithologic Subunit IIC at 350 mbsf, the ammonium concentration is 103 µM. Thereafter, the concentration rises to 210 µM at 488 mbsf then falls again to 152 µM in the lowermost sample at 505 mbsf.

Pore water magnesium concentration decreases from a near-seawater value of 56.45 to ~42 mM from the top to bottom of lithologic Subunit IA (Fig. F17E). Through lithologic Subunits IB and IIA, the concentration increases to 48 mM. Below the interval in which pore waters could not be sampled, the magnesium concentration is initially 52 mM and remains between 52 and 50 mM to a depth of 450 mbsf. From 480 to 505 mbsf, the magnesium concentration decreases rapidly to 29.5 mM at the base of Hole 1198B.

Calcium concentration remains almost constant at ~10 mM in the upper 60 mbsf then rises linearly to 19.1 mM at the base of lithologic Unit I (Fig. F17F). At the top of lithologic Unit III, the calcium concentration is 17.1 mM. Below this point, the calcium concentration rises rapidly with depth, reaching 135.3 mM at 505 mbsf, just above the basaltic basement.

Strontium concentration rises rapidly in the upper 60 mbsf, reaching a concentration of 616 µM at 58 mbsf (Fig. F17G). Concentration remains between 624 and 588 µM from 58 to 144 mbsf and then decreases downhole to a value of 246 µM at 204.4 mbsf, the base of lithologic Unit I. The increase in strontium with depth at this site is more rapid than for other Leg 194 sites as a result of the significant aragonite component in the sediments. The constant concentration between 60 and 140 mbsf suggests a solubility control, possibly as saturation with celestite is reached. In lithologic Unit III, the strontium concentration is 276 µM at the top and increases to ~700 µM between 440 and 460 mbsf.

Potassium concentration changes little in the upper 200 mbsf (Fig. F17H), varying between 11 and 9.6 mM. Nevertheless, a clear curved pattern of initially rising then falling concentration is seen. From 200 to 350 mbsf is found the interval of no recovery. At 350 mbsf, the concentration is 10.4 mM, and it decreases steadily through the remainder of the cored interval to a value of 3.58 mM near the base of Hole 1198B.

For several pore water constituents, nearly symmetrical, arcuate pore water profiles are found in the upper 200 mbsf. Concentrations increase (decrease) from near seawater values in the interval from 0 to 100 mbsf then decrease (increase) in the interval from 100 to 200 mbsf, returning to concentrations close to those found in seawater. The changes in concentration seen in the lower half of this sediment package are quite unusual. Sulfate concentration, for example, initially decreases as a result of bacterial sulfate reduction. A cessation of this process in the lower part of lithologic Unit IB is an unlikely cause for the increase in sulfate concentration because there is no decrease in the organic carbon content within this unit. More likely is that sulfate reduction occurs throughout this sediment package, but sulfate is supplied by diffusion from both above and below. The near-seawater concentration of sulfate (and other constituents) at the base of these sediments strongly suggests active circulation of seawater through the sediment package between 200 and 350 mbsf. Neither the mechanism nor direction of fluid flow can be determined from the available data.

The high concentration of calcium in the lower portion of the hole is clear evidence for a diagenetic flux of calcium out of basaltic basement (Fig. F17F). During this mineralogical reaction, calcium production must be balanced by the uptake of another element. The observed magnesium concentrations cannot alone provide a balance for calcium. The only other significant cation in solution is sodium. Sodium concentration, however, is usually calculated by charge balance, which automatically leads to rapidly decreasing sodium concentration as calcium rises be-

cause there is no offsetting rise in the concentration of any anion. Sodium is also measured during ion-chromatographic determination of calcium, magnesium, and potassium, although the values are not usually reported. Figure F18 shows a comparison of sodium concentration as determined by both charge balance and ion chromatography. The results match well except for the lower 50 m of Hole 1198B, where results from the charge-balance calculation are significantly below the ion chromatography measurements. Both pore water profiles, however, show a large decrease in sodium concentration in the lower portion of the hole. Thus, the large increase in calcium concentration is dominantly offset by a decrease in sodium, suggesting formation of a sodium-rich mineral in the basaltic basement. The most likely candidate is natrolite ($Na_2Al_2Si_3O_{10} \cdot 2H_2O$), a zeolite that is a common alteration product in the vugs and pore spaces of the basalt.

F18. Dissolved sodium, p. 44.

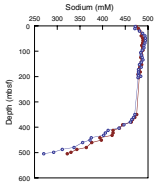

X-Ray Diffraction Carbonate Mineralogy

A total of 109 samples were analyzed for carbonate mineralogy from Site 1198 (Fig. F19; Table T10). At the sediment surface, lithologic Unit I contains ~30% aragonite and 60% calcite. The latter is a near-equal mixture of high- and low-magnesium calcite. The aragonite and high-magnesium calcite content decrease over the upper 120 mbsf and are not present below this depth. From 110 to 200 mbsf, minor amounts of dolomite are found. The transition from lithologic Units II to III is marked by an increase in dolomite content to ~5–8%, with one sample at 230 mbsf containing 20% dolomite. Below 300 mbsf, dolomite content decreases to between 0% and 3%. Dolomite content increases again in lithologic Unit IV, accompanied by a decrease in overall calcium carbonate content. Dolomite varies between 5% and 10% between 400 and 480 mbsf and then is absent to the bottom of the cored interval.

F19. Carbonate and noncarbonate fractions, p. 45.

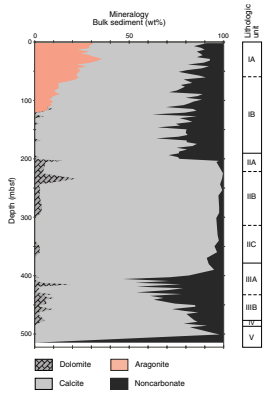

T10. Aragonite, calcite, dolomite, and noncarbonate mineral percentages, p. 71.

Sedimentary Geochemistry

Results

Calcium carbonate ($CaCO_3$) content at Site 1198 ranges from ~47 to 99 wt% and generally covaries inversely with total organic carbon (TOC) content, which ranges from 0.0 to 0.38 wt% (Fig. F20; Tables T11, T12). Note that TOC values from Rock-Eval pyrolysis and carbon-nitrogen-sulfur analyses provide similar downsection profiles.

Hydrogen index (HI) values at Site 1198 range from 28 to 328 mg HC/g TOC (Fig. F20; Table T12), but the low TOC values of some intervals limit the reliability of these results. We performed duplicate and triplicate analyses on low organic carbon samples, and the results were within 10% of the mean value. Oxygen index (OI) values vary from 0 to 57,000 mg CO_2/g TOC (Table T12). In general, the high OI values are attributed to the thermal degradation of carbonate minerals during pyrolysis and are not considered in this interpretation. T_{max} values range from 316° to 433°C (Table T12), although the most reliable values lie between 370° and 420°C and have a mean value of 392°C.

Total sulfur content in Site 1198 sediments ranges from 0 to ~0.78 wt% (Fig. F20; Table T11), and its distribution is similar to that of TOC. C/N and C/S ratios (Fig. F20; Table T11) are compatible with interpretations of a dominantly marine depositional environment.

F20. Carbon, HI, and sulfur plots, p. 46.

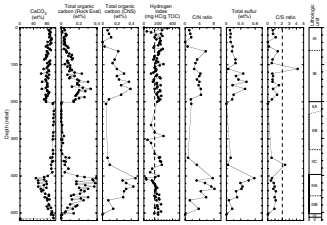

T11. Carbon, nitrogen, sulfur, and hydrogen results, p. 72.

T12. Rock-Eval pyrolysis results, p. 74.

Discussion

The inverse covariation between $CaCO_3$ and TOC content mostly reflects fluctuations in the ratio of biogenic carbonate and terrigenous sedimentation through time. Calcium carbonate content displays an overall decrease from ~90 wt% near the seafloor to ~77 wt% at ~200 mbsf. Through the same interval, TOC content displays an overall increase from values <0.1 wt% to values >0.2 wt%, although TOC values decrease from ~190 to 200 mbsf, where effectively no organic carbon was measured; total S content shows the same generalized profile as TOC. Superimposed on these trends are higher-frequency, inversely covariant TOC and $CaCO_3$ content excursions. These excursions are particularly well developed in lithologic Subunit IB and coincide with alternations of white to yellow skeletal grainstones and packstones and olive-gray packstones (see **"Lithostratigraphy and Sedimentology,"** p. 3). Here, relatively elevated total S content also shows high variability, although the sample frequency is lower than for calcium carbonate and TOC, so an accurate definition of TOC-S-$CaCO_3$ relationships cannot clearly be determined. The variations are suggestive, however, of changes in redox conditions at the seafloor, perhaps tied to episodes of increased terrigenous sedimentation.

At ~200 mbsf seismic Megasequence C/D boundary (see **"Seismic Stratigraphy,"** p. 22) is marked by a hardground (see **"Lithostratigraphy and Sedimentology,"** p. 3) that coincides with an abrupt change to higher $CaCO_3$ (~97 wt%) and lower TOC (~0 wt%) and S (0%) contents. This abrupt change exists at the boundary between lithologic Units I and II (see **"Lithostratigraphy and Sedimentology,"** p. 3) and may record a downhole shift to a more stable oxic seafloor and/or water column. TOC and $CaCO_3$ content remain at similarly low (average = <0.01 wt%) and high (average = ~96 wt%) values, respectively, until ~350 mbsf. This horizon of lower $CaCO_3$ and higher TOC corresponds to seismic Megasequence B/C boundary (see **"Seismic Stratigraphy,"** p. 22) and marks the beginning of a gradual transition to lower carbonate and higher organic carbon contents through the remainder of lithologic Subunit IIC.

Lithologic Subunit IIIA, compared to those values observed in the overlying Unit II, is distinguished by an abrupt drop in carbonate content and an increase in TOC and total S content. The highest total S content (0.78%) measured at Site 1198 coincides with the lowest $CaCO_3$ value at ~406 mbsf, and the highest TOC values exist just below this horizon, at ~409 and 418 mbsf. Interestingly, HI values within this interval of Subunit IIA (~405–410 mbsf) are low, suggesting input of more oxidized or terrigenous organic matter associated with low calcium carbonate and relatively high TOC and S deposition.

Lithologic Subunit IIIA is further characterized by inversely covariant alternations in carbonate and TOC content superimposed on the general trends observable in the data. These alternations are similar to those observed in lithologic Subunit IB. In lithologic Subunit IIIB, "cyclic" alternations are best developed in the TOC profile where they coincide with alternations of white to yellow skeletal grainstones and packstones and olive-gray packstones (see **"Lithostratigraphy and Sedimentology,"** p. 3).

Lithologic Subunit IV is characterized by high $CaCO_3$ and low TOC. Below this subunit, all measured geochemical parameters decrease to zero in the basaltic basement rock.

CORE PHYSICAL PROPERTIES

Physical properties at Site 1198 were measured and evaluated on whole cores, split cores, and discrete core samples. The multisensor track (MST) was used on whole cores to perform nondestructive measurements of bulk density, magnetic susceptibility (MS), and natural gamma radiation (NGR). Color reflectance was measured on the archive halves of split cores. Compressional wave velocity was measured in the x-, y-, and z-directions on split cores and core samples. Moisture and density (MAD) analyses were performed on core samples. Thermal conductivity was evaluated on unlithified whole cores and on samples from semilithified and lithified cores.

Density and Porosity

Gamma ray attenuation (GRA) and MAD analyses provided two independent measures of bulk density at Site 1198. From 0 to 200 mbsf, which corresponds to the interval cored with the APC, GRA bulk density values are an average of 0.1 g/cm³ higher than MAD bulk density values (Fig. F21). Low core recovery prevented bulk density measurements from 200 to 350 mbsf. Below 350 mbsf, MAD bulk density exceeds the average GRA bulk density by 0.1–0.2 g/cm³ (Fig. F21). The low GRA bulk density below 350 mbsf is likely a result of undersized cores and/or sample disturbance as a result of RCB coring (see "Core Physical Properties," p. 18, in the "Site 1192" chapter). Downhole bulk density trends of both data sets, however, are similar.

Bulk density within lithologic Unit I is nearly constant, averages 1.75 g/cm³, and ranges from 1.65 to 2.00 g/cm³ (Fig. F21). Throughout lithologic Units III and IV, bulk density increases from an average of 2.1 to 2.3 g/cm³. The highly altered olivine basalt basement (lithologic Unit V; see "Lithostratigraphy and Sedimentology," p. 3) is characterized by the highest bulk density of 2.4 g/cm³.

Grain density decreases downhole from 2.8 to 2.7 g/cm³ within lithologic Unit I (0–200 mbsf). Lithologic Units III and IV have an average grain density of 2.7 g/cm³. Acoustic basement has the lowest grain density (2.5–2.6 g/cm³) at Site 1198 (Fig. F21).

Porosity, calculated from MAD data (Fig. F21; also see "Core Physical Properties," p. 21, in the "Explanatory Notes" chapter), is nearly constant at 60% throughout lithologic Unit I. A slightly lower porosity (50%–55%) is observed from 45 to 55 mbsf and correlates with the transition between lithologic Subunits IA and IB (see "Lithostratigraphy and Sedimentology," p. 3). The general lack of compaction, shown by the nearly constant porosity, may result from high fluid pressures generated during deposition or induced by fluid migration. High porosity and potentially elevated fluid pressures may have reduced sediment stability, contributed to sediment deformation, or aided in the initiation of the mud slumps observed within lithologic Unit I (see "Lithostratigraphy and Sedimentology," p. 3) and on seismic data (see "Seismic Stratigraphy," p. 22).

Throughout lithologic Units III and IV, porosity decreases from 40% to 25%. The porosity (ϕ) profile in these units can be related to depth (z) using an exponential function and a porosity decay parameter (k) (e.g., Athy, 1930),

$$\phi(z) = \phi_o e^{-kz}.$$

F21. Bulk density, grain density, and porosity, p. 47.

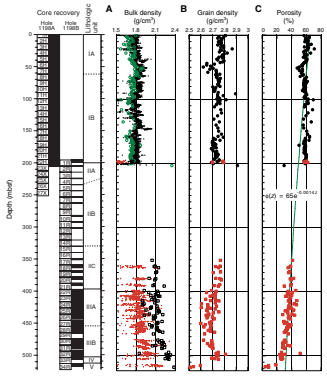

The interpreted normal compaction trend for lithologic Units III and IV (ϕ_o = 65%; k = 0.0014; Fig. F21) is similar to that observed in similar hemipelagic sediments from other sites (see "Core Physical Properties," p. 18, in the "Site 1192" chapter; "Core Physical Properties," p. 24, in the "Site 1193" chapter; "Core Physical Properties," p. 19, in the "Site 1194" chapter; and "Core Physical Properties," p. 16, in the "Site 1195" chapter). Lithologic Unit I was excluded from the porosity regression because this porosity relation assumes hydrostatic fluid pressures (Athy, 1930). Porosity in the olivine basalt basement is <10%.

Compressional Wave Velocity

Compressional wave velocity was measured at discrete intervals for Site 1198. PWS velocity is nearly constant within lithologic Unit I at ~1625 m/s (Fig. F22). This corresponds to the constant porosity of this unit (Fig. F21). Few velocity measurements were obtained from 200 to 400 mbsf (lithologic Unit II) because of poor recovery. Of the obtained data, average velocity is 2225 m/s with two high velocity measurements (4250 and 3750 m/s) (Fig. F22). The higher velocity corresponds to a horizon containing phosphatic nodules (200 mbsf; boundary of lithologic Units I and II) (see "Lithostratigraphy and Sedimentology," p. 3). From lithologic Unit III to IV velocity increases from ~2000 to ~2800 m/s. The basalt of lithologic Unit V is characterized by an abrupt velocity increase to values ranging from 3750 to 4250 m/s.

The overall velocity structure at Site 1198 is isotropic (Fig. F22) (see "Core Physical Properties," p. 21, in the "Explanatory Notes" chapter). Anisotropy calculations were made in zones where transverse (x- and y-direction) and longitudinal (z-direction) velocity values were obtained.

Velocity can often be related to porosity. The porosity and velocity data from Site 1198 do not match the time-average relationship of Wyllie et al. (1956) (Fig. F23) (see "Core Physical Properties," p. 24, in the "Site 1193" chapter) but can be described with a power law relation,

$$V_P(\phi) = a\phi^{-b},$$

where V_P is the compressional wave velocity, and a (12232 m/s) and b (0.49) are empirical constants determined from a least-squares regression (correlation coefficient = 0.90) (Fig. F23). One high velocity/high porosity outlier deviates significantly from the model (496 mbsf, ϕ = 52%, and V_P = 2750 m/s; Fig. F23). This high porosity-velocity point correlates with the onset of the laminated packstone/grainstone intervals at the base of lithologic Subunit IIIB (see "Lithostratigraphy and Sedimentology," p. 3). Low porosity and compositional changes control the high basement velocity.

Temperature and Thermal Conductivity

Four APC temperature tool temperature measurements were taken in lithologic Unit I without success. The observed temperature decay curves are erratic, possibly due to heave-induced probe movement. Reliable in situ temperatures, therefore, are not available.

Thermal conductivity values are nearly constant at 1.2 W/(m·K) in lithologic Unit I and are consistent with the porosity within this interval (Figs. F21, F24). From 0 to 40 mbsf, thermal conductivity increases from 0.8 to 1.2 W/(m·K). Such a variation is not observed in any other

F22. Compressional wave velocity and anisotropy, p. 48.

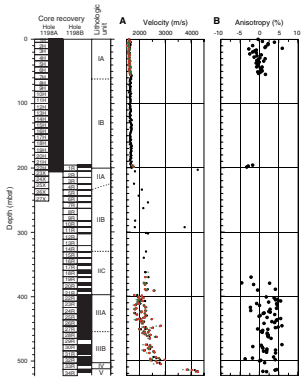

F23. Velocity-porosity crossplot, p. 49.

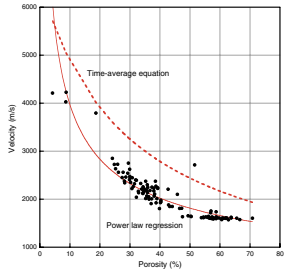

F24. Thermal conductivity, p. 50.

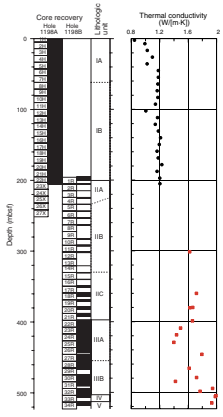

data and may be the result of poor contact between the needle probe and the high water-content sediment. From 350 to 450 mbsf, thermal conductivity decreases slightly with depth and then increases below 450 mbsf with significant data scatter (Fig. F24).

Thermal conductivity (K_{bulk}) can be described with a power law relationship (e.g., Keen and Beaumont, 1990),

$$K_{bulk}(\phi) = K_w \phi K_{grain}^{(1-\phi)},$$

where K_w is the thermal conductivity of the interstitial water and K_{grain} is the thermal conductivity of the solid grain (see "Core Physical Properties," p. 21, in the "Explanatory Notes" chapter). The observed thermal conductivity follows this relationship within the range for the encountered sediments (Fig. F25), which gives confidence to the observations.

F25. Thermal conductivity as a function of porosity, p. 51.

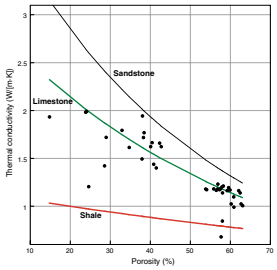

Magnetic Susceptibility, Natural Gamma Radiation, and Color Reflectance

MS and NGR increase, on average, from 0 to 200 mbsf, and have significantly high values at the hardground between lithologic Units I and II (200 mbsf) (Fig. F26). The gradual increase in MS and NGR correlates with the steady downhole increase in clay content (see "Lithostratigraphy and Sedimentology," p. 3, and "Geochemistry," p. 15). The wireline gamma radiation log shows a similar increase over this interval (see "Downhole Measurements," p. 21). MS shows 25–50 m scale variations (0–10 × 10^{-6} SI) superimposed on the average trend. These variations may relate to variations in clay content or the presence of pyrite (see "Lithostratigraphy and Sedimentology," p. 3). NGR data are scattered throughout lithologic Unit I (Fig. F26), but small-scale (< 25 m) variations seem to exist. Similar NGR variations also can be observed in wireline log data (see "Downhole Measurements," p. 21). The MS and NGR trends inversely correlate with sediment lightness, which decreases downcore from ~70% to 50% over this interval (Fig. F26).

Lithologic Units III and IV are characterized by MS that decreases downhole from 10 × 10^{-6} SI to nearly 0 SI (Fig. F26). This overall gradual decrease is mirrored by a gradual increase in lightness (45% to 55%). NGR throughout this interval is highly variable (Fig. F26). Local MS maxima may correspond to phosphate and pyrite-rich intervals at the top of lithologic Unit IV (see "Lithostratigraphy and Sedimentology," p. 3). Within the olivine basalt basement, NGR and MS values increase greatly.

F26. Magnetic susceptibility, natural gamma radiation, and lightness, p. 52.

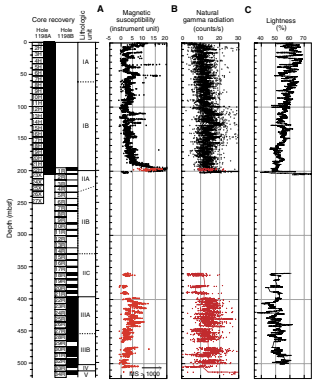

DOWNHOLE MEASUREMENTS

Logging Operations

Logging operation in Hole 1198B started at 2020 hr on 10 February with rigging up the triple combo tool string (Table T13). At 2140 hr, the tools were lowered into the hole but only reached a depth of 235.5 mbsf. When the triple combo tried to pass this tight spot, the hole diameter narrowed to ~4 in and trapped the tool string. The tools were pulled free, and logging started at 231 mbsf. Because of the bad hole condition, no further logging was attempted, ending the operation at 0145 hr on 11 February.

T13. Logging operations, Hole 1198B, p. 75.

Data Quality

The hole was dramatically enlarged above 192 mbsf, thus negatively affecting the quality of the porosity and density data and, to a lesser extent, resistivity data (Fig. F27). Even though the log density values are slightly lower than the shipboard GRA density values measured on corresponding cores, the data profiles show good agreement in local trends and corroborate a good depth match (Fig. F28). The MST natural gamma ray data are highly scattered but follow the general log trend.

The total spectral gamma ray (HSGR) log is the most reliable log because it is corrected up to a borehole size of 17 in. Consequently, the HSGR log is used to distinguish two log units in the logged 135-m interval.

F27. Summary of logging results, p. 53.

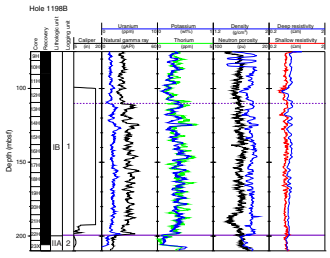

Logging Results

Logging Unit 1 (74–199 mbsf)

Logging Unit 1 is characterized by low HSGR values of 20–30 gAPI with moderate variability. An upper interval (74–110.5 mbsf) has constantly low values of ~20 gAPI. At 110.5 mbsf, HSGR values increase to 30 gAPI with small-scaled variations superimposed on a nearly linear downhole trend. Logging Unit 1 corresponds to the skeletal packstones of the drift deposits of lithologic Subunit IB. In the cores, a gradual downhole increase in clay content can be observed from 138 mbsf to the bottom of the unit (see **"Lithostratigraphy and Sedimentology"** p. 3). The top of the clay interval is thus 28 m deeper than the change in the logs to higher HSGR values. The clay content in the sediments is reflected by a positive correlation of potassium and thorium logs with average values of 0.5 wt% for potassium and 2.5 ppm for thorium. At the bottom of logging Unit 1, a peak in the uranium log occurs. It corresponds to a hardground with rounded phosphatic nodules, developed on top of Subunit IIA (see **"Lithostratigraphy and Sedimentology,"** p. 3).

F28. Comparison of downhole and core logging data, p. 54.

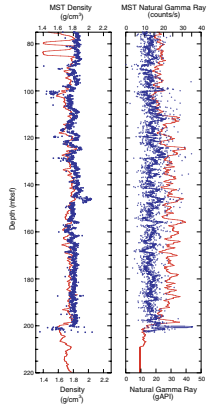

Logging Unit 2 (199–210 mbsf)

A sharp decrease in the HSGR values down to ~12 gAPI at 199 mbsf marks the top of logging Unit 2. Only ~10 m of this unit were logged by the tool string. This interval coincides with the top of lithologic Unit IIA and seismic Megasequence C. Lithologic Subunit IIA consists of coarse-grained carbonate-rich rudstone and floatstone, capped by the dark hardground with phosphatic nodules.

SEISMIC STRATIGRAPHY

Site 1198 penetrated a 523-m-thick sedimentary succession and recovered 5 m of volcanic basement. The site is located on regional multichannel seismic line MAR07 at SP 2262 and on local grid line MAR54 at SP 900 (Fig. F29; also see Fig. F8, p. 68, in the "Leg 194 Summary" chapter). Site 1198 is located ~5 km northwest of the paleoplatform escarpment of the SMP (Fig. F29). The escarpment dips ~10° to the northwest. The lower section of this Miocene escarpment was buried by oncapping and downcapping sediments of Megasequence D. Strong currents close to the platform margin, however, reduced sedimentation

F29. Multichannel seismic line MAR07, p. 55.

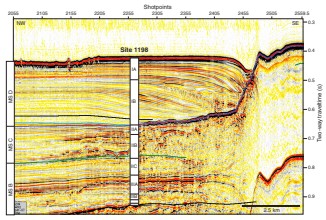

rates adjacent to the escarpment, producing platformward-dipping reflections within Megasequence D. Consequently, a moat was formed at this current-exposed side of the margin so that the topmost section of the paleoescarpment is still outcropping at the seafloor (Fig. F29).

The main objective at this site was to drill the late Miocene platform proximal sedimentary record of the SMP within Megasequence C. The thickening of Megasequence C sediments toward the platform was interpreted to be a result of platform shedding to the northwest during active platform production, bypassing the nondepositional slope and creating an apron at the toe of slope. The sedimentary geometry indicates that these platform slope deposits, which were shed from the SMP, overlie platform-derived distal sediments that might have been shed from the NMP from the northwest.

Time-Depth Conversion

Because of the deteriorating hole condition after drilling, Site 1198 could only be logged in the uppermost 160 m of the borehole and no check shot data are available. As a result, the time-depth conversion for this site was calculated for the upper 201 mbsf using the shipboard velocity data collected from cores (see "Core Physical Properties," p. 19). For the lower part, where velocity data are scarce because of low recovery, two prominent physical and lithological surfaces were used as tie points to relate the seismic traveltimes to depth in the cores. The first horizon is a hardground at 201 mbsf at the base of the hemipelagic drift deposits of lithologic Unit I (see "Lithostratigraphy and Sedimentology," p. 3). This first downcore hard surface is correlated with the high-amplitude reflection of the Megasequence C/D boundary at 655 ms two-way traveltime (TWT) (Fig. F29). The second fix point corresponds to the basalt at the bottom of the hole at 513 mbsf, which produces the strong basement reflection at 922 ms TWT. The resulting time-depth correlation is shown in Figure F10, p. 72, in the "Leg 194 Summary" chapter. Since a continuous velocity record was not available, no synthetic seismogram was generated.

Megasequence D

Seismic Facies and Geometries

Megasequence D is characterized, in general, by laterally continuous low- to medium-amplitude reflections within a 200-m-thick mounded drift. Along line MAR07, 2 km to the northwest, erosional truncations cut into the top of Megasequence D, indicating ongoing erosion at the modern seafloor (Fig. F29). Such erosional features are only seen on the modern seafloor, and no major unconformities occur within Megasequence D northwest of Site 1198. Closer to the SMP margin, the reflections gently dip with progressively steeper angles to the southeast into the moat created in front of the platform margin. Several disturbances in these dipping reflections, such as contorted beds, document sediment slumping and accumulation of these slump sediments at the bottom of the of the paleomoat (Fig. F29). The basal reflections of Megasequence D downlap onto Megasequence C, indicating a hiatus at the Megasequence C/D boundary at 232 ms TWT, or 203 mbsf.

Correlation with Cores

Megasequence D coincides with lithologic Unit I (0–201 mbsf), which consists of hemipelagic wackestone to grainstone with varying input of terrigenous sediments. In the bioturbated ooze, possible slumped intervals occur in the upper 70 m of this unit (see "Lithostratigraphy and Sedimentology," p. 3). Seismic data from line MAR07 show large-scale slump geometries on topographically lower levels toward the moat to the southwest. The conformable reflections of the slumped interval coincide with the top of Subunit IB and the potential slump interval between ~70 and 60 mbsf (Fig. F29). Thus, the observed slump structures seen in the cores could be the upslope equivalent of the larger-scale disturbed intervals, although the layering along the seismic line and the local site survey grid indicate horizontal bedding. Hemipelagic sediments directly overlie a hardground surface at 201 mbsf, coinciding with the Megasequence C/D boundary. The surface represents a hiatus from 4.5 to 7.2 Ma (see "Age Model," p. 14).

Megasequence C

Seismic Facies and Geometries

The top of Megasequence C is marked by a high-amplitude reflection that dips to the northwest, away from the platform escarpment. The Megasequence C/D boundary is defined by toplap below the boundary and downlap above, resulting in an unconformity. This change in reflection dip across the boundary indicates a change in transport direction between Megasequences D and C. This geometry led to the interpretation that the C/D boundary marks the end of platform shedding from the SMP and, thus, the timing of platform drowning and the subsequent onset of current-controlled hemipelagic deposition in Megasequence D. Close to the escarpment, the seismic facies is chaotic to transparent, with numerous small-scale, erosional high-amplitude cut and fill patterns (Fig. F29). These geometries are typical for channelized lower-slope deposits (Anselmetti et al., 2000). Farther away from the platform, the reflection geometry of Megasequence C becomes more regular, indicating a reduced influence of platform-derived gravity flow deposits. Site 1198 is located roughly at the transition between these two seismic facies within Megasequence C. Only the strongest of the intra-Megasequence C erosional surfaces reaches basinward of Site 1198. Already 3 km northwest of Site 1198, or ~9 km away from the platform, continuous low-amplitude reflections indicate that sediments within Megasequence C form a generally continuous succession.

Correlation with Cores

The top of Megasequence C coincides with the top of lithologic Unit II (see "Lithostratigraphy and Sedimentology," p. 3), which is mostly of late Miocene age (see "Age Model," p. 14). The contact between lithologic Units I and II (201 mbsf) is recovered in the cores as a 10-cm-thick layer of dark phosphatic nodules. The occurrence of these nodules correlates well with the high-amplitude reflection character of C/D and its interpretation as an unconformity as well as the hiatus in the chronostratigraphy (see "Age Model," p. 14). Megasequence C correlates with Subunits IIA and IIB. Based on their high content of neritic constituents, Unit II sediments are interpreted as periplatform deposits

(see "Lithostratigraphy and Sedimentology," p. 3). Subunit IIA consists of fine-grained packstone to grainstone, whereas Subunit IIB has a much coarser carbonate lithology that was deposited in a more proximal periplatform setting, such as a reef talus (see "Lithostratigraphy and Sedimentology," p. 3). The lithology of Subunit IIB correlates well with the chaotic seismic facies seen in Megasequence C. The base of Megasequence C is placed using the time-depth correlation at 320 mbsf.

Megasequence B

Seismic Facies and Geometries

At Site 1198, the Megasequence B/C boundary does not have a strong seismic signature. The upper 100 ms TWT of Megasequence B displays a facies similar to Megasequence C: chaotic to transparent close to the escarpment and more regular and coherent further from the platform (Fig. F29). Below that interval, a series of coherent high-amplitude reflections extend to the southwest underneath the platform edge where they are masked by the transparent platform facies and multiples. West of the platform, reflections in the lower part of Megasequence B display variable amplitudes with few erosional geometries. The lowermost reflection above the basement downlaps onto its surface to the northwest and in turn is onlapped from the northwest, indicating a laterally restricted unit overlying basement. Seismic Megasequence A cannot be traced to this area.

Correlation with Cores

The top ~100 ms of Megasequence B corresponds to middle Miocene Subunit IIC, which consists of fine-grained carbonates rich in neritic components deposited in a periplatform setting similar to Subunit IA. Thus, periplatform carbonates occur above and below the Megasequence B/C boundary and record the shedding of neritic components from the nearby carbonate platform into the bathyal environment during the middle Miocene, as well as during the late Miocene (see "Lithostratigraphy and Sedimentology," p. 3). The lower part of Megasequence B consists of the hemipelagic lithologic Unit III, characterized by a downcore increase in carbonate content from ~50 wt% at the top to ~95 wt% at the bottom, and of lithologic Unit IV (504–513 mbsf). The top of lithologic Unit III coincides with the high-amplitude reflections within Megasequence B that can be traced from the distal areas to the platform margin (Fig. F29). Unit IV consists of floatstone to rudstone, with rhodoliths and abundant large benthic foraminifers, and is capped by a phosphatic hardground surface. This interval can be correlated to the seismic data as the lowermost sequence overlying the basement reflection, which is onlapped by the hemipelagic lithologic Unit III.

Acoustic Basement

Acoustic basement at Site 1198 is defined by a strong reflection and a drastic change in seismic facies. It is slightly dipping to the northwest and cannot be traced below the SMP, as the overlying platform sediments attenuate the signal and mask most subsurface information. Basement at this site, reached at 513 mbsf, consists of an olivine basalt.

REFERENCES

Allan, T.L., Trotter, J.A., Whitford, D.J., and Korsch, M.J., 2000. Strontium isotope stratigraphy and the Oligocene-Miocene T-letter "stages" in Papua New Guinea. *In* Buchanan, P.G., Grainge, A.M., and Thornton, R.C.N. (Eds.), *Proc. Fourth Petrol. Conv:* Port Moresby, 155–168.

Anselmetti, F.S., Eberli, G.P., and Diug, Z.-D., 2000. From the Great Bahama Bank into the Straits of Florida: a margin architecture controlled by sea level fluctuations and ocean currents. *Geol. Soc. Am. Bull.,* 112:829–844.

Athy, L.F., 1930. Density, porosity, and compaction of sedimentary rocks. *AAPG Bull.,* 14:1–24.

Betzler, C., 1997. Ecological control on geometries of carbonate platforms: Miocene/Pliocene shallow-water microfaunas and carbonate biofacies from the Queensland Plateau (NE Australia). *Facies,* 37:147–166.

Betzler, C., and Chaproniere, G.C.H., 1993. Paleogene and Neogene larger foraminifers from the Queensland Plateau: biostratigraphy and environmental significance. *In* McKenzie, J.A., Davies, P.J., Palmer-Julson, A., et al., *Proc. ODP, Sci. Results,* 133: College Station, TX (Ocean Drilling Program), 51–66.

Chaproniere, G.C.H., 1981. Australasian mid-Tertiary larger foraminiferal associations and their bearing on the East Indian Letter Classification. *BMR J. Aust. Geol. Geophys.,* 6:145–151.

Chaproniere, G.C.H., 1984. The Neogene larger foraminiferal sequence in the Australian and New Zealand regions, and its relevance to the East Indian Letter Stage classification. *Palaeogeogr., Palaeoclimatol., Palaeoecol.,* 46:25–35.

Chaproniere, G.C.H., and Betzler, C., 1993. Larger foraminiferal biostratigraphy of Sites 815, 816, and 826, Leg 133, northeastern Australia. *In* McKenzie, J.A., Davies, P.J., Palmer-Julson, A., et al., *Proc. ODP, Sci. Results,* 133: College Station, TX (Ocean Drilling Program), 39–49.

Keen, C., and Beaumont, C., 1990. Geodynamics of rifted continental margins. *In* Keen, M.J., and Williams, G.L. (Eds.), *Geology of the Continental Margin of Eastern Canada.* Geol. Soc. Am., 1:391–472.

Prévot, M., and Grommé, S., 1975. Intensity of magnetization of subaerial basalts and its possible change with time. *Geophys. J. R. Astron. Soc.,* 40:207–224.

Tsuji, Y., 1993. Tide influenced high energy environments and rhodolith-associated carbonate deposition on the outer shelf and slope off the Miyako Islands, southern Ryukyu island arc, Japan. *Mar. Geol.,* 113:255–271.

Wyllie, M.R.J., Gregory, A.R., and Gardner, L.W., 1956. Elastic wave velocities in heterogeneous and porous media. *Geophysics,* 21:41–70.

Figure F1. Seismic line MAR07 with location of Site 1198, along with Site 1196 drilled into the southern carbonate platform and Site 1197 drilled on the leeward margin of the platform. * = projected into the seismic section parallel to the northwestern Southern Marion Platform (SMP) margin. MS = Megasequence.

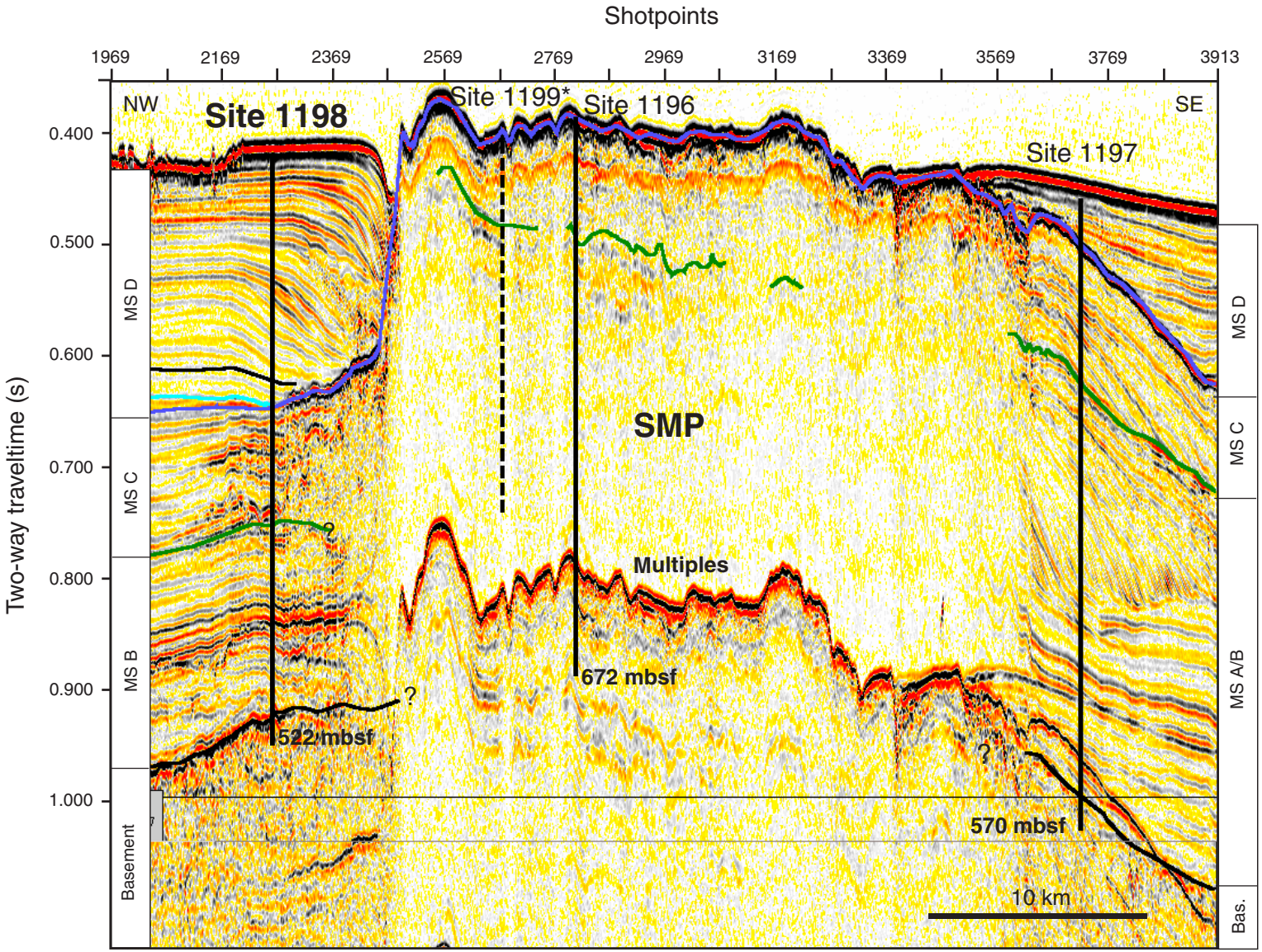

Figure F2. Bathymetry map showing locations of Leg 194 sites.

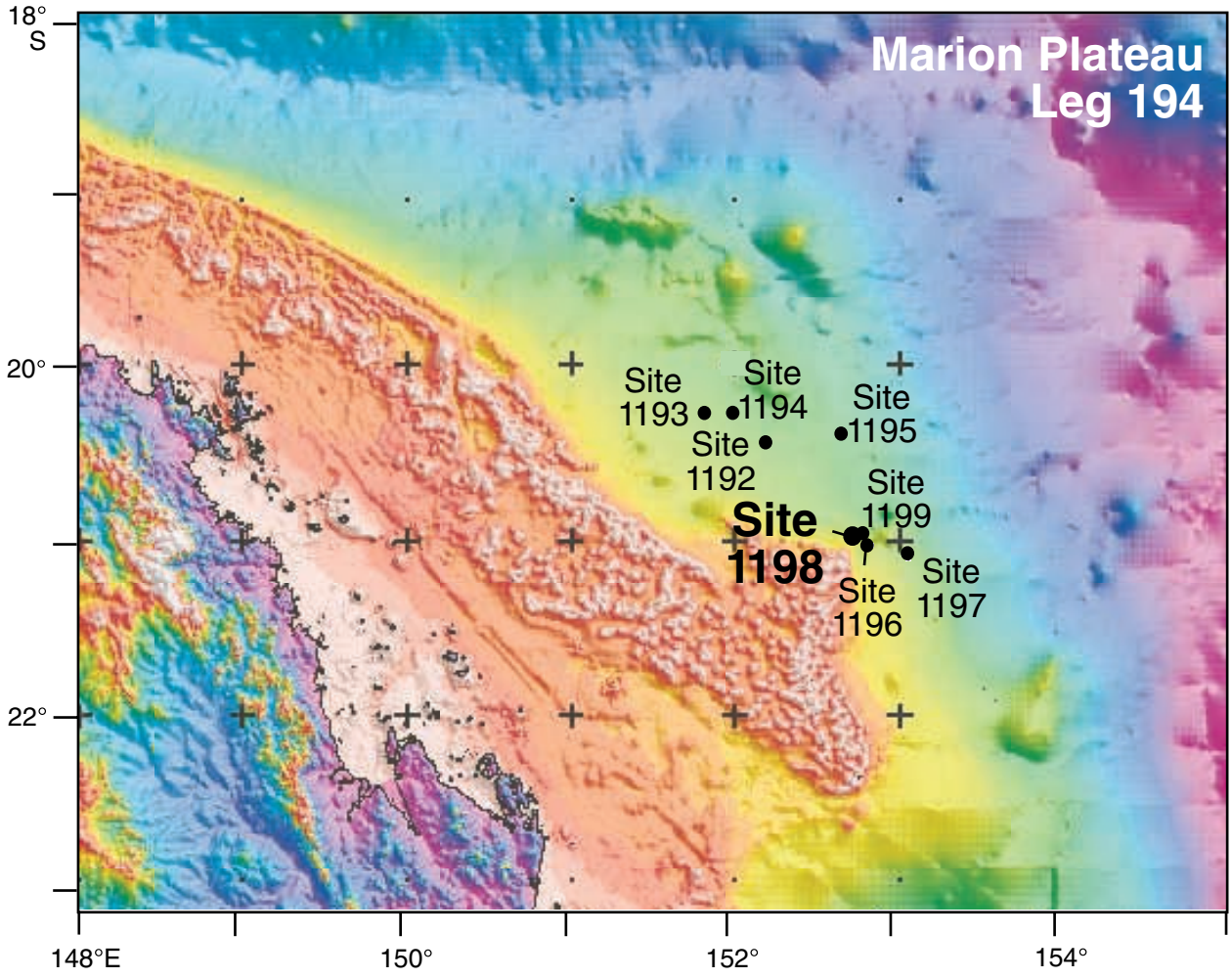

Figure F3. Lithologic summary for Site 1198. **A.** Core recovery. Black = recovery, white = gap (<100% recovery). **B.** Lithologic units as defined in this section. **C.** Lithology. **D.** Calcium carbonate vs. the noncarbonate fraction (see "Geochemistry," p. 15). **E.** Dunham texture. **F.** Grain size. **G.** Interpretation of the recovered facies. **H.** Geologic age (see "Biostratigraphy and Paleoenvironments," p. 8).

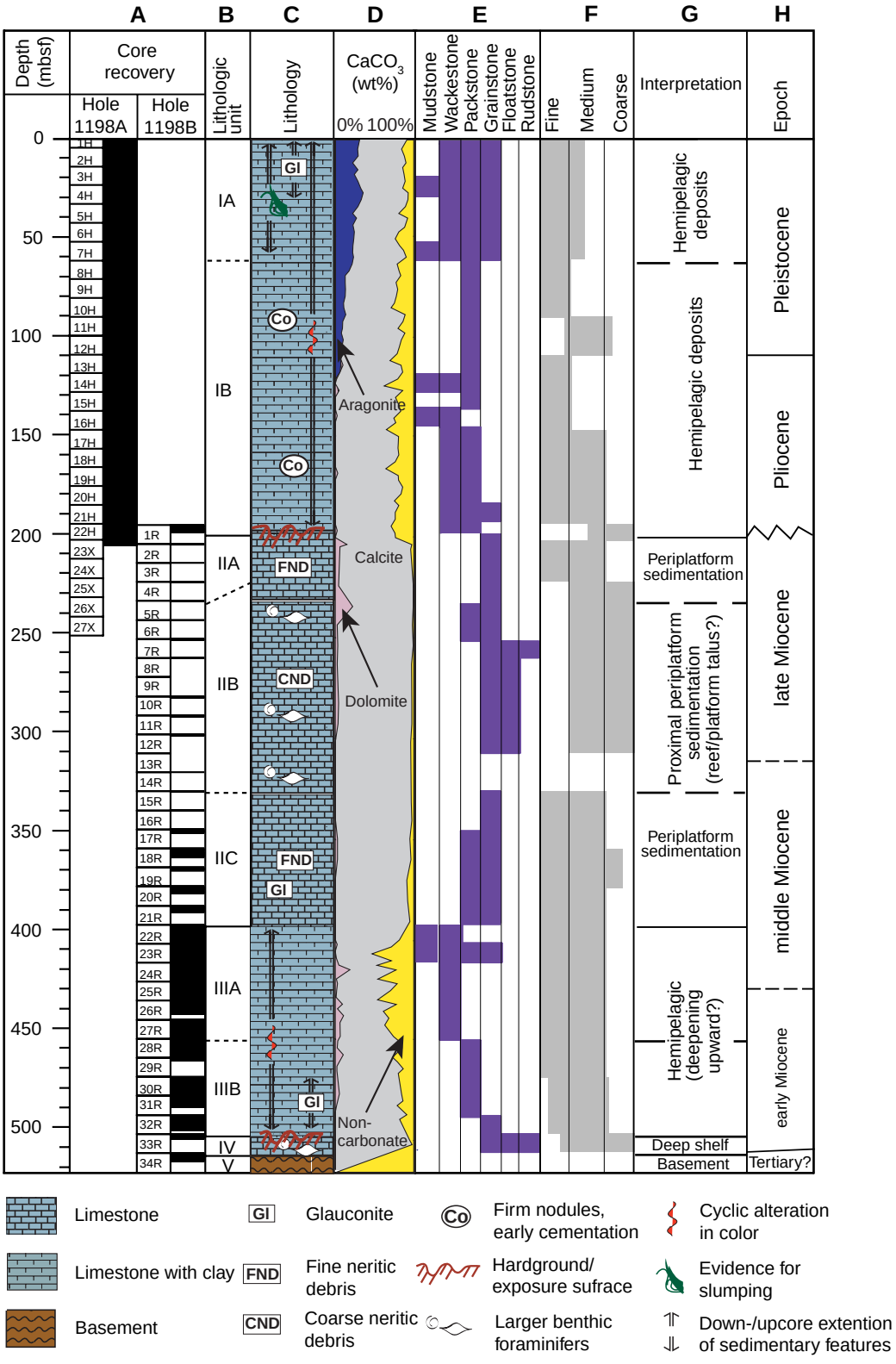

Figure F4. Close-up photograph of synsedimentary soft sediment deformation (slump) (interval 194-1198A-8H-6, 56–75 cm; 70.06–70.26 mbsf), revealed by the vertical slurred-like structure. This divides a lighter and darker part in the sediment, which cannot be explained by coring processes.

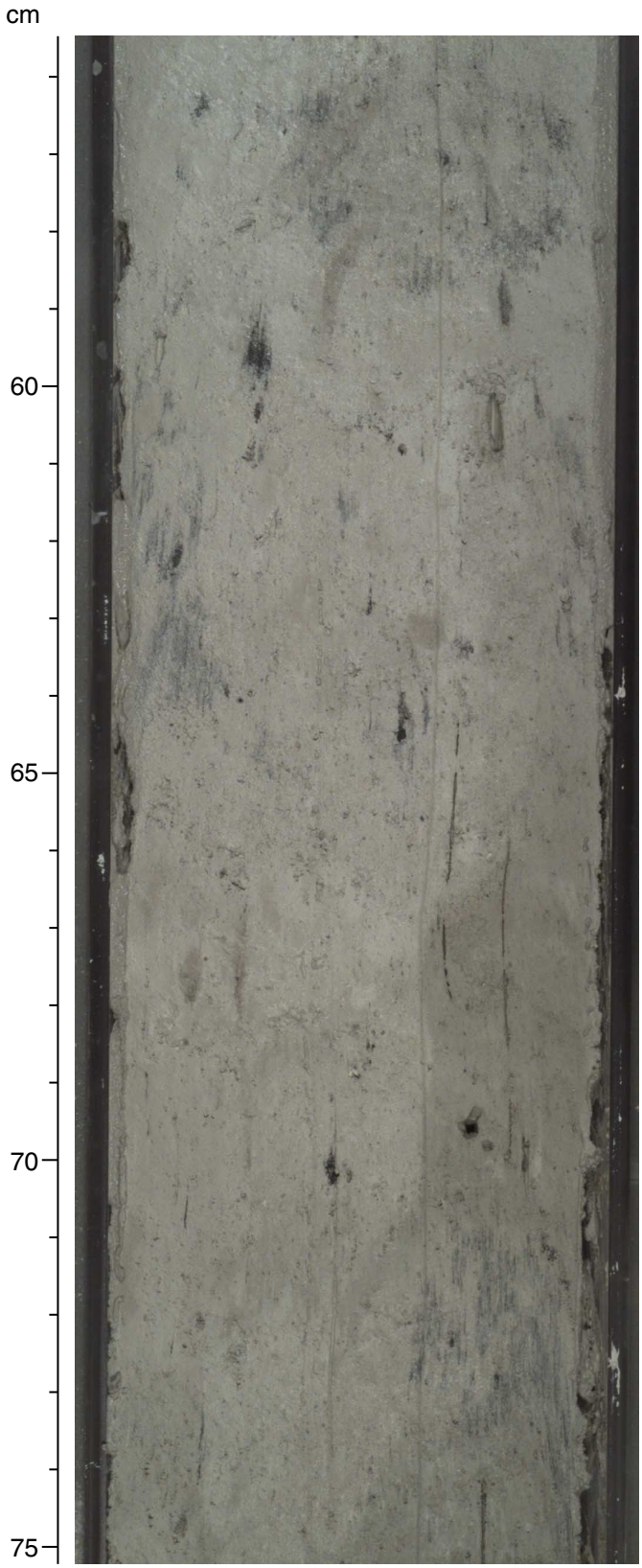

Figure F5. Close-up photograph of boundary between a whitish periplatform sediment (32–38 cm) and a layer of dark phosphatic nodules (interval 194-1198A-23X-1, 19–38 cm; 203.19–203.38 mbsf). This layer is interpreted as a hardground. The texture within each individual nodule is a skeletal packstone dominated by planktonic foraminifer and minor amounts of small benthic foraminifers.

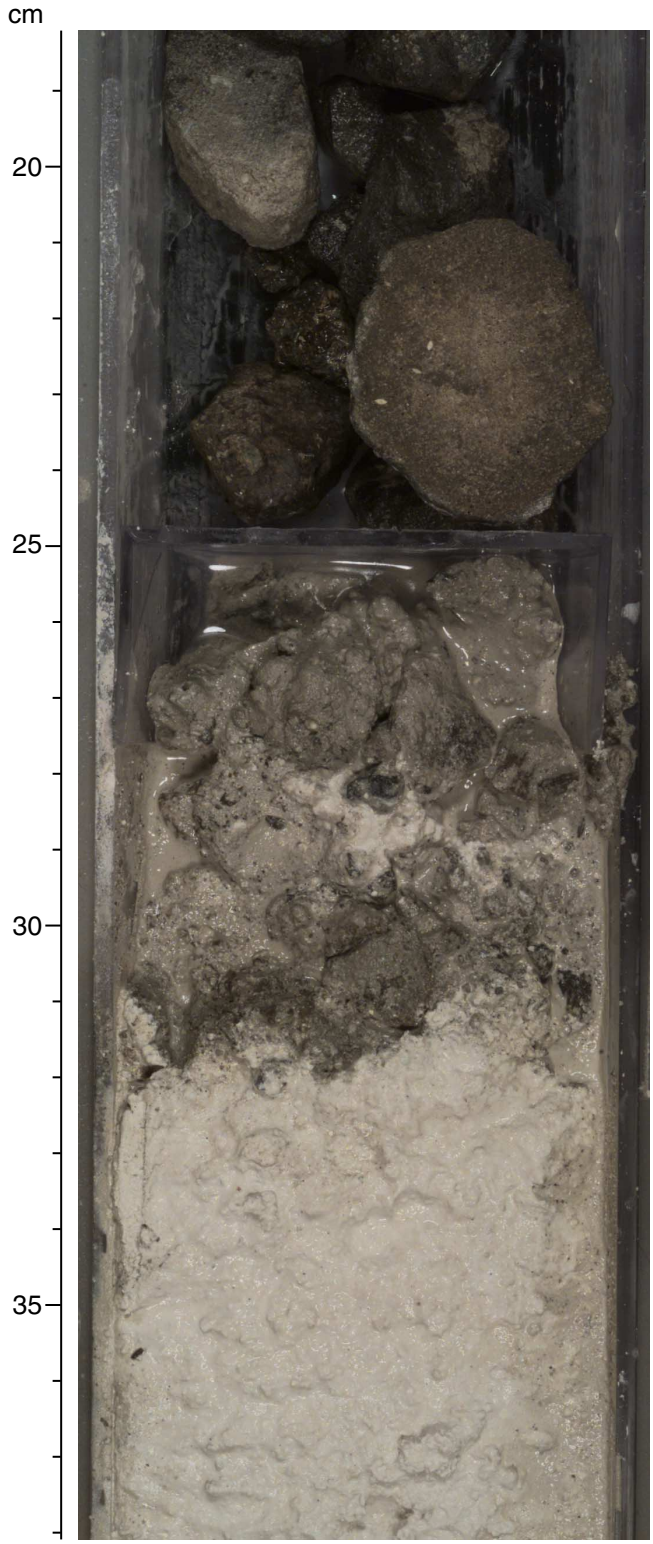

Figure F6. Close-up photograph of coarse-grained periplatform sediment facies (Subunit IIB; interval 194-1198B-12R-1, 11–27 cm; 301.52–301.67 mbsf). Coarse neritic benthic foraminifers occur in a grainstone texture of small benthic and planktonic foraminifers, bryozoan fragments, and algal fragments.

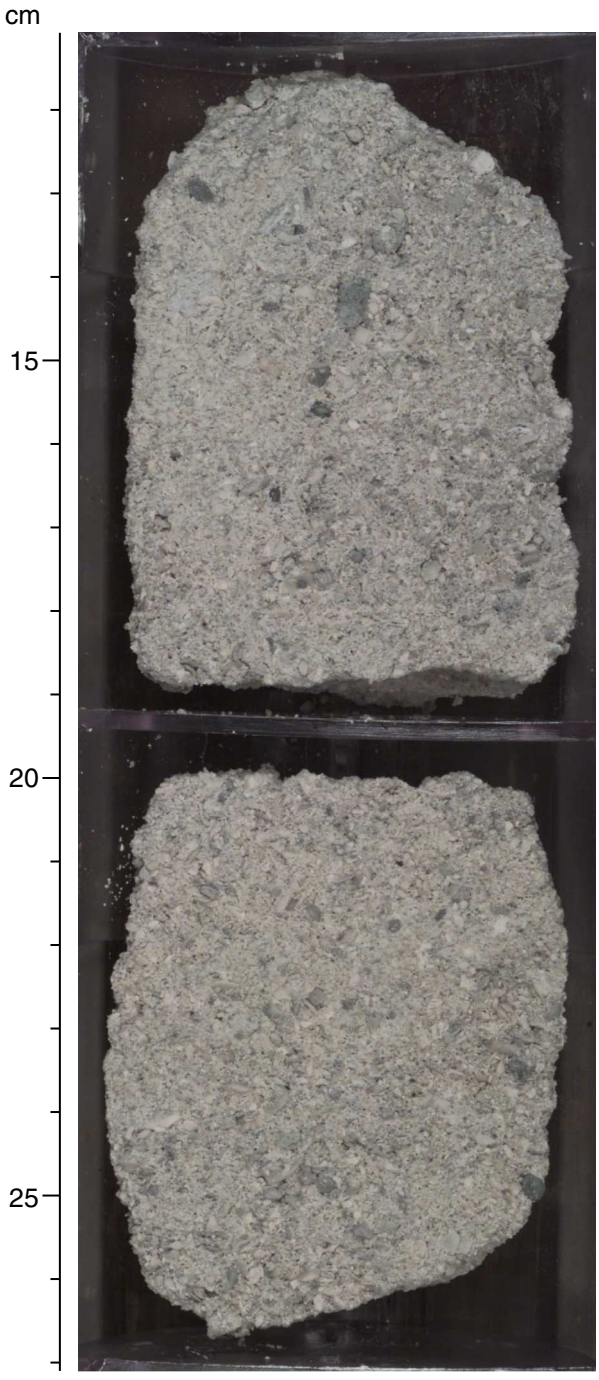

Figure F7. Photomicrograph of Sample **194-1198B-20R-2, 9–12 cm** (379.76–379.79 mbsf), showing fine-grained periplatform sediment facies (Subunit IIC) consisting of larger benthic foraminifers, algal fragments, and mollusk shells, within a planktonic foraminifer dominated facies.

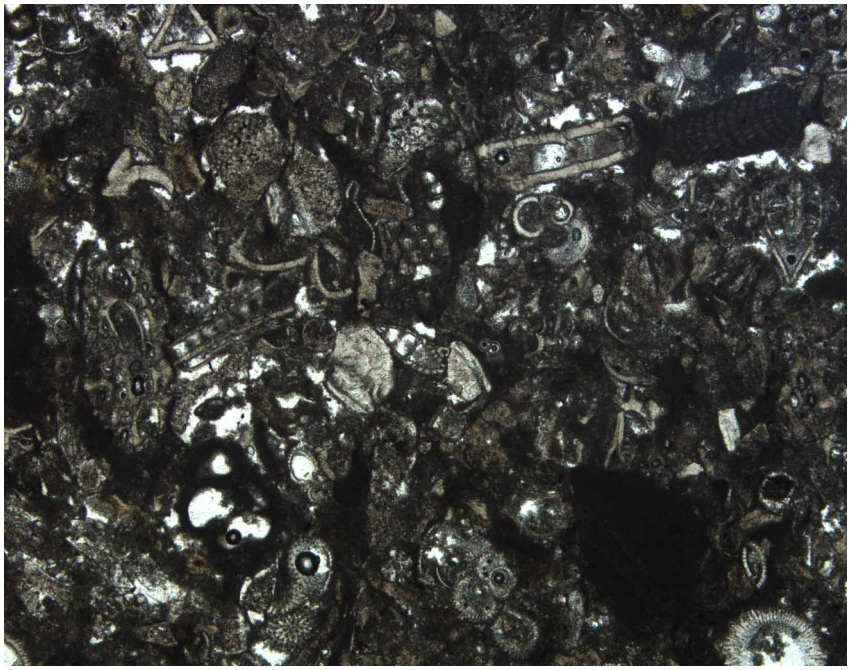

Figure F8. Close-up photograph of the Unit III/IV boundary, seen at ~22–23 cm (interval 194-1198B-33R-1, 18–37 cm; 503.58–503.78 mbsf). Alternations of submillimeter-scaled unoxidized pyrite and phosphate layers encrust the top of Unit IV, indicating a hardground layer. Below this, altered(?) rhodoliths in a fine-grained, brownish-stained matrix with few planktonic foraminifers and neritic-derived grains are observed.

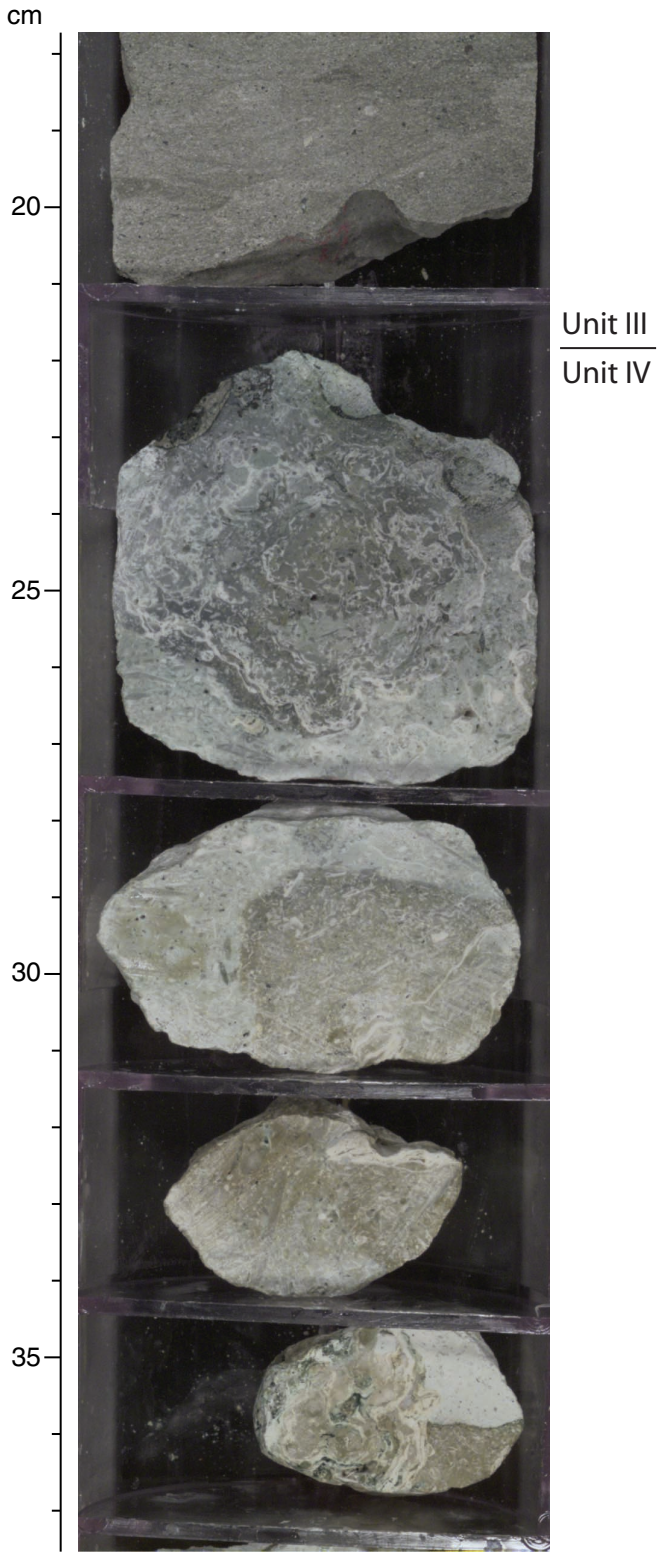

Figure F9. Photomicrograph of submillimeter laminae of pyrite and phosphate at the top of Unit IV (Sample **194-1198B-33R-1, 23–25 cm;** 503.58–503.78 mbsf). Below, fine dark micritic sediment with minor amounts of planktonic foraminifers and altered rhodoliths are observed.

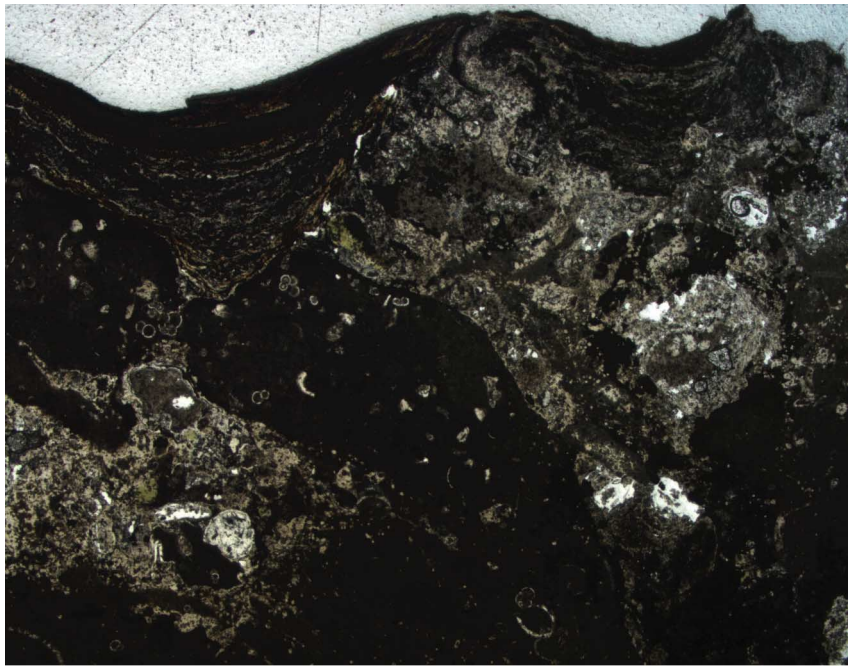

Figure F10. Close-up photograph of deep euphotic shelf facies with rhodoliths and larger benthic foraminifers (skeletal floatstone) (interval 194-1198A-33R-2, 37–56 cm; 505.18–503.39 mbsf). The two principal skeletal components (platy rhodoliths and larger benthic foraminifers) are oriented horizontally in a light greenish gray clay- to silt-sized matrix, which yields a laminated texture.

Figure F11. Photomicrograph showing foraminiferal boundstone consisting of large, very thin larger benthic foraminifers, primarily *Lepidocyclina* (*Eulepidina*) sp. (El), bound together by thin red algal crusts (RA) (Sample **194-1198B-33R-1, 97 cm;** 504.37 mbsf).

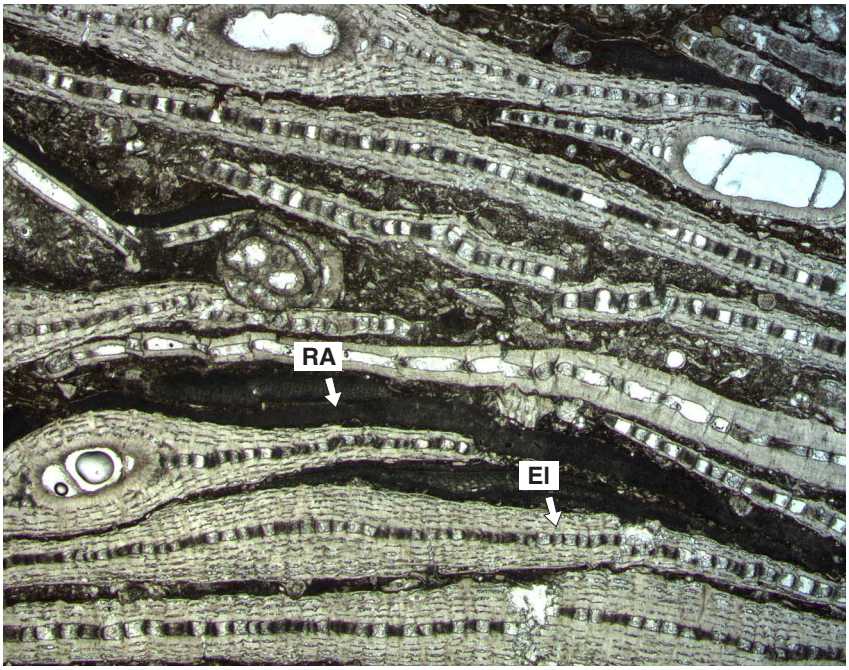

Figure F12. Long-core measurements of inclination and interpreted magnetostratigraphy for the interval 0–200 mbsf in Hole 1198A.

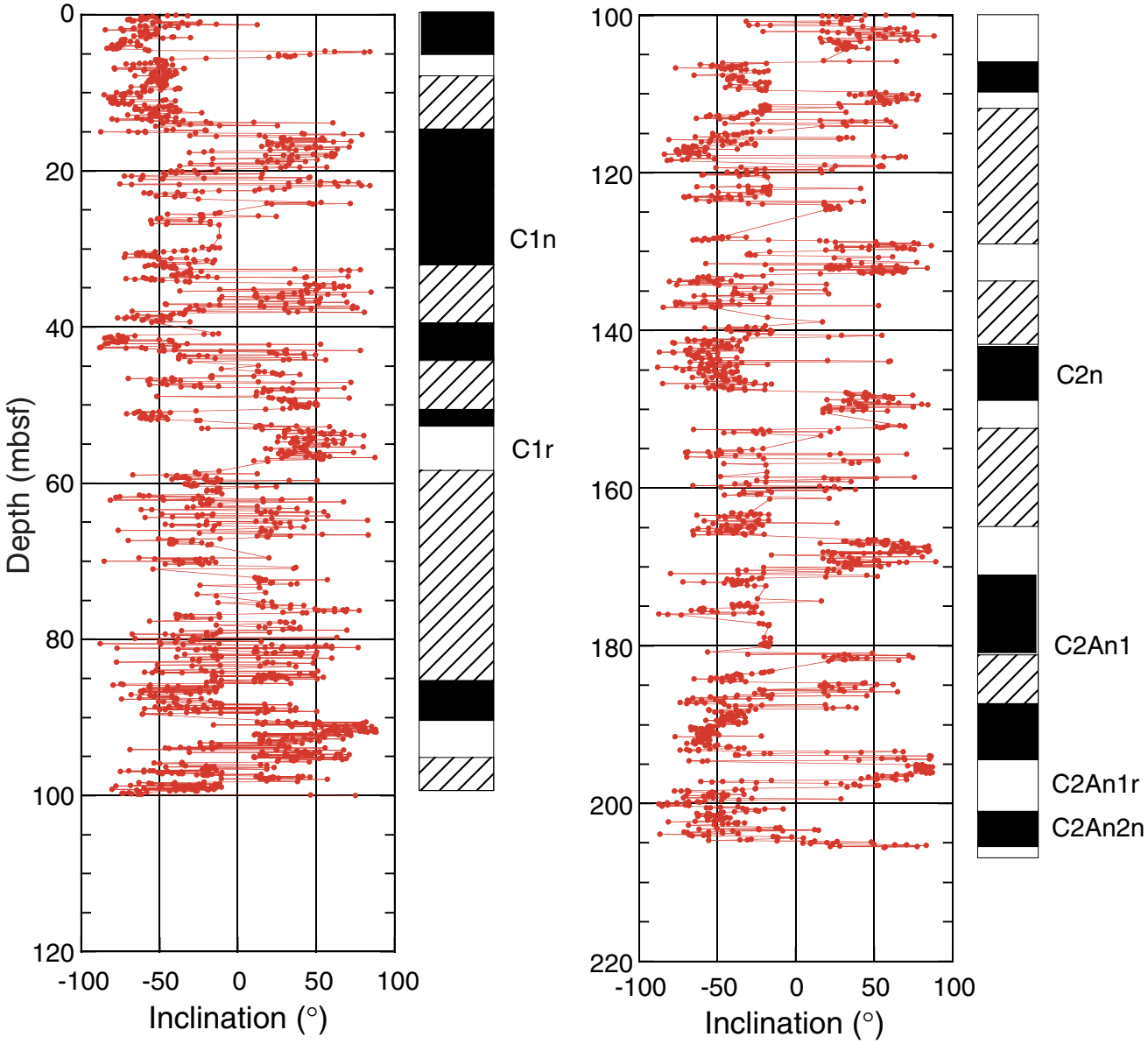

Figure F13. Long-core measurements of inclination for the interval 200–520 mbsf in Hole 1198B.

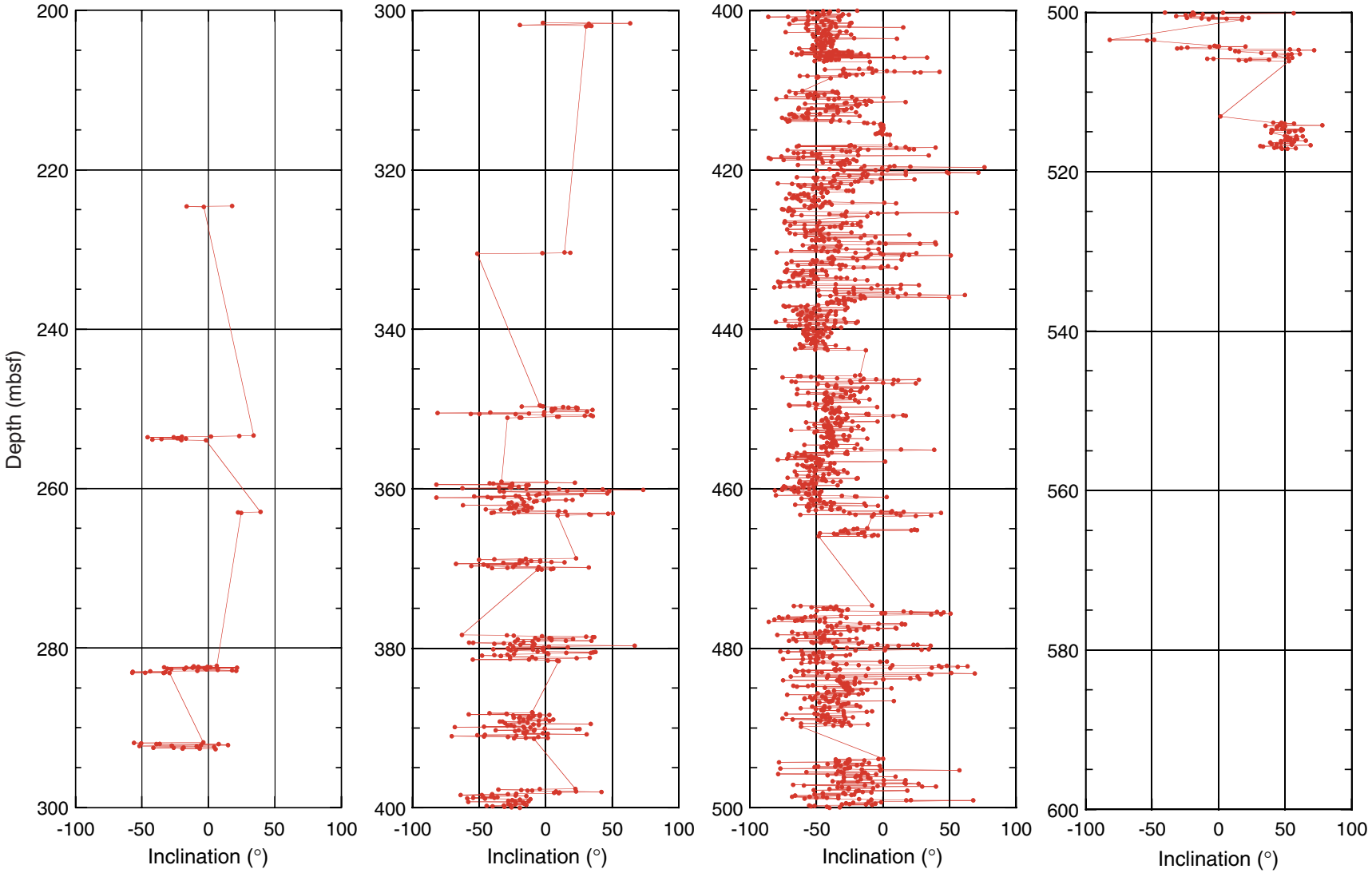

Figure F14. Remanent magnetism characteristics of (**A**) Sample 194-1198A-7H-4, 110–112 cm, and (**B**) Sample 194-1198B-34R-1, 66–68 cm. NRM = natural remanent magnetization, ARM = anhysteretic remanent magnetization, IRM = isothermal remanent magnetization, demag = demagnetization, acq = acquisition.

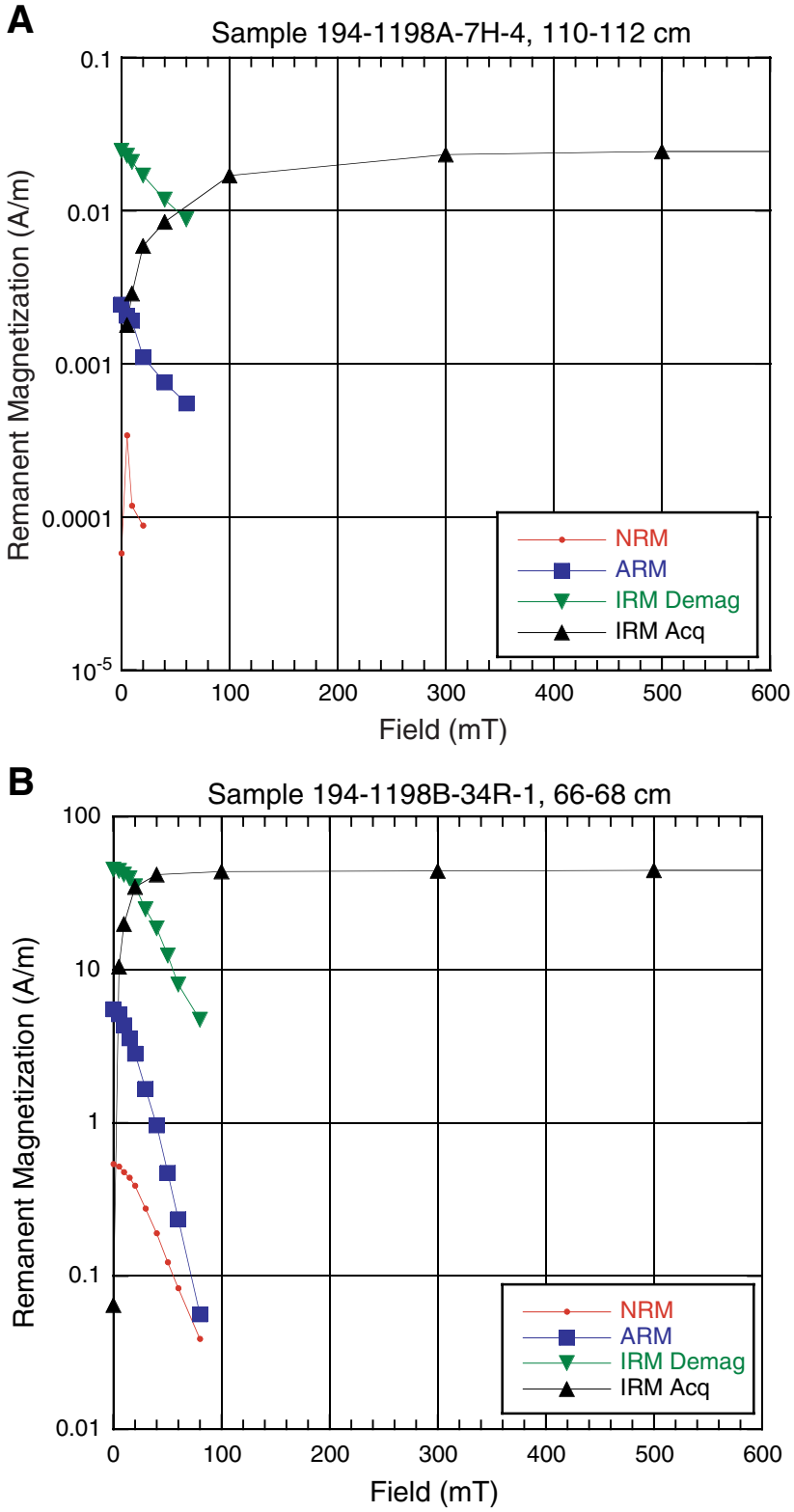

Figure F15. Downcore variation of intensity of natural remanent magnetization (NRM), anhysteretic remanent magnetization (ARM), and isothermal remanent magnetization (IRM), and ratios of IRM 40 mT demag./IRM, IRM 100 mT acq./IRMs, and ARM susceptibility/IRM.

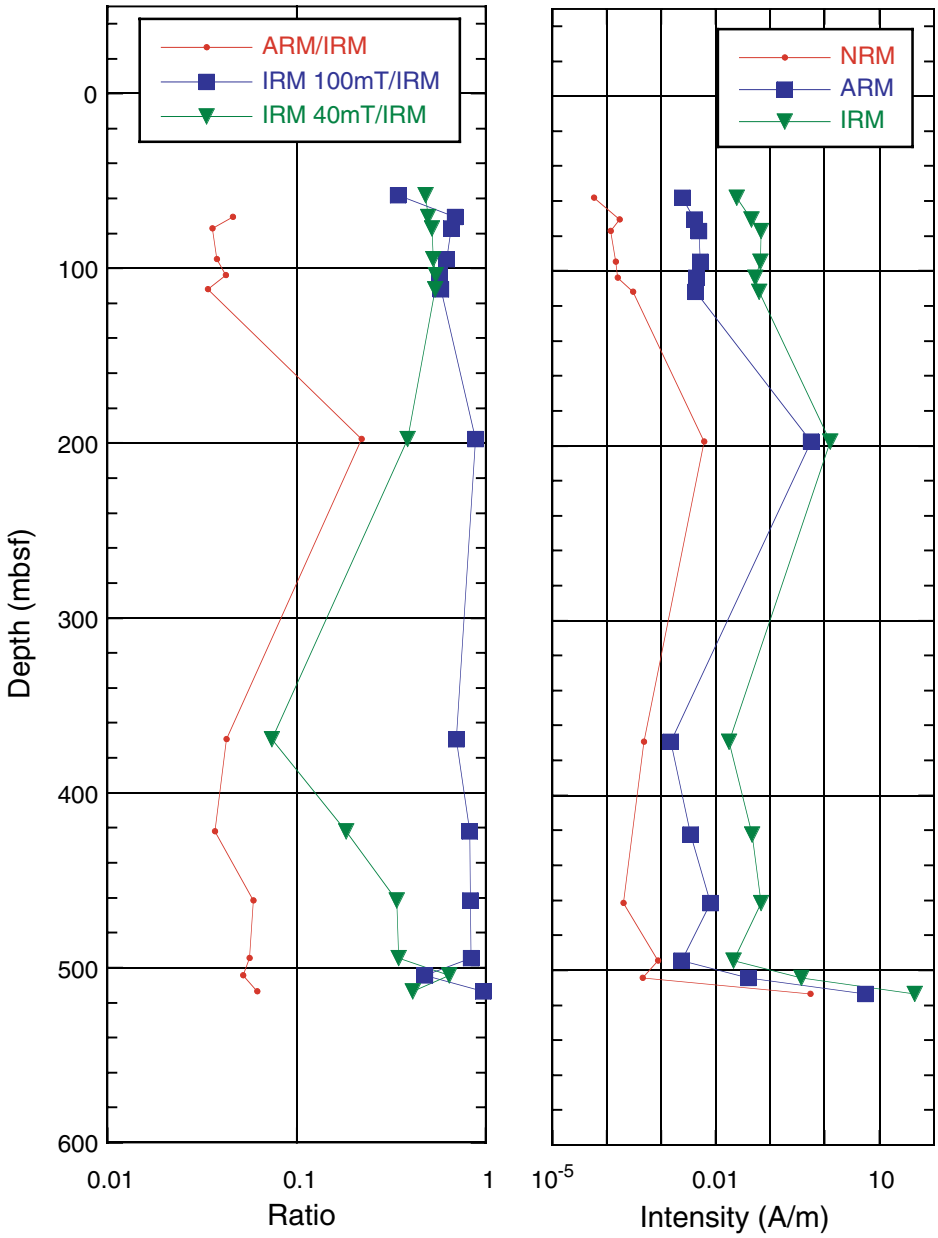

Figure F16. Age-depth model and sedimentation rates at Site 1198. Horizontal lines spanning from the left figure margin to the age-depth curve are lithologic unit (solid) and subunit (dashed) boundaries. Horizontal lines spanning from the right margin of the figure to the age-depth curve are seismic megasequence boundaries (solid) and major reflectors within megasequences (dashed). Vertical lines are epoch boundaries as labeled at the top of the diagram. MS = Megasequence, BSMT = basement.

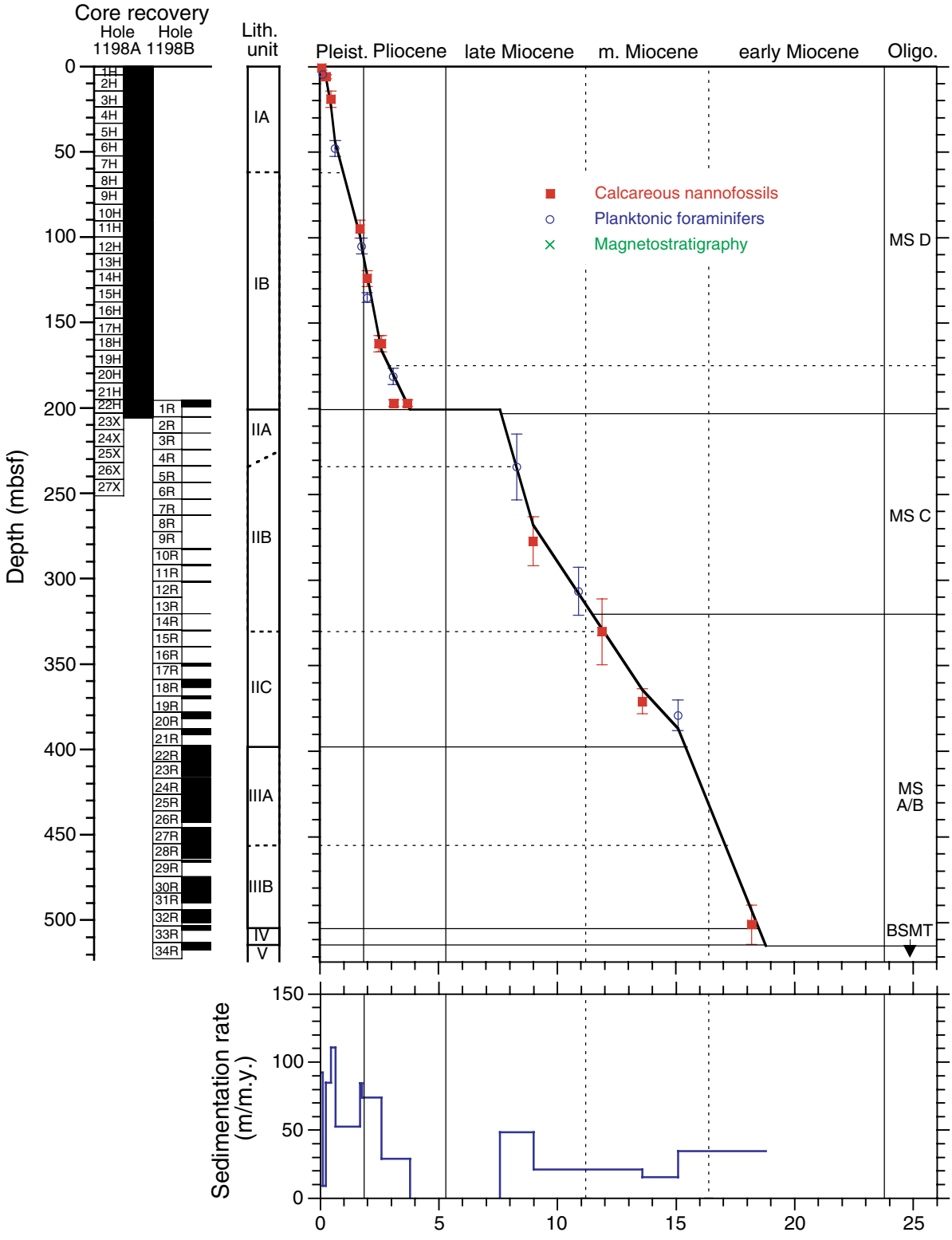

Figure F17. Concentrations of dissolved constituents vs. depth for Site 1198. Solid circles = Hole 1198A, open circles = Hole 1198B. **A.** Chloride. **B.** Alkalinity. **C.** Sulfate. **D.** Ammonium. **E.** Magnesium. **F.** Calcium. **G.** Strontium. **H.** Potassium.

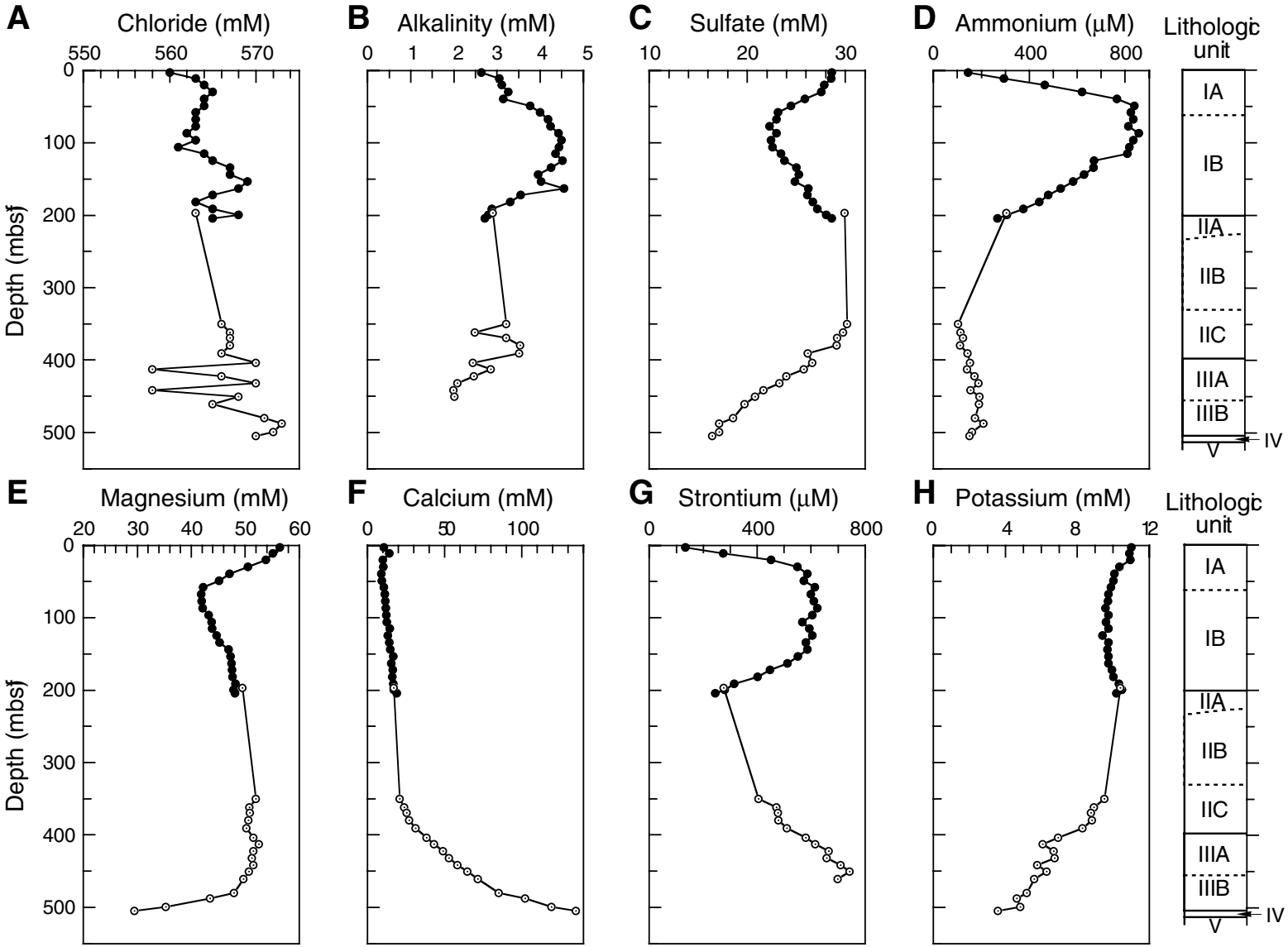

Figure F18. Dissolved sodium in Site 1198 pore water. Blue symbols and line = data determined by charge balance, red symbols and line = data measured by ion chromatography.

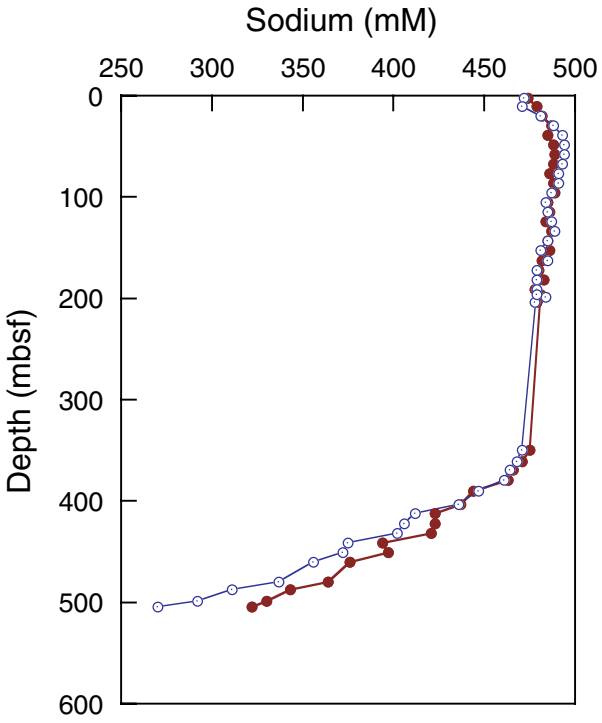

Figure F19. Percentages of carbonate minerals and noncarbonate fraction for Site 1195.

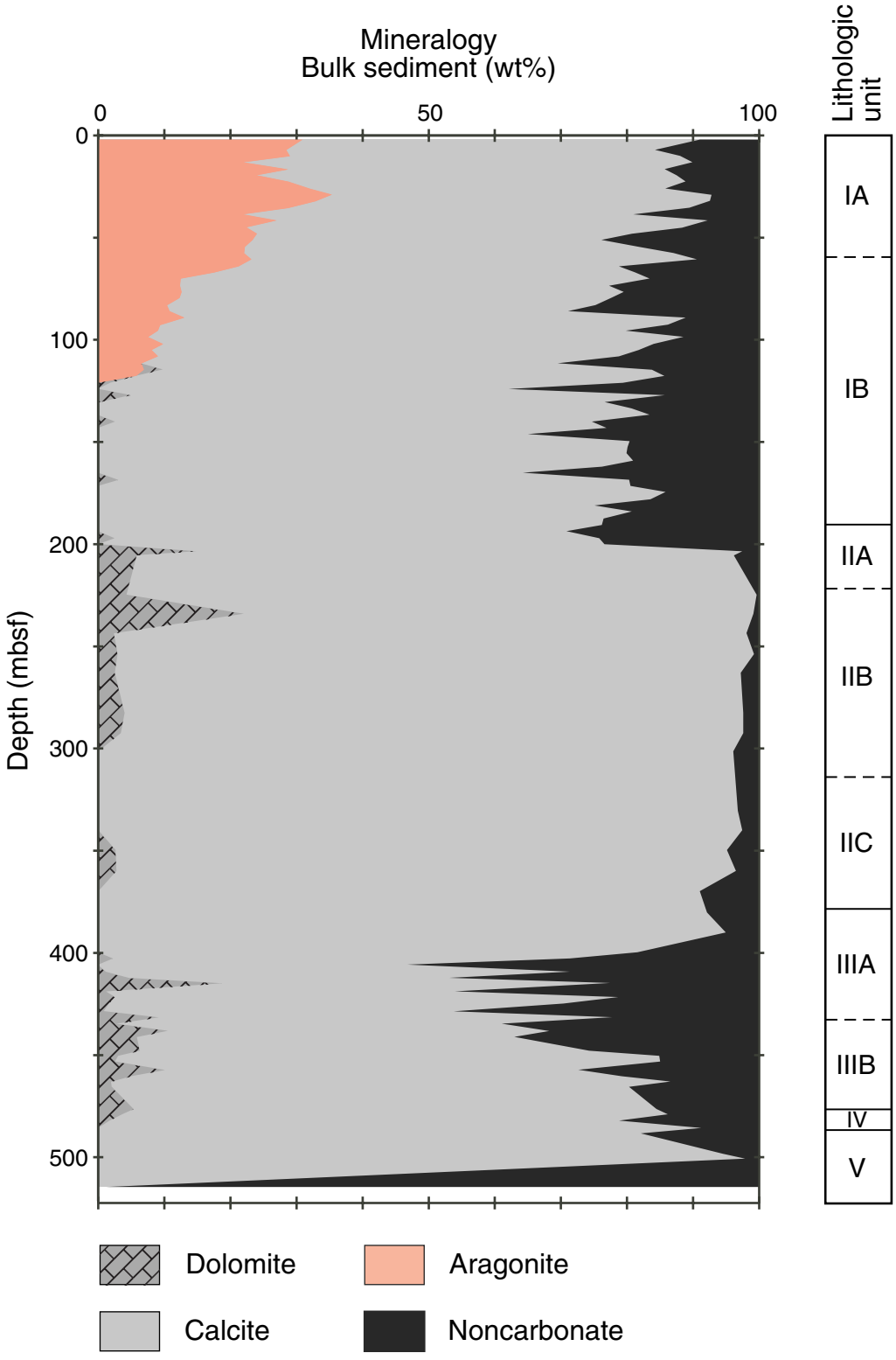

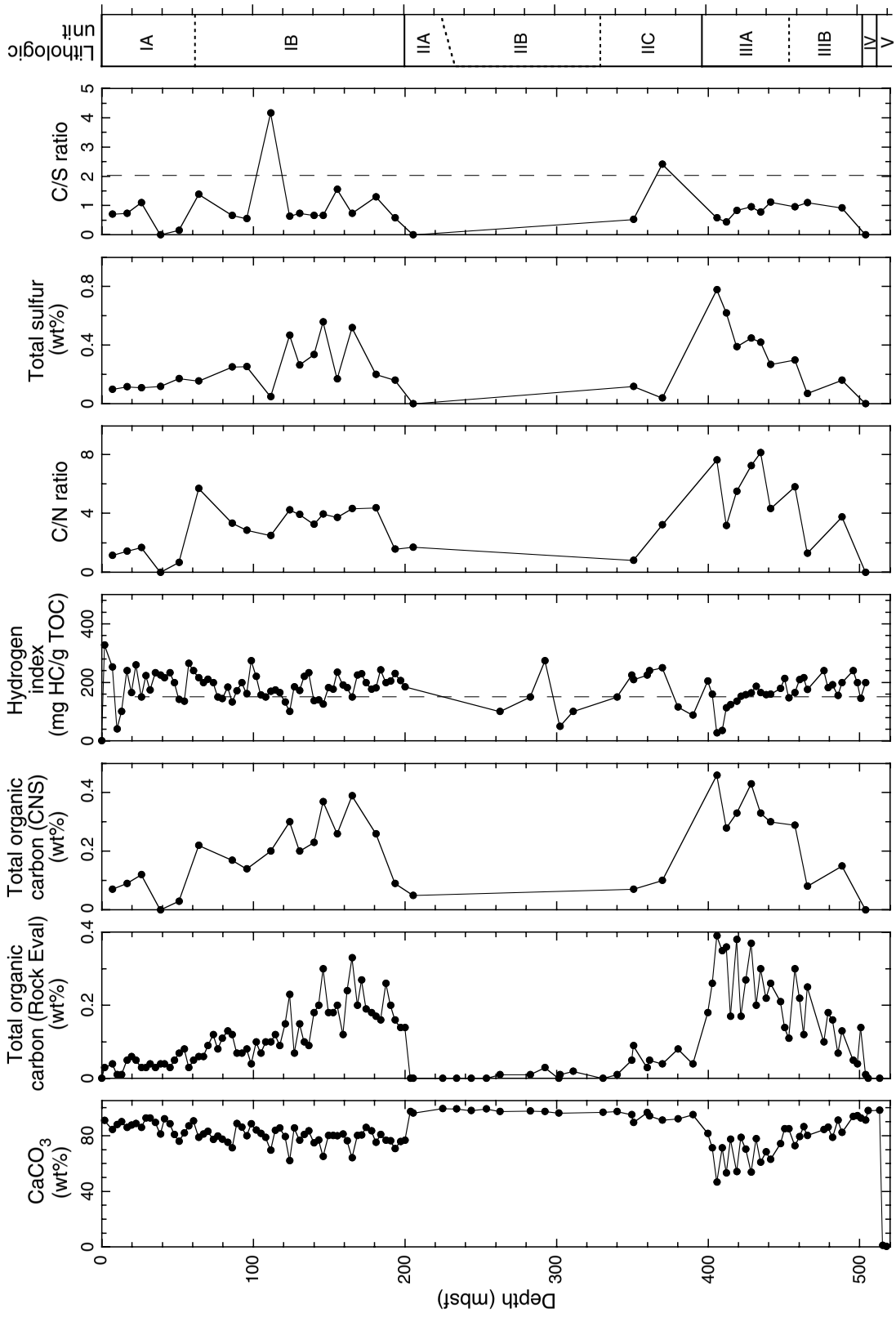

Figure F20. Plots of carbonate and total organic content, hydrogen index values, total sulfur content, and C/N and C/S ratios, Site 1198. The solid vertical lines at HI = 150 and C/S = 2 mark the approximate boundary between terrigenous (<150) and marine organic matter and the transition between marine (<2) and brackish environments of formation, respectively.

Figure F21. A. Bulk density (solid dots = GRA bulk density, open circles = MAD bulk density for Hole 1198A, open squares = MAD bulk density for Hole 1198B). **B.** Grain density from MAD data. Solid circles = Hole 1198A data, solid squares = Hole 1198B data. **C.** Porosity determined from MAD data (symbols) and modeled with an exponential porosity-depth model (line). Circles = Hole 1198A data, squares = Hole 1198B data.

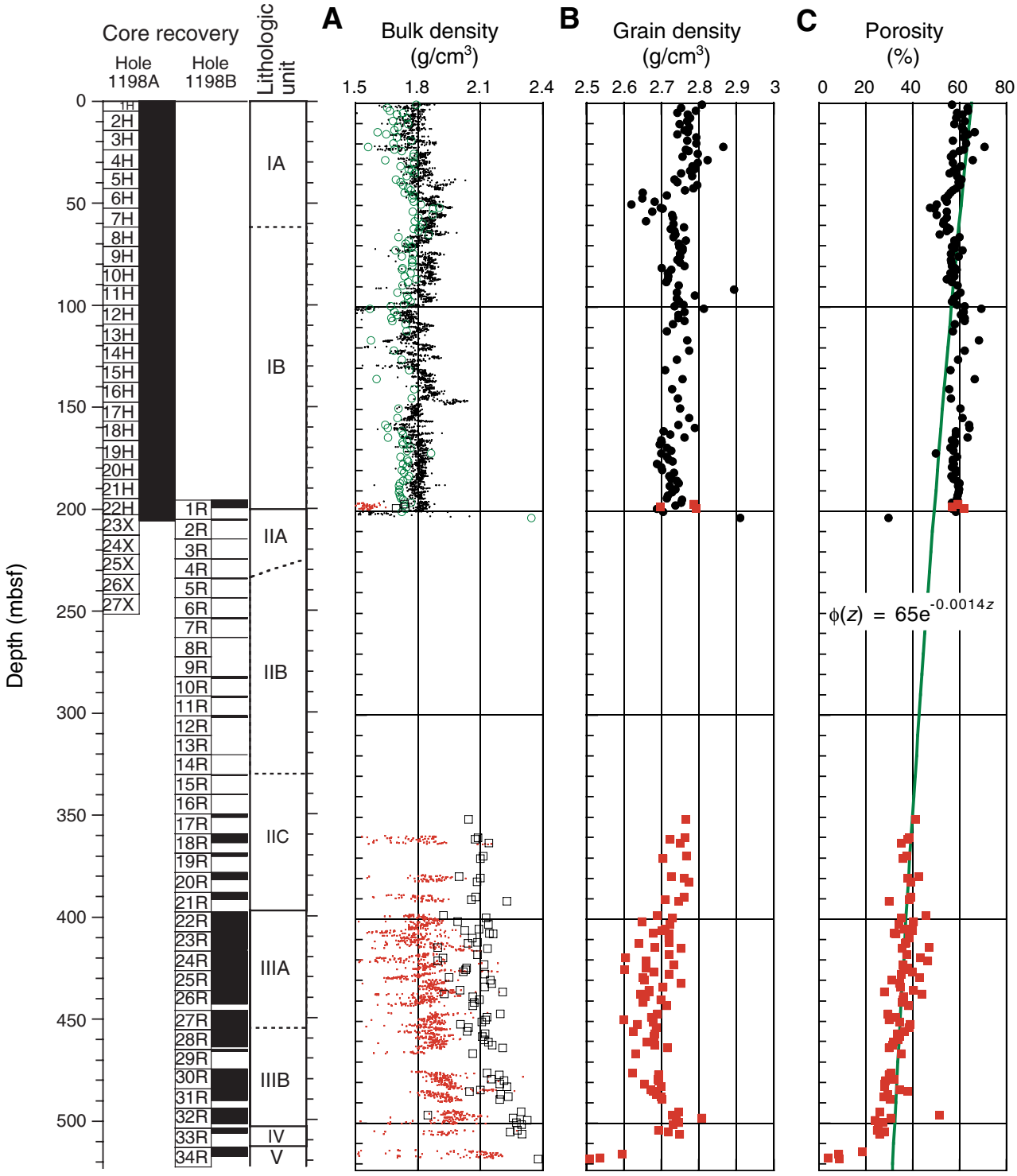

Figure F22. A. Compressional wave velocity as a function of depth. Circles = x-direction, squares = y-direction, diamonds = z-direction. **B.** Anisotropy (average transverse velocity to longitudinal velocity) of compressional wave velocity.

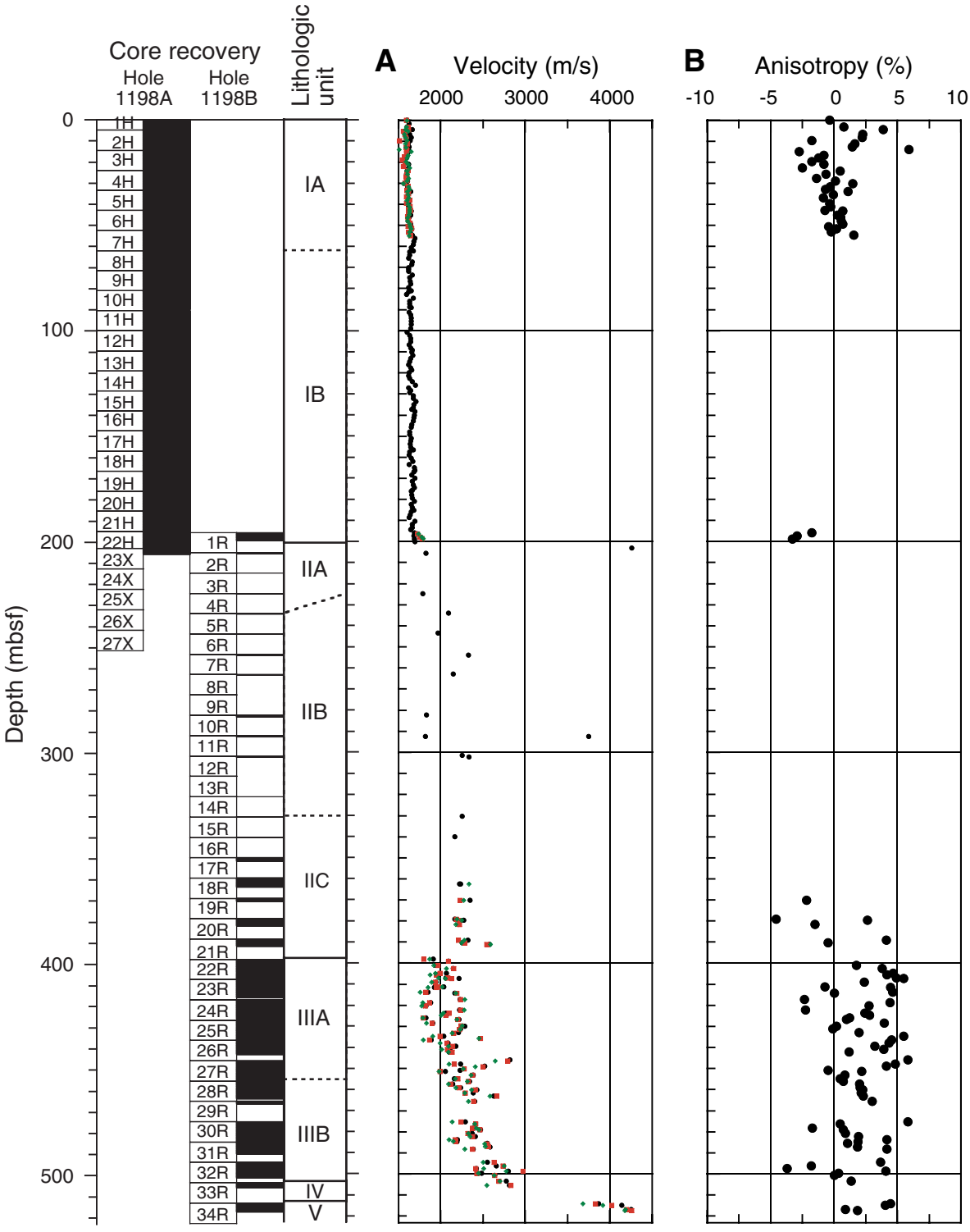

Figure F23. Velocity-porosity crossplot for Site 1198. Solid line = power law porosity-velocity model. Dashed line = time-average equation for calcite (Wyllie et al., 1956).

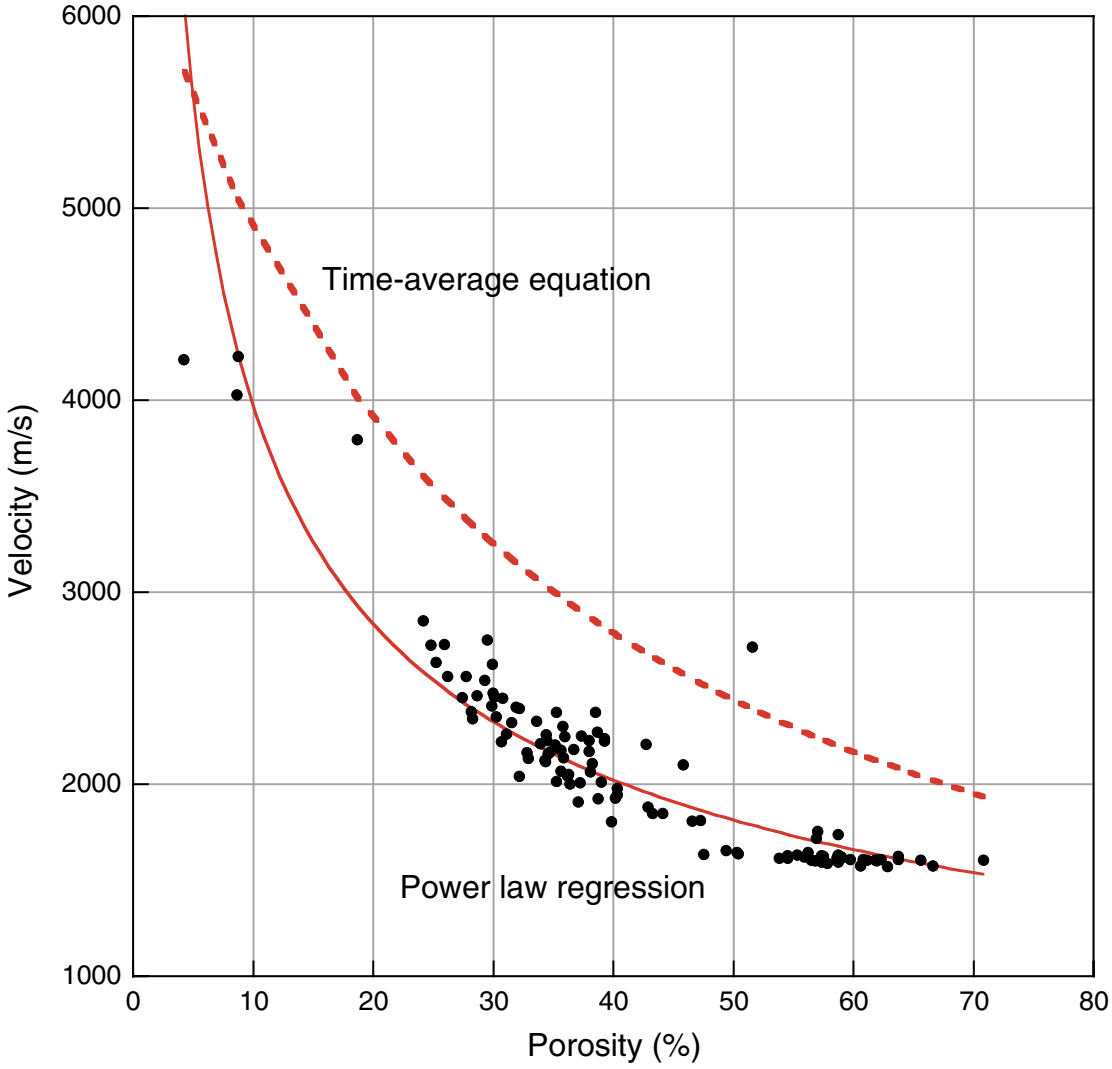

Figure F24. Thermal conductivity (W/[m·K]) at Site 1198. Circles = Hole 1198A data, squares = Hole 1198B data. Plotted values are averages of three needle probe measurements or four half-space probe measurements.

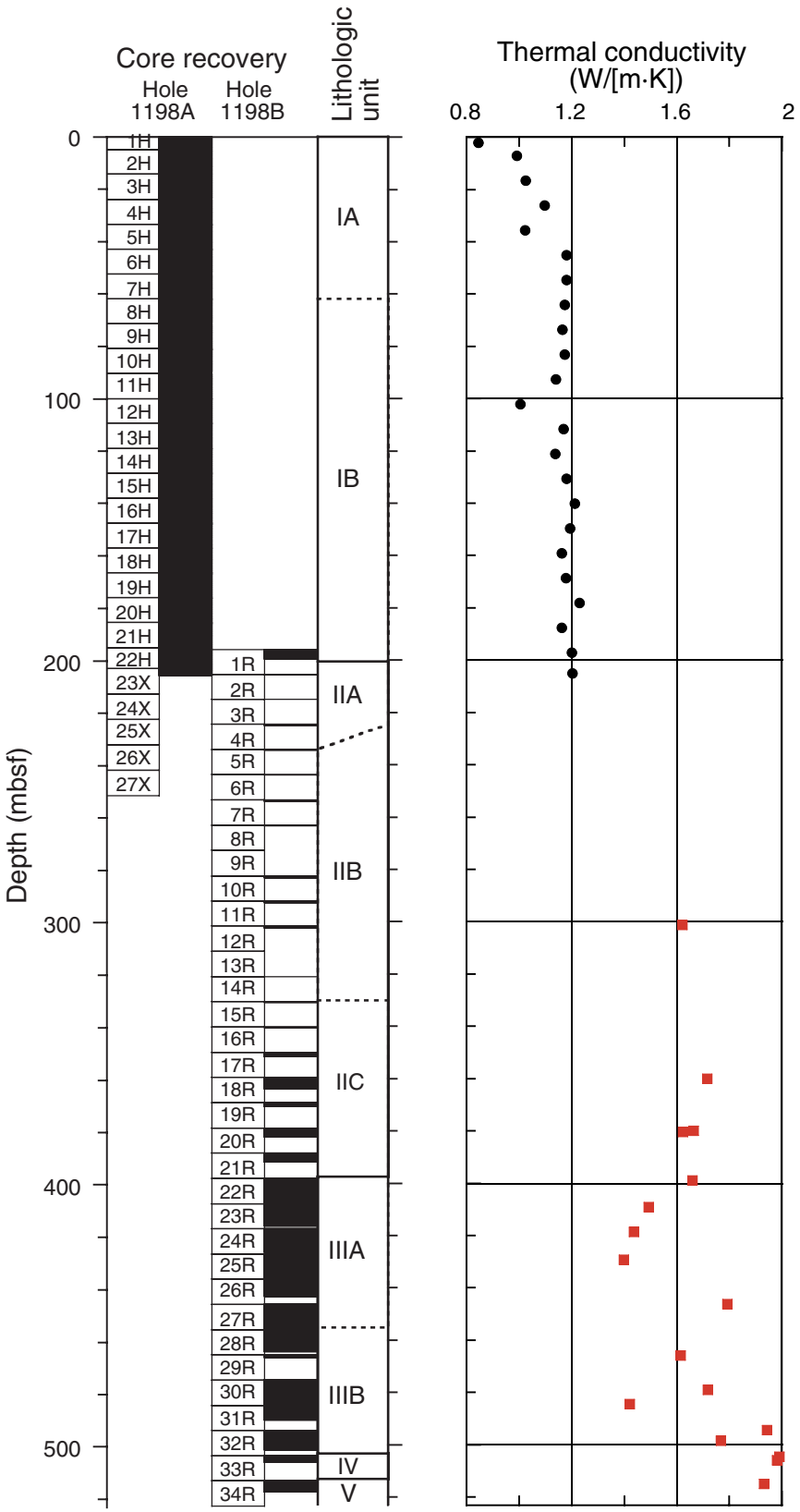

Figure F25. Thermal conductivity as a function of porosity. Curves are theoretical values for pure, single-lithology systems (sandstone, limestone, and shale).

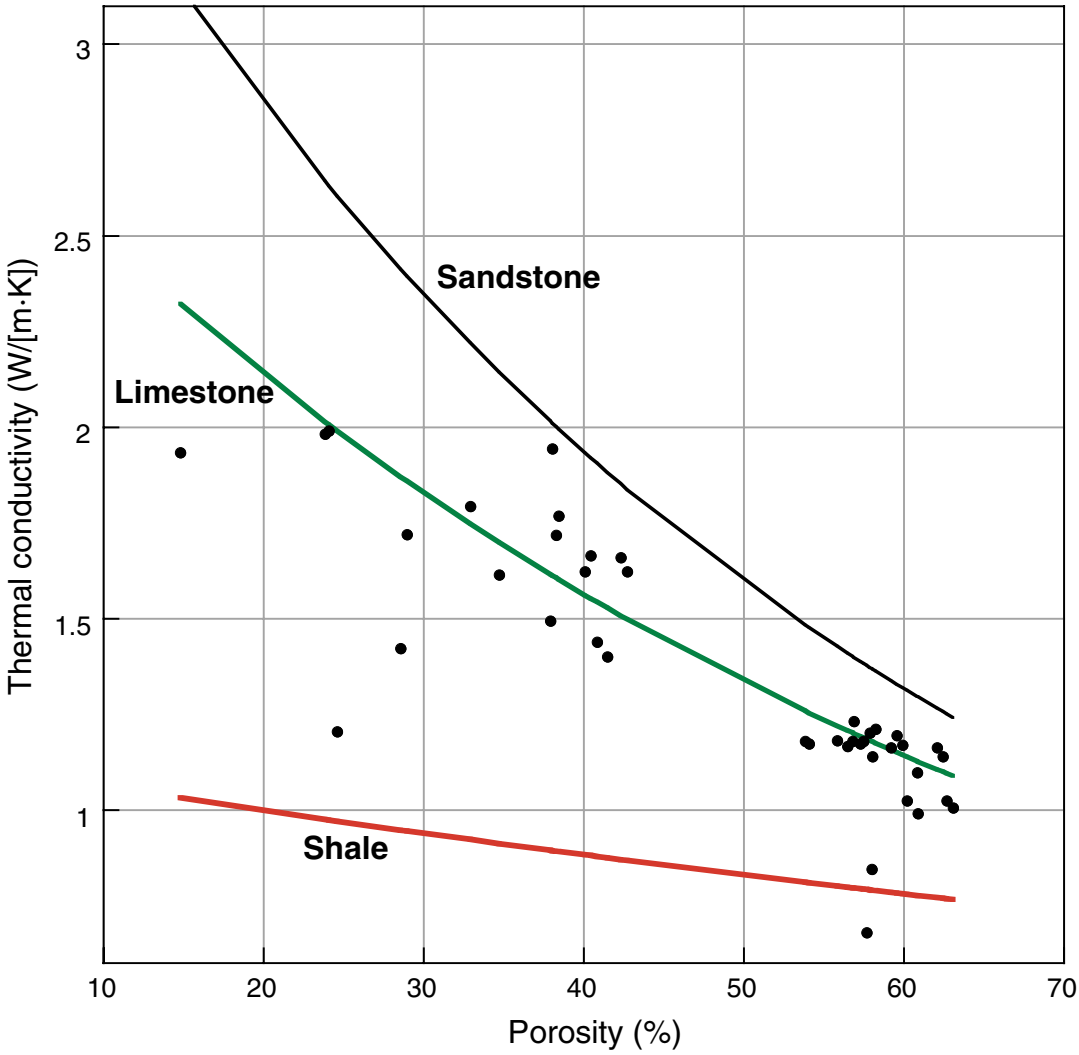

Figure F26. Site 1198 (A) magnetic susceptibility, (B) natural gamma radiation, and (C) lightness (L* parameter). Solid line (NGR) is smoothed (10-point moving average) data. Note that magnetic susceptibility for lithologic Unit V ranges from 1000 to 1500 × 10^{-6} SI. These data are not shown. Circles = Hole 1198A data, squares = Hole 1198B data.

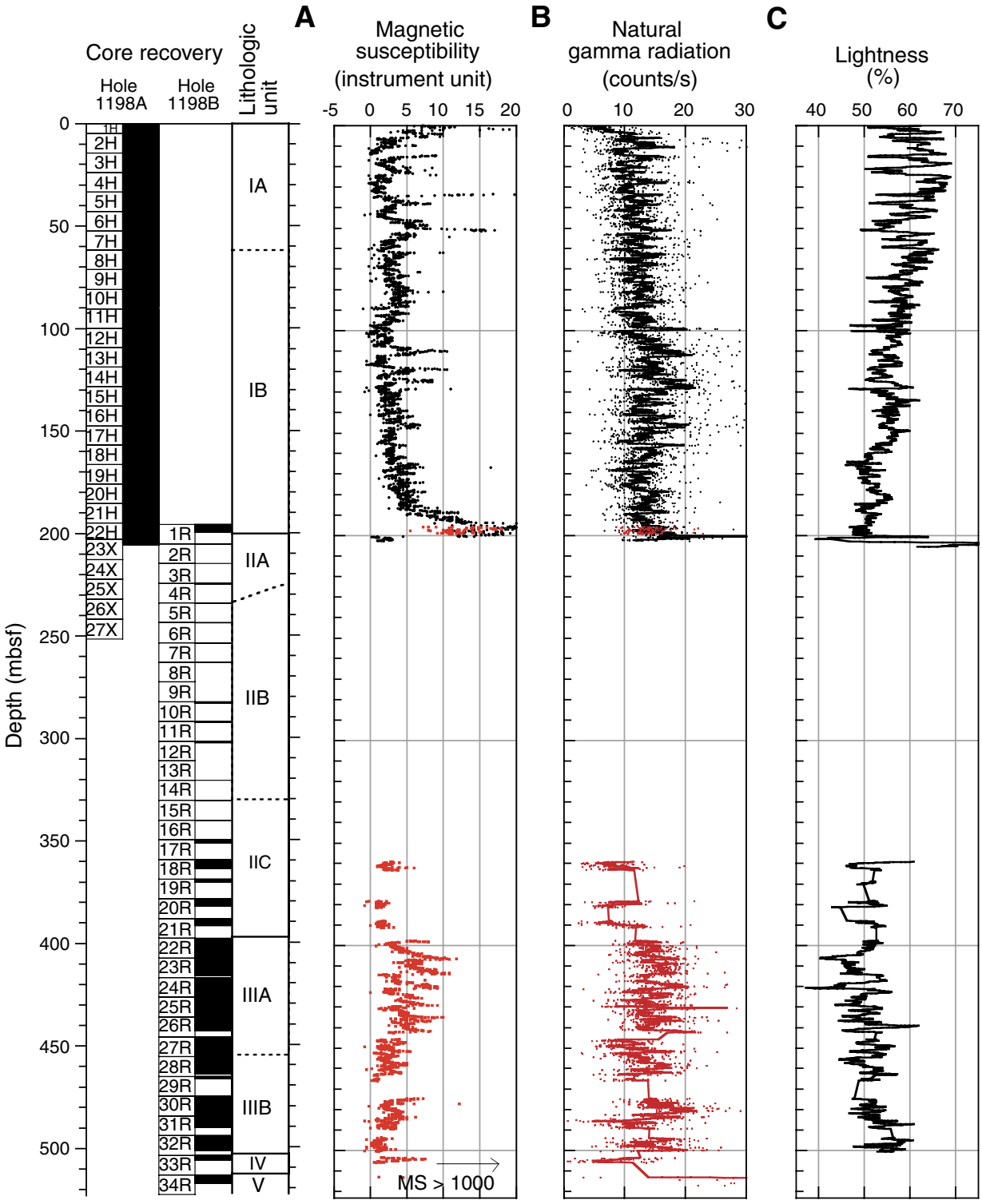

Figure F27. Summary of logging results and correlation with lithologic units. The caliper is open to its maximum throughout most of the logged interval, indicating a borehole diameter >17 in.

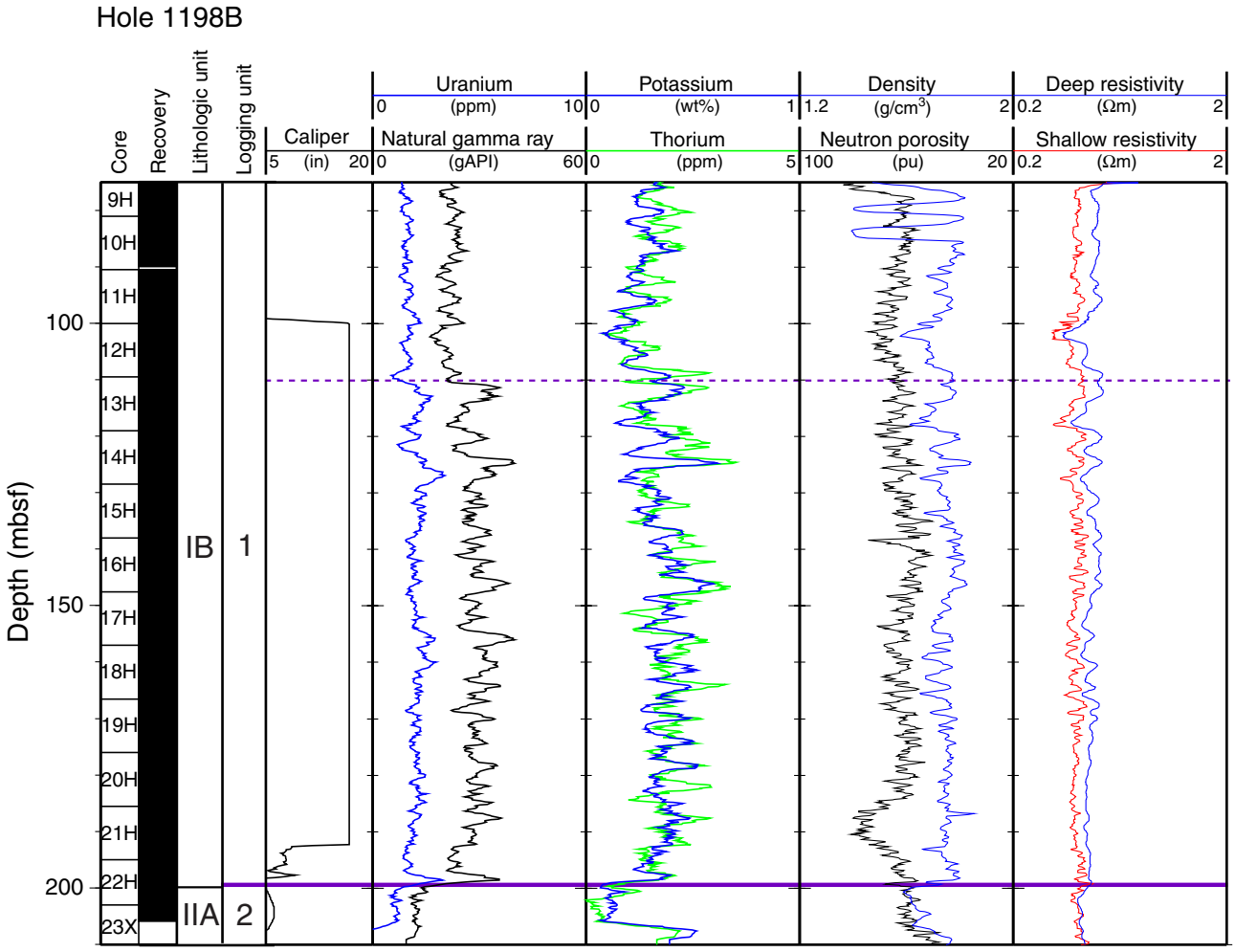

Figure F28. Comparison of corresponding downhole and core logging data. The multisensor track (MST) natural gamma ray data are smoothed over 10 data points (solid line) to reduce scattering. A good correlation can be seen for both the density and natural gamma ray data sets.

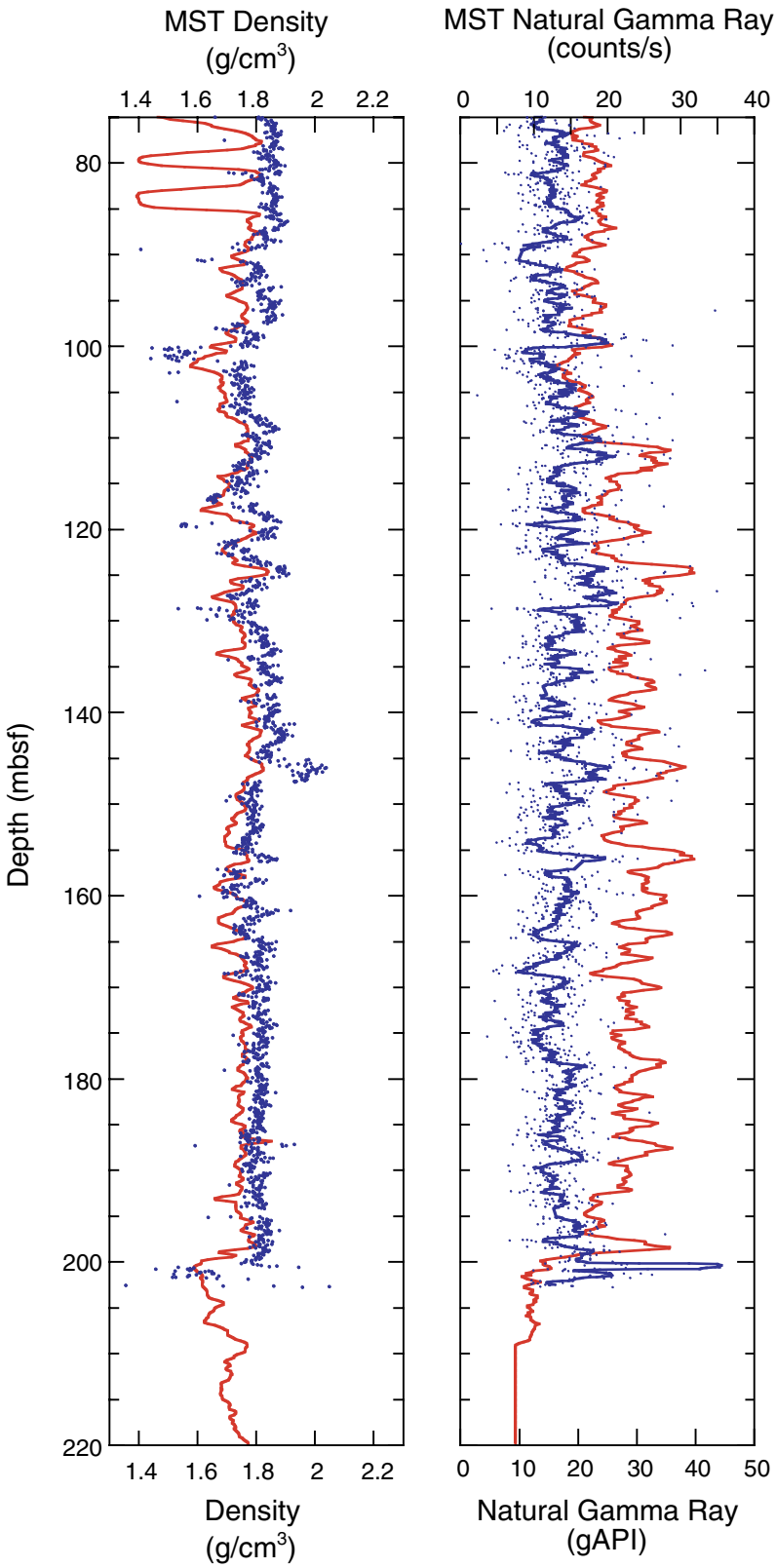

Figure F29. Multichannel seismic line MAR07 with location, penetration depth, and lithologic units at Site 1198 located at SP 2262. The seismic sequences and the basement are marked and traced along the section. MS = Megasequence.

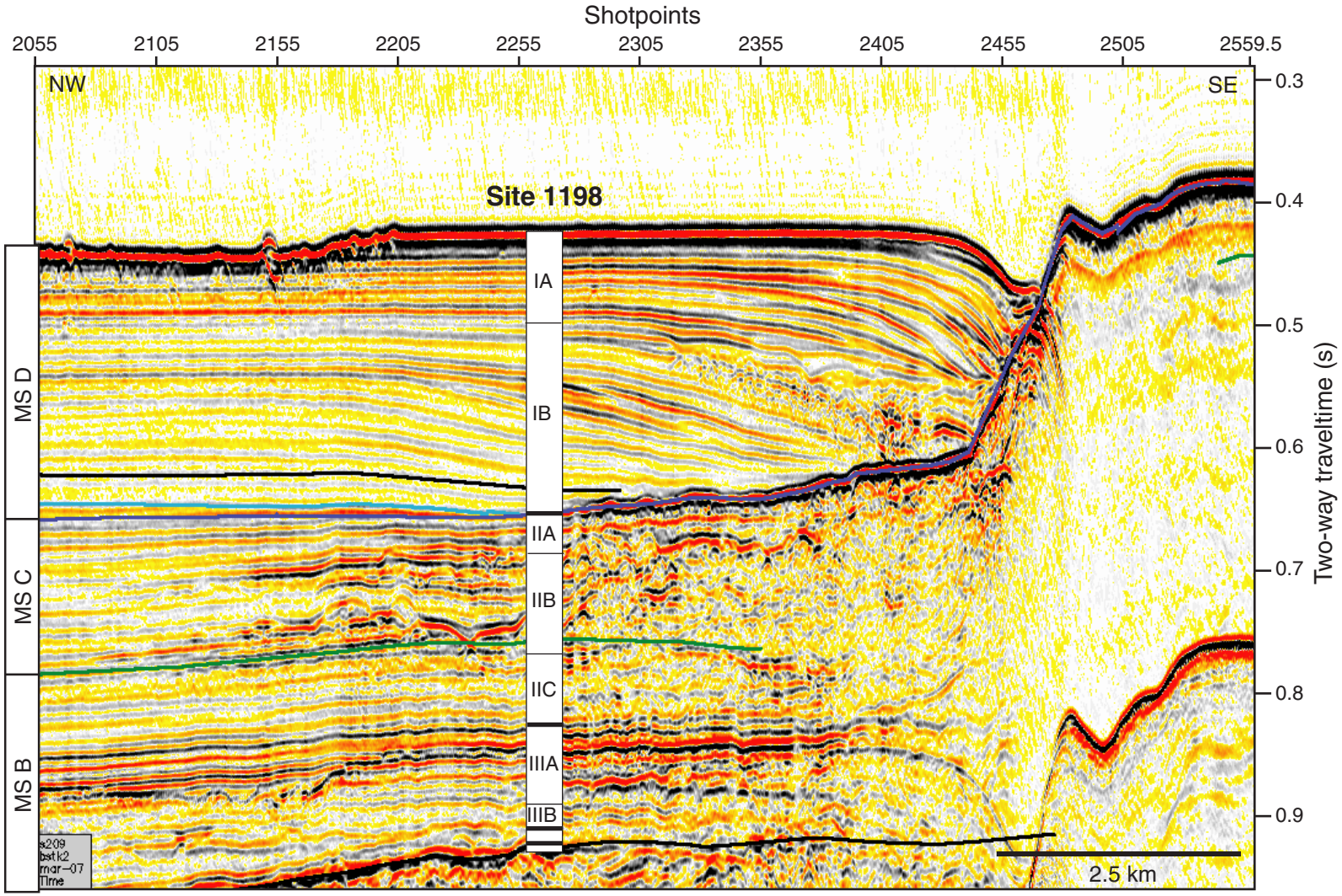

Table T1. Coring summary, Site 1198.

Core	Date (Feb 2001)	Time (local)	Depth (mbsf) Top	Depth (mbsf) Bottom	Length (m) Cored	Length (m) Recovered	Recovery (%)
194-1198A-							
1H	7	2040	0.0	5.0	5.0	5.00	100.0
2H	7	2145	5.0	14.5	9.5	9.57	100.7
3H	7	2210	14.5	24.0	9.5	9.33	98.2
4H	7	2310	24.0	33.5	9.5	9.92	104.4
5H	7	2340	33.5	43.0	9.5	9.93	104.5
6H	8	0015	43.0	52.5	9.5	9.29	97.8
7H	8	0120	52.5	62.0	9.5	9.92	104.4
8H	8	0150	62.0	71.5	9.5	9.39	98.8
9H	8	0220	71.5	81.0	9.5	10.04	105.7
10H	8	0305	81.0	90.5	9.5	8.91	93.8
11H	8	0335	90.5	100.0	9.5	9.81	103.3
12H	8	0405	100.0	109.5	9.5	9.82	103.4
13H	8	0455	109.5	119.0	9.5	9.87	103.9
14H	8	0525	119.0	128.5	9.5	9.83	103.5
15H	8	0610	128.5	138.0	9.5	9.53	100.3
16H	8	0700	138.0	147.5	9.5	10.07	106.0
17H	8	0725	147.5	157.0	9.5	9.77	102.8
18H	8	0755	157.0	166.5	9.5	9.94	104.6
19H	8	0840	166.5	176.0	9.5	9.90	104.2
20H	8	0910	176.0	185.5	9.5	10.01	105.4
21H	8	0940	185.5	195.0	9.5	9.55	100.5
22H	8	1020	195.0	203.0	8.0	8.01	100.1
23X	8	1120	203.0	212.7	9.7	2.84	29.3
24X	8	1145	212.7	222.4	9.7	0.00	0.0
25X	8	1240	222.4	232.1	9.7	0.00	0.0
26X	8	1325	232.1	241.8	9.7	0.00	0.0
27X	8	1420	241.8	251.5	9.7	0.00	0.0
				Cored total:	251.5	210.25	83.6
				Drilled total:	0.0		
				Total:	251.5		
194-1198B-							
10	9	0115	0.0	195.7	0.0	0.00	NA
1R	9	0150	195.7	205.2	9.5	3.75	39.5
2R	9	0230	205.2	214.8	9.6	0.35	3.6
3R	9	0315	214.8	224.4	9.6	0.05	0.5
4R	9	0400	224.4	234.0	9.6	0.41	4.3
5R	9	0445	234.0	243.6	9.6	0.23	2.4
6R	9	0730	243.6	253.3	9.7	0.10	1.0
7R	9	0900	253.3	262.9	9.6	0.51	5.3
8R	9	1000	262.9	272.5	9.6	0.16	1.7
9R	9	1050	272.5	282.2	9.7	0.00	0.0
10R	9	1130	282.2	291.8	9.6	0.80	8.3
11R	9	1230	291.8	301.4	9.6	0.60	6.3
12R	9	1320	301.4	311.0	9.6	0.78	8.1
13R	9	1420	311.0	320.6	9.6	0.02	0.2
14R	9	1505	320.6	330.3	9.7	0.05	0.5
15R	9	1550	330.3	339.9	9.6	0.20	2.1
16R	9	1630	339.9	349.5	9.6	0.26	2.7
17R	9	1710	349.5	359.1	9.6	1.71	17.8
18R	9	1815	359.1	368.7	9.6	4.49	46.8
19R	9	1905	368.7	378.3	9.6	1.56	16.3
20R	9	1950	378.3	388.0	9.7	3.62	37.3
21R	9	2050	388.0	397.6	9.6	3.46	36.0
22R	10	0115	397.6	407.2	9.6	9.90	103.1
23R	10	0215	407.2	416.8	9.6	8.66	90.2
24R	10	0310	416.8	426.4	9.6	9.11	94.9
25R	10	0410	426.4	436.0	9.6	9.90	103.1
26R	10	0515	436.0	445.7	9.7	6.71	69.2
27R	10	0615	445.7	455.3	9.6	9.50	99.0
28R	10	0720	455.3	464.9	9.6	8.49	88.4
29R	10	0830	464.9	474.6	9.7	1.19	12.3
30R	10	0945	474.6	484.2	9.6	9.90	103.1
31R	10	1055	484.2	493.8	9.6	5.71	59.5
32R	10	1215	493.8	503.4	9.6	7.48	77.9
33R	10	1340	503.4	513.0	9.6	2.59	27.0
34R	10	1555	513.0	522.6	9.6	4.39	45.7
				Cored total:	326.9	116.64	35.7
				Drilled total:	195.7		
				Total:	522.6		

Note: NA = not applicable.

Table T2. Expanded coring summary, Site 1198. (See table notes. Continued on next five pages.)

Core	Date (Feb 2001)	Time (local)	Core depth (mbsf) Top	Core depth (mbsf) Bottom	Length (m) Cored	Length (m) Recovered	Recovery (%)	Section	Length (m) Liner	Length (m) Curated	Section depth (mbsf) Top	Section depth (mbsf) Bottom	Catwalk samples	Comment
194-1198A-														
1H	7	2040	0.0	5.0	5.0	5.00	100.0							
								1	1.50	1.50	0.00	1.50		
								2	1.50	1.50	1.50	3.00	IW	
								3	1.50	1.50	3.00	4.50	HS	
								4	0.37	0.37	4.50	4.87		
								CC (w/4)	0.13	0.13	4.87	5.00	PAL	
								Totals:	5.00	5.00				
2H	7	2145	5.0	14.5	9.5	9.57	100.7							
								1	1.50	1.50	5.00	6.50		
								2	1.50	1.50	6.50	8.00		
								3	1.50	1.50	8.00	9.50		
								4	1.50	1.50	9.50	11.00	IW	
								5	1.50	1.50	11.00	12.50	HS	
								6	1.50	1.50	12.50	14.00		
								7	0.39	0.39	14.00	14.39		
								CC (w/7)	0.18	0.18	14.39	14.57	PAL	
								Totals:	9.57	9.57				
3H	7	2210	14.5	24.0	9.5	9.33	98.2							
								1	1.50	1.50	14.50	16.00		
								2	1.50	1.50	16.00	17.50		
								3	1.50	1.50	17.50	19.00		
								4	1.50	1.50	19.00	20.50	IW	
								5	1.50	1.50	20.50	22.00	HS	
								6	1.40	1.40	22.00	23.40		
								7	0.27	0.27	23.40	23.67		
								CC (w/7)	0.16	0.16	23.67	23.83	PAL	
								Totals:	9.33	9.33				
4H	7	2310	24.0	33.5	9.5	9.92	104.4							
								1	1.50	1.50	24.00	25.50		
								2	1.50	1.50	25.50	27.00		
								3	1.50	1.50	27.00	28.50		
								4	1.50	1.50	28.50	30.00	IW	
								5	1.50	1.50	30.00	31.50	HS	
								6	1.50	1.50	31.50	33.00		
								7	0.71	0.71	33.00	33.71		
								CC (w/7)	0.21	0.21	33.71	33.92	PAL	
								Totals:	9.92	9.92				
5H	7	2340	33.5	43.0	9.5	9.93	104.5							
								1	1.50	1.50	33.50	35.00		
								2	1.50	1.50	35.00	36.50		
								3	1.50	1.50	36.50	38.00		
								4	1.50	1.50	38.00	39.50	IW	
								5	1.50	1.50	39.50	41.00	HS	
								6	1.50	1.50	41.00	42.50		
								7	0.67	0.67	42.50	43.17		
								CC (w/7)	0.26	0.26	43.17	43.43	PAL	
								Totals:	9.93	9.93				
6H	8	0015	43.0	52.5	9.5	9.29	97.8							
								1	1.50	1.50	43.00	44.50		
								2	1.50	1.50	44.50	46.00		
								3	1.50	1.50	46.00	47.50		
								4	1.50	1.50	47.50	49.00	IW	
								5	1.50	1.50	49.00	50.50		
								6	1.01	1.01	50.50	51.51		
								7	0.58	0.58	51.51	52.09		
								CC (w/7)	0.20	0.20	52.09	52.29	PAL	
								Totals:	9.29	9.29				
7H	8	0120	52.5	62.0	9.5	9.92	104.4							
								1	1.50	1.50	52.50	54.00		
								2	1.50	1.50	54.00	55.50		
								3	1.50	1.50	55.50	57.00		
								4	1.50	1.50	57.00	58.50	HS, IW	
								5	1.50	1.50	58.50	60.00		
								6	1.50	1.50	60.00	61.50		
								7	0.75	0.75	61.50	62.25		
								CC (w/7)	0.17	0.17	62.25	62.42	PAL	
								Totals:	9.92	9.92				

Table T2 (continued).

Core	Date (Feb 2001)	Time (local)	Core depth (mbsf) Top	Core depth (mbsf) Bottom	Length (m) Cored	Length (m) Recovered	Recovery (%)	Section	Length (m) Liner	Length (m) Curated	Section depth (mbsf) Top	Section depth (mbsf) Bottom	Catwalk samples	Comment
8H	8	0150	62.0	71.5	9.5	9.39	98.8							
								1	1.50	1.50	62.00	63.50		
								2	1.50	1.50	63.50	65.00		
								3	1.50	1.50	65.00	66.50		
								4	1.50	1.50	66.50	68.00	IW	
								5	1.50	1.50	68.00	69.50	HS	
								6	1.40	1.40	69.50	70.90		
								7	0.21	0.21	70.90	71.11		
								CC (w/7)	0.28	0.28	71.11	71.39	PAL	
								Totals:	9.39	9.39				
9H	8	0220	71.5	81.0	9.5	10.04	105.7							
								1	1.50	1.50	71.50	73.00		
								2	1.50	1.50	73.00	74.50		
								3	1.50	1.50	74.50	76.00		
								4	1.50	1.50	76.00	77.50	IW	
								5	1.50	1.50	77.50	79.00	HS	
								6	1.50	1.50	79.00	80.50		
								7	0.76	0.76	80.50	81.26		
								CC (w/7)	0.28	0.28	81.26	81.54	PAL	
								Totals:	10.04	10.04				
10H	8	0305	81.0	90.5	9.5	8.91	93.8							
								1	1.50	1.50	81.00	82.50		
								2	1.50	1.50	82.50	84.00		
								3	1.50	1.50	84.00	85.50		
								4	1.50	1.50	85.50	87.00	IW	
								5	1.50	1.50	87.00	88.50	HS	
								6	1.19	1.19	88.50	89.69		
								CC (w/6)	0.22	0.22	89.69	89.91	PAL	
								Totals:	8.91	8.91				
11H	8	0335	90.5	100.0	9.5	9.81	103.3							
								1	1.50	1.50	90.50	92.00		
								2	1.50	1.50	92.00	93.50		
								3	1.50	1.50	93.50	95.00		
								4	1.50	1.50	95.00	96.50	IW	
								5	1.50	1.50	96.50	98.00	HS	
								6	1.50	1.50	98.00	99.50		
								7	0.71	0.71	99.50	100.21		
								CC (w/7)	0.10	0.10	100.21	100.31	PAL	
								Totals:	9.81	9.81				
12H	8	0405	100.0	109.5	9.5	9.82	103.4							
								1	1.50	1.50	100.00	101.50		
								2	1.50	1.50	101.50	103.00		
								3	1.50	1.50	103.00	104.50		
								4	1.50	1.50	104.50	106.00	IW	
								5	1.50	1.50	106.00	107.50	HS	
								6	1.50	1.50	107.50	109.00		
								7	0.56	0.56	109.00	109.56		
								CC (w/7)	0.26	0.26	109.56	109.82	PAL	
								Totals:	9.82	9.82				
13H	8	0455	109.5	119.0	9.5	9.87	103.9							
								1	1.50	1.50	109.50	111.00		
								2	1.50	1.50	111.00	112.50		
								3	1.50	1.50	112.50	114.00	DUGWR	
								4	1.50	1.50	114.00	115.50	IW	
								5	1.50	1.50	115.50	117.00	HS	
								6	1.50	1.50	117.00	118.50		
								7	0.64	0.64	118.50	119.14		
								CC (w/7)	0.23	0.23	119.14	119.37	PAL	
								Totals:	9.87	9.87				
14H	8	0525	119.0	128.5	9.5	9.83	103.5							
								1	1.50	1.50	119.00	120.50		
								2	1.50	1.50	120.50	122.00		
								3	1.50	1.50	122.00	123.50		
								4	1.50	1.50	123.50	125.00	IW	
								5	1.50	1.50	125.00	126.50	HS	
								6	1.50	1.50	126.50	128.00		
								7	0.67	0.67	128.00	128.67		
								CC (w/7)	0.16	0.16	128.67	128.83	PAL	
								Totals:	9.83	9.83				

Table T2 (continued).

Core	Date (Feb 2001)	Time (local)	Core depth (mbsf) Top	Core depth (mbsf) Bottom	Length (m) Cored	Length (m) Recovered	Recovery (%)	Section	Length (m) Liner	Length (m) Curated	Section depth (mbsf) Top	Section depth (mbsf) Bottom	Catwalk samples	Comment
15H	8	0610	128.5	138.0	9.5	9.53	100.3							
								1	1.50	1.50	128.50	130.00		
								2	1.50	1.50	130.00	131.50		
								3	1.50	1.50	131.50	133.00	DUGWR	
								4	1.50	1.50	133.00	134.50	IW	
								5	1.50	1.50	134.50	136.00	HS	
								6	1.20	1.20	136.00	137.20		
								7	0.42	0.42	137.20	137.62		
								CC (w/7)	0.41	0.41	137.62	138.03	PAL	
								Totals:	9.53	9.53				
16H	8	0700	138.0	147.5	9.5	10.07	106.0							
								1	1.50	1.50	138.00	139.50		
								2	1.50	1.50	139.50	141.00		
								3	1.50	1.50	141.00	142.50		
								4	1.50	1.50	142.50	144.00	IW	
								5	1.50	1.50	144.00	145.50	HS	
								6	1.50	1.50	145.50	147.00		
								7	0.69	0.69	147.00	147.69		
								CC (w/7)	0.38	0.38	147.69	148.07	PAL	
								Totals:	10.07	10.07				
17H	8	0725	147.5	157.0	9.5	9.77	102.8							
								1	1.50	1.50	147.50	149.00		
								2	1.50	1.50	149.00	150.50		
								3	1.50	1.50	150.50	152.00		
								4	1.50	1.50	152.00	153.50	IW	
								5	1.41	1.41	153.50	154.91	HS	
								6	1.50	1.50	154.91	156.41		
								7	0.62	0.62	156.41	157.03		
								CC (w/7)	0.24	0.24	157.03	157.27	PAL	
								Totals:	9.77	9.77				
18H	8	0755	157.0	166.5	9.5	9.94	104.6							
								1	1.50	1.50	157.00	158.50		
								2	1.50	1.50	158.50	160.00		
								3	1.50	1.50	160.00	161.50	DUGWR	
								4	1.50	1.50	161.50	163.00	IW	
								5	1.50	1.50	163.00	164.50	HS	
								6	1.50	1.50	164.50	166.00		
								7	0.75	0.75	166.00	166.75		
								CC (w/7)	0.19	0.19	166.75	166.94	PAL	
								Totals:	9.94	9.94				
19H	8	0840	166.5	176.0	9.5	9.90	104.2							
								1	1.50	1.50	166.50	168.00		
								2	1.50	1.50	168.00	169.50		
								3	1.50	1.50	169.50	171.00		
								4	1.50	1.50	171.00	172.50	IW	
								5	1.50	1.50	172.50	174.00	HS	
								6	1.50	1.50	174.00	175.50		
								7	0.69	0.69	175.50	176.19		
								CC (w/7)	0.21	0.21	176.19	176.40	PAL	
								Totals:	9.90	9.90				
20H	8	0910	176.0	185.5	9.5	10.01	105.4							
								1	1.50	1.50	176.00	177.50		
								2	1.50	1.50	177.50	179.00		
								3	1.50	1.50	179.00	180.50		
								4	1.50	1.50	180.50	182.00	IW	
								5	1.50	1.50	182.00	183.50	HS	
								6	1.50	1.50	183.50	185.00		
								7	0.78	0.78	185.00	185.78		
								CC (w/7)	0.23	0.23	185.78	186.01	PAL	
								Totals:	10.01	10.01				
21H	8	0940	185.5	195.0	9.5	9.55	100.5							
								1	1.50	1.50	185.50	187.00		
								2	1.50	1.50	187.00	188.50		
								3	1.50	1.50	188.50	190.00	DUGWR	
								4	1.50	1.50	190.00	191.50	IW	
								5	1.50	1.50	191.50	193.00	HS	
								6	1.20	1.20	193.00	194.20		
								7	0.51	0.51	194.20	194.71		

Table T2 (continued).

Core	Date (Feb 2001)	Time (local)	Core depth (mbsf) Top	Core depth (mbsf) Bottom	Length (m) Cored	Length (m) Recovered	Recovery (%)	Section	Length (m) Liner	Length (m) Curated	Section depth (mbsf) Top	Section depth (mbsf) Bottom	Catwalk samples	Comment
								CC (w/7)	0.34	0.34	194.71	195.05	PAL	
								Totals:	9.55	9.55				
22H	8	1020	195.0	203.0	8.0	8.01	100.1							
								1	1.50	1.50	195.00	196.50		
								2	1.50	1.50	196.50	198.00		
								3	1.50	1.50	198.00	199.50	IW	
								4	0.90	0.90	199.50	200.40	HS	
								5	1.50	1.50	200.40	201.90		
								6	0.91	0.91	201.90	202.81		
								CC (w/6)	0.20	0.20	202.81	203.01	PAL	
								Totals:	8.01	8.01				
23X	8	1120	203.0	212.7	9.7	2.84	29.3							
								1	1.50	1.50	203.00	204.50	IW	
								2	1.24	1.24	204.50	205.74		
								CC (w/CC)	0.10	0.10	205.74	205.84	PAL	
								Totals:	2.84	2.84				
24X	8	1145	212.7	222.4	9.7	0.00	0.0							
25X	8	1240	222.4	232.1	9.7	0.00	0.0							
26X	8	1325	232.1	241.8	9.7	0.00	0.0							
27X	8	1420	241.8	251.5	9.7	0.00	0.0							
				Totals:	251.5	210.25	83.6							
194-1198B-														
10	9	0115	0.0	195.7	0.0	0.00	NA							
1R	9	0150	195.7	205.2	9.5	3.75	39.5							
								1	1.44	1.44	195.70	197.14	HS, IW	
								2	1.09	1.09	197.14	198.23		
								3	1.07	1.07	198.23	199.30		
								CC (w/3)	0.15	0.15	199.30	199.45	PAL	
								Totals:	3.75	3.75				
2R	9	0230	205.2	214.8	9.6	0.35	3.6							
								1	0.35	0.42	205.20	205.62	PAL	
								Totals:	0.35	0.42				
3R	9	0315	214.8	224.4	9.6	0.05	0.5							
								1	0.05	0.05	214.80	214.85	PAL	
								Totals:	0.05	0.05				
4R	9	0400	224.4	234.0	9.6	0.41	4.3							
								1	0.41	0.55	224.40	224.95	PAL	
								Totals:	0.41	0.55				
5R	9	0445	234.0	243.6	9.6	0.23	2.4							
								1	0.23	0.32	234.00	234.32	PAL	
								Totals:	0.23	0.32				
6R	9	0730	243.6	253.3	9.7	0.10	1.0							
								1	0.10	0.12	243.60	243.72	PAL	
								Totals:	0.10	0.12				
7R	9	0900	253.3	262.9	9.6	0.51	5.3							
								1	0.51	0.71	253.30	254.01	PAL	
								Totals:	0.51	0.71				
8R	9	1000	262.9	272.5	9.6	0.16	1.7							
								1	0.16	0.21	262.90	263.11	PAL	
								Totals:	0.16	0.21				
9R	9	1050	272.5	282.2	9.7	0.00	0.0							
10R	9	1130	282.2	291.8	9.6	0.80	8.3							
								1	0.80	1.00	282.20	283.20	PAL	
								Totals:	0.80	1.00				
11R	9	1230	291.8	301.4	9.6	0.60	6.3							
								1	0.60	0.95	291.80	292.75	HS, PAL	
								Totals:	0.60	0.95				
12R	9	1320	301.4	311.0	9.6	0.78	8.1							
								1	0.78	0.98	301.40	302.38	PAL	
								Totals:	0.78	0.98				
13R	9	1420	311.0	320.6	9.6	0.02	0.2							
								1	0.02	0.02	311.00	311.02	PAL	All to PAL
								Totals:	0.02	0.02				
14R	9	1505	320.6	330.3	9.7	0.05	0.5							
								1	0.05	0.05	320.60	320.65	PAL	All to PAL
								Totals:	0.05	0.05				

Table T2 (continued).

Core	Date (Feb 2001)	Time (local)	Core depth (mbsf) Top	Core depth (mbsf) Bottom	Length (m) Cored	Length (m) Recovered	Recovery (%)	Section	Length (m) Liner	Length (m) Curated	Section depth (mbsf) Top	Section depth (mbsf) Bottom	Catwalk samples	Comment
15R	9	1550	330.3	339.9	9.6	0.20	2.1							
								1	0.20	0.26	330.30	330.56	PAL	
								Totals:	0.20	0.26				
16R	9	1630	339.9	349.5	9.6	0.26	2.7							
								1	0.26	0.46	339.90	340.36	PAL	
								Totals:	0.26	0.46				
17R	9	1710	349.5	359.1	9.6	1.71	17.8							
								1	0.74	0.74	349.50	350.24	IW	
								2	0.97	0.97	350.24	351.21	PAL, HS	
								Totals:	1.71	1.71				
18R	9	1815	359.1	368.7	9.6	4.49	46.8							
								1	1.38	1.38	359.10	360.48		
								2	1.44	1.44	360.48	361.92	IW	
								3	1.50	1.50	361.92	363.42	HS	
								CC (w/CC)	0.17	0.17	363.42	363.59	PAL	
								Totals:	4.49	4.49				
19R	9	1905	368.7	378.3	9.6	1.56	16.3							
								1	0.93	0.93	368.70	369.63	IW	
								2	0.63	0.63	369.63	370.26	HS, PAL	
								Totals:	1.56	1.56				
20R	9	1950	378.3	388.0	9.7	3.62	37.3							
								1	1.37	1.37	378.30	379.67	IW	
								2	1.50	1.50	379.67	381.17	HS	
								3	0.52	0.52	381.17	381.69		
								CC (w/3)	0.23	0.23	381.69	381.92	PAL	
								Totals:	3.62	3.62				
21R	9	2050	388.0	397.6	9.6	3.46	36.0							
								1	1.48	1.48	388.00	389.48		
								2	1.10	1.10	389.48	390.58	IW	
								3	0.88	0.88	390.58	391.46	HS, PAL	
								Totals:	3.46	3.46				
22R	10	0115	397.6	407.2	9.6	9.90	103.1							
								1	1.50	1.50	397.60	399.10		
								2	1.50	1.50	399.10	400.60		
								3	1.50	1.50	400.60	402.10		
								4	1.50	1.50	402.10	403.60	IW	
								5	1.50	1.50	403.60	405.10	HS	
								6	1.40	1.40	405.10	406.50		
								7	0.81	0.81	406.50	407.31		
								CC (w/7)	0.19	0.19	407.31	407.50	PAL	
								Totals:	9.90	9.90				
23R	10	0215	407.2	416.8	9.6	8.66	90.2							
								1	1.35	1.35	407.20	408.55		
								2	1.50	1.50	408.55	410.05		
								3	1.52	1.52	410.05	411.57		
								4	1.16	1.16	411.57	412.73	IW	
								5	1.50	1.50	412.73	414.23	HS	
								6	1.45	1.45	414.23	415.68		
								CC (w/CC)	0.18	0.18	415.68	415.86	PAL	
								Totals:	8.66	8.66				
24R	10	0310	416.8	426.4	9.6	9.11	94.9							
								1	1.45	1.45	416.80	418.25		
								2	1.50	1.50	418.25	419.75		
								3	1.50	1.50	419.75	421.25		
								4	1.50	1.50	421.25	422.75	IW	
								5	1.50	1.50	422.75	424.25	HS	
								6	1.00	1.00	424.25	425.25		
								7	0.66	0.66	425.25	425.91	PAL	
								Totals:	9.11	9.11				
25R	10	0410	426.4	436.0	9.6	9.90	103.1							
								1	1.50	1.50	426.40	427.90		
								2	1.50	1.50	427.90	429.40		
								3	1.50	1.50	429.40	430.90		
								4	1.50	1.50	430.90	432.40	IW	
								5	1.50	1.50	432.40	433.90	HS	
								6	1.50	1.50	433.90	435.40		
								7	0.68	0.68	435.40	436.08		
								CC (w/7)	0.22	0.22	436.08	436.30	PAL	
								Totals:	9.90	9.90				

Table T2 (continued).

Core	Date (Feb 2001)	Time (local)	Core depth (mbsf) Top	Core depth (mbsf) Bottom	Length (m) Cored	Length (m) Recovered	Recovery (%)	Section	Length (m) Liner	Length (m) Curated	Section depth (mbsf) Top	Section depth (mbsf) Bottom	Catwalk samples	Comment
26R	10	0515	436.0	445.7	9.7	6.71	69.2							
								1	1.50	1.50	436.00	437.50		
								2	1.50	1.50	437.50	439.00		
								3	1.50	1.50	439.00	440.50		
								4	1.50	1.50	440.50	442.00	IW	
								5	0.71	0.71	442.00	442.71	PAL, HS	
								Totals:	6.71	6.71				
27R	10	0615	445.7	455.3	9.6	9.50	99.0							
								1	1.46	1.46	445.70	447.16		
								2	1.11	1.11	447.16	448.27		
								3	1.47	1.47	448.27	449.74		
								4	1.22	1.22	449.74	450.96	IW	
								5	1.50	1.50	450.96	452.46		
								6	1.30	1.30	452.46	453.76		
								7	1.44	1.44	453.76	455.20	PAL	
								Totals:	9.50	9.50				
28R	10	0720	455.3	464.9	9.6	8.49	88.4							
								1	1.35	1.35	455.30	456.65		
								2	1.50	1.50	456.65	458.15		
								3	1.50	1.50	458.15	459.65		
								4	1.50	1.50	459.65	461.15	IW	
								5	1.29	1.29	461.15	462.44	HS	
								6	1.12	1.12	462.44	463.56		
								CC (w/6)	0.23	0.23	463.56	463.79	PAL	
								Totals:	8.49	8.49				
29R	10	0830	464.9	474.6	9.7	1.19	12.3							
								1	1.19	1.19	464.90	466.09	PAL	
								Totals:	1.19	1.19				
30R	10	0945	474.6	484.2	9.6	9.90	103.1							
								1	1.26	1.26	474.60	475.86		
								2	1.25	1.25	475.86	477.11		
								3	1.50	1.50	477.11	478.61		
								4	1.50	1.50	478.61	480.11	IW	
								5	1.50	1.50	480.11	481.61		
								6	1.50	1.50	481.61	483.11		
								7	1.19	1.19	483.11	484.30		
								CC (w/7)	0.20	0.20	484.30	484.50	PAL	
								Totals:	9.90	9.90				
31R	10	1055	484.2	493.8	9.6	5.71	59.5							
								1	0.90	0.90	484.20	485.10		
								2	1.50	1.50	485.10	486.60		
								3	1.50	1.50	486.60	488.10	IW, IW	
								4	1.52	1.52	488.10	489.62	HS	
								5	0.29	0.29	489.62	489.91		
								Totals:	5.71	5.71				
32R	10	1215	493.8	503.4	9.6	7.48	77.9							
								1	1.50	1.50	493.80	495.30		
								2	1.14	1.14	495.30	496.44		
								3	1.50	1.50	496.44	497.94		
								4	1.31	1.31	497.94	499.25	IW	
								5	1.29	1.29	499.25	500.54	HS	
								6	0.45	0.45	500.54	500.99		
								CC (w/6)	0.29	0.29	500.99	501.28	PAL	
								Totals:	7.48	7.48				
33R	10	1340	503.4	513.0	9.6	2.59	27.0							
								1	1.43	1.42	503.40	504.82		
								2	1.16	1.49	504.82	506.31	HS, PAL, IW	
								Totals:	2.59	2.91				
34R	10	1555	513.0	522.6	9.6	4.39	45.7							
								1	0.00	1.44	513.00	514.44		
								2	1.43	1.28	514.44	515.72		
								3	1.50	1.50	515.72	517.22		
								4	1.46	0.89	517.22	518.11	PAL	
								Totals:	4.39	5.11				
				Totals:	326.9	116.64	35.7							

Notes: CC = core catcher (number in parentheses indicates which section the core catcher is stored with). Catwalk samples: IW = interstitial water, HS = headspace, PAL = paleontology sample, DUGWR = sample request code.

Table T3. Lithologic units and subunits, Site 1198.

Unit	Subunit	Hole 1198A Core, section, interval (cm) Top	Hole 1198A Core, section, interval (cm) Base	Hole 1198A Depth (mbsf) Top	Hole 1198A Depth (mbsf) Base	Hole 1198B Core, section, interval (cm) Top	Hole 1198B Core, section, interval (cm) Base	Hole 1198B Depth (mbsf) Top	Hole 1198B Depth (mbsf) Base	Description	Interpretation
I	IA	1H-1, 0	7H-CC, 17	0.0	62.0					Skeletal wackestone to grainstone with planktonic foraminifers, pteropods, and variety of microfossils. Light gray to greenish gray.	Hemipelagic setting (drift deposits)
	IB	7H-CC, 17	22H-5, 18	62.0	200.6					Mudstone to skeletal packstone with predominantly planktonic foraminifers. Light greenish gray to olive-gray.	Hemipelagic setting (drift deposits)
II	IIA	22H-5, 18	?	200.6	224.8	?	4R-1, 55	?	225.0	Skeletal packstone to grainstone, predominantly fine grained with planktonic foraminifers, abundant larger benthic foraminifers, and neritic material. White to pale brownish white and slightly dolomitized.	Periplatform setting
	IIB					4R-1, 55	15R-1, 0	225.0	330.3	Skeletal packstone to grainstone and skeletal grainstone/floatstone to rudstone, coarse grained, with lepidocyclinids, rhodoliths, and corals. White to pale yellow and slightly dolomitized.	Proximal slope, periplatform setting
	IIC					15R-1, 0	22R-1, 0	330.3	397.6	Skeletal grainstone to packstone (brownish white), fine grained, and silt-sized packstone to grainstone with clay. Light gray to light olive-gray and slightly dolomitized between 330 and 360 mbsf.	Periplatform setting
III	IIIA					22R-1, 0	27R-1, 144	397.6	447.1	Mudstone to silt-sized packstone with clay, cyclic alternation of lithologies. Light to dark greenish gray and slightly dolomitized. Occurrence of small fining-upward sequences.	Hemipelagic (deepening upward?); cyclic sedimentation
	IIIB					27R-1, 144	33R-1, 23	447.1	503.6	Silt-sized packstone to grainstone with more abundant glauconite (at base of subunit) and less clay than Subunit IIIA. Light greenish gray to light olive-gray and slightly dolomitized.	Hemipelagic (deepening upward?); cyclic sedimentation, some influence of distal periplatform shedding?
IV						33R-1, 23	34R-1, 23	503.6	513.2	Skeletal floatstone/rudstone with larger benthic foraminifers (*Cycloclypeus* sp.) and rhodoliths. White to light greenish gray.	Deep shelf facies
V						34R-1, 23		513.2		Olivine basalt with smectite-, hematite-, feldspar- and opal-(?) filled veins. Dark gray.	Basement

Note: Depth: ? = not defined.

Table T4. Biostratigraphic datums, Site 1198.

Datum	Core, section, interval (cm)	Depth (mbsf)		Mean depth (mbsf)	Age (Ma)
		First absence or presence	Last presence or absence		
	194-1198A-				
Acme *Emiliania huxleyi*	1H-1, 0 to 1H-2, 80	0.00	2.30	1.15	0.08
LO *Globigerinoides ruber* (pink)	1H-4, 20–22 to 1H-CC	4.70	4.95	4.83	0.12
FO *Emiliania huxleyi*	1H-CC to 2H-2, 80	4.87	7.30	6.09	0.26
LO *Pseudoemiliania lacunosa*	2H-CC to 3H-CC	14.52	23.78	19.15	0.46
LO *Globorotalia tosaensis*	5H-CC to 6H-CC	43.38	52.24	47.81	0.65
LO *Calcidiscus macintyrei*	10H-CC to 11H-CC	89.86	100.26	95.06	1.70
LO *Globigerinoides fistulosus*	11H-CC to 12H-CC	100.26	109.56	104.91	1.77
LO *Discoaster brouweri*	13H-CC to 14H-CC	119.32	128.78	124.05	2.00
FO *Globorotalia truncatulinoides*	15H-3, 85–87 to 15H-CC	132.35	137.98	135.17	2.00
LO *Discoaster pentaradiatus*	17H-CC to 18H-CC	157.24	166.89	162.07	2.50
LO *Discoaster surculus*	17H-CC to 18H-CC	157.24	166.89	162.07	2.60
LO *Dentoglobigerina altispira*	19H-CC to 20H-CC	176.38	185.96	181.17	3.09
LO *Sphaeroidinellopsis seminulina*	21H-CC to 22H-3, 85–87	195.02	198.85	196.94	3.12
LO *Reticulofenestra pseudoumbilica*	21H-CC to 22H-3, 85–87	195.02	198.85	196.94	3.70
	194-1198B-				
FO *Globigerinoides extremus*	3R-CC to 6R-CC	214.80	243.70	229.25	8.30
LO *Reticulofenestra pseudoumbilicus* (>7 µm)	8R-CC to 10R-CC	263.09	283.18	273.14	9.00
FO *Globorotalia plesiotumida*	11R-CC to 13R-CC	292.73	311.00	301.87	10.90
LO *Cyclicargolithus floridanus*	13R-CC to 16R-CC	311.00	340.31	325.66	11.90
LO *Sphenolithus heteromorphus*	18R-CC to 19R-CC	363.57	370.24	366.91	13.60
FO *Orbulina* spp.	19R-CC to 20R-CC	370.24	381.88	376.06	15.10

Note: LO = last occurrence, FO = first occurrence.

Table T5. Summary of biostratigraphic and paleoenvironmental interpretations, Site 1198. (See table notes. Continued on next page.)

Hole, core, section (cm)	Depth (mbsf)	Zone	Age (Ma)	Foraminiferal assemblages				Comments on core catcher samples, >63 µm-fraction	Paleowater depth (m)	Depositional setting	Lithologic unit
				PF	ONBF	LBF	Pres				
194-											
1198A-1H-CC, 8–13	4.95	N23	0.08–0.26	A	A, Div	T	G	Coarse: DHM and pteropods; fines mostly debris	>200	Hemipelagic	IA
1198A-2H-CC, 13–18	14.52	N23	0.26–0.45	Dom	C, Div		G	Coarse: DPM and pteropods; fines mostly PF	>200	Hemipelagic	
1198A-3H-CC, 11–16	23.78	N22?	0.46–1.7	A	A, Div	T	G	Fines dominate; PF, pteropods, DHM, reworked fragments common	>200	Hemipelagic	
1198A-4H-CC, 16–21	33.87	N22	0.46–1.7	Dom	C, Div		G	Fines dominate; PF, pteropods, DHM, reworked fragments common	>200	Hemipelagic	
1198A-5H-CC, 21–26	43.38	N22	0.46–1.7	A	A, Div		G	Fines dominate; PF, pteropods, DHM, reworked fragments common	>200	Hemipelagic	
1198A-6H-CC, 15–20	52.24	N22	0.46–1.7	Dom	C, Div		G	Fines dominate; PF, pteropods, DHM, reworked fragments common	>200	Hemipelagic	
1198A-7H-CC, 12–17	62.37	N22	0.46–1.7	Dom	C, Div		M	PF dominate; minor neritics in fines	>200	Hemipelagic	IB
1198A-8H-CC, 23–28	71.34	N22	0.46–1.7	Dom	C		G	PF dominate; minor neritics in fines	>200	Hemipelagic	
1198A-9H-CC, 23–28	81.49	N22	0.46–1.7	Dom	C, Div		G	PF dominate; minor neritics in fines	>200	Hemipelagic	
1198A-10H-CC, 17–22	89.86	N22	0.46–1.7	Dom	C, Div		G	PF dominate; minor neritics in fines; minor reworked glauconite/pyrite	>200	Hemipelagic	
1198A-11H-CC, 5–10	100.26	N21–N22	1.7–2	Dom	R		G	Very small PF dominate; echinoid material common	>200	Hemipelagic	
1198A-12H-CC, 21–26	109.77	N21–N22	1.7–2	Dom	C, Div		G	Very small PF dominate medium and fine fractions; minor reworked PF and ONBF	>200	Hemipelagic	
1198A-13H-CC, 18–23	119.32	N21–N22	1.7–2	Dom	C, Div		M	Very small PF dominate; minor reworked PF and ONBF	>200	Hemipelagic	
1198A-14H-CC, 11–16	128.78	N21–N22	2–2.5	Dom	C, Div			Very small PF dominate; minor reworked PF and ONBF	>200	Hemipelagic	
1198A-15H-CC, 36–41	137.98	N21	2–2.5	Dom	R		G	Very small PF dominate; abundant infilled grains	>200	Hemipelagic	
1198A-16H-CC, 33–38	148.02	N21	2–2.5	Dom	R		G	Very small PF dominate; some infilled grains and pieces of pyrite	>200	Hemipelagic	
1198A-17H-CC, 21–24	157.24	N21	2–2.5	Dom	R		G	Very small PF dominate; some infilled grains and pieces of pyrite	>200	Hemipelagic	
1198A-18H-CC, 14–19	166.89	N21	2.6–3.7	Dom	R		G	Very small PF dominate; some infilled grains and pieces of pyrite	>200	Hemipelagic	
1198A-19H-CC, 19–21	176.38	N21	2.8–3.7	Dom	A		G	PF overwhelmingly dominate, minor other debris	>200	Hemipelagic	
1198A-20H-CC, 18–23	185.96	N20–N21	2.8–3.7	Dom	A		G	PF overwhelmingly dominate, minor other debris	>200	Hemipelagic	
1198A-21H-CC, 31–34	195.02	N20	2.8–3.7	Dom	R		G	PF overwhelmingly dominate, commonly pyrite or phosphate filled	>200	Hemipelagic	
1198B-1R-CC, 13–15	199.43	N18–N19	3.8–5.6	A	C	A	G	PF dominate, neritic material common, abundant LBF	>200	Proximal periplatform	IIA
1198A-22H-CC, 15–20	202.96	N19?	5.6–7.5	Dom	R	A	G	PF dominate, neritic material common, abundant LBF	>200	Proximal periplatform	
1198B-2R-1, 40–42	205.60	N18–N19		A	R	C	G	PF about equal to neritic debris	>200	Proximal periplatform	
1198A-23X-CC, 5–10	205.79	N19?		Dom	R	A	G	PF dominate, neritic material common, abundant LBF	>200	Proximal periplatform	
1198B-3R-1, 0–5	214.80	N17–N20		A		A	P–M	Bimodal: diverse LBF in neritic silt/fine sand	>200	Proximal periplatform	
1198B-4R-1, 53–55	224.93					A	P	Lithified: LBF in neritic silt/fine sand	>200	Proximal periplatform	
1198B-5R-1, 27–32	234.27					A	P	*Lepidocyclina* grainstone/packstone	>200	Proximal periplatform	IIB
1198B-6R-1, 10–12	243.70	N17?	5.6–11.9	A	R	A	P–M	*Lepidocyclina*/PF grainstone/packstone	>200	Proximal periplatform	
1198B-7R-1, 69–71	253.99					A	P	Lithified: *Lepidocyclina* rudstone/grainstone	>200	Proximal periplatform	
1198B-8R-1, 19–21	263.09					A	P	Lithified: rhodoliths, RA fragments, coral, and robust LBF	>200	Proximal periplatform	
1198B-10R-1, 98–100	283.18	N16–N17?	9–11.9	A	R	A	P–M	Lithified: *Lepidocyclina* rudstone/grainstone	>200	Proximal periplatform	
1198B-11R-1, 93–95	292.73	N16?	9–11.9	A		A	P	Lithified: *Lepidocyclina* rudstone/grainstone	>200	Proximal periplatform	
1198B-12R-1, 96–98	302.36					A	P	Lithified: rhodoliths, RA fragments, coral, robust LBF, some black/green clasts	>200	Proximal periplatform	
1198B-13R-1, 0–2	311.00	N16	9–11.9	A	R	A	P–M	Medium sands, include PF, diverse LBF, and bryozoan debris	>200	Proximal periplatform	
1198B-14R-1, 0–5	320.60					A	P–M	Lithified: rhodoliths, RA fragments, coral, robust LBF, some black/green clasts	>200	Proximal periplatform	
1198B-15R-1, 24–26	330.54					A	P–M	Lithified medium grainstone, includes PF, diverse LBF and bryozoan debris	>200	Proximal periplatform	
1198B-16R-1, 41–46	340.31	N12–N15	11.9–13.6			A	P–M	Partly lithified, PF and neritic debris (bryozoans and LBF)	>200	Proximal periplatform	IIC
1198B-17R-2, 95–97	351.19		11.9–13.6	A	C		VP	Partly lithified, PF and neritic debris	>200	Distal periplatform	
1198B-18R-CC, 15–17	363.57	N13	11.9–13.6	A	A	A	VP	Glauconitized neritic debris with common planktonics and ONBF	>200	Distal periplatform	
1198B-19R-2, 61–63	370.24	N10–N12	13.6–18.2	A	C	A	VP	PF and neritic debris, poorly preserved, also partly lithified into larger clasts	>200	Distal periplatform	
1198B-20R-CC, 19–23	381.88	N10–N12?	13.6–18.2	A			VP	Partly lithified PF and neritic debris	>200	Distal periplatform	
1198B-21R-3, 86–88	391.44	N9?	13.6–18.2	Dom	R	R	VP	PF dominate, neritic debris secondary; mostly medium sands	>200	Distal periplatform	
1198B-22R-CC, 17–19	407.48		13.6–18.2	C			P	Very fine neritic debris, minor identifiable components include PF	>200	Distal periplatform	IIIA

Table T5 (continued).

Hole, core, section (cm)	Depth (mbsf)	Zone	Age (Ma)	Foraminiferal assemblages				Comments on core catcher samples, >63 µm-fraction	Paleowater depth (m)	Depositional setting	Lithologic unit
				PF	ONBF	LBF	Pres				
1198B-23R-CC, 16–18	415.84	N8–N9	13.6–18.2	A	C		P	PF, ONBF, sponge spicules, and very fine neritic debris	>200	Distal periplatform	
1198B-24R-7, 64–66	425.89	N8–N9	13.6–18.2	A		R	P	PF dominate; abundant reworked clasts, LBF, PF, ONBF, pyrite	>200	Distal periplatform	
1198B-25R-CC, 20–22	436.28		13.6–18.2	C		R	P	Fine debris: planktonic, neritic, glauconite	>200	distal periplatform	
1198B-26R-5, 70—71	442.70		13.6–18.2	C	R	R	P	Fine debris: planktonic, neritic, sponge spicules common	>200	Distal periplatform	
1198B-27R-7, 142–144	455.18		13.6–18.2	R	R	Rjuv	P	Fine debris: planktonic and neritic, minor coarser component, dispersed fine pyrite	>200	Distal periplatform	
1198B-28R-CC, 21–23	463.77		13.6–18.2					Fine debris: nothing recognizable	>200	Distal periplatform	IIIB
1198B-29R-1, 117–119	466.07		13.6–18.2	R				Fine debris: planktonic and neritic, minor coarser component, dispersed fine pyrite	>200	Distal periplatform	
1198B-30R-CC, 18–20	484.48		13.6–18.2	R	R	R	P	Fine debris: planktonic and neritic, minor coarser component	>200	Distal periplatform	
1198B-31R-5, 27–29	489.89		18.2–18.5	R				Fine debris: planktonic and neritic, minor coarser component, abundant black grains	>200	Distal periplatform	
1198B-32R-CC, 24–29	501.23			R				Fine debris: planktonic and neritic, minor coarser component	>200	Distal periplatform	
1198B-33R-2, 114–116	505.97					A		Red algal crusts and large, very flat *Lepidocyclina* (*Eulepidina*) sp.	<150	Deep shelf	IV
1198B-34R-4, 78–80	518.00							Volcanic basement	?		V

Notes: Based on microscopic analysis of biogenic sediment constituents >63 µm, particularly benthic foraminifers, from core catcher samples. Foraminiferal assemblages: PF = planktonic foraminifers, ONBF = outer neritic to upper bathyal benthic foraminifers, LBF = larger benthic foraminifers, Pres = preservation; A = abundant, Div = diverse, T = trace, G = good, Dom = dominant, C = common, M = moderate, R = rare, P = poor, juv = juvenile. Comments: DHM = deep hardbottom macrofauna, RA = red alga, fines = silt to fine sand. Paleowater depth: ? = uncertain.

Table T6. Age-depth control points, Site 1198.

Source	Datum	Age (Ma)	Top: FO presence or LO absence		Bottom: LO presence or FO absence		Average depth (mbsf)	Uncertainty (m)	
			Core, section, interval (cm)	Depth (mbsf)	Core, section, interval (cm)	Depth (mbsf)		Up-section	Down-section
			194-1198A-		194-1198A-				
CN	Acme *Emiliania huxleyi*	0.08	1H-1, 0	0.00	1H-2, 80	2.30	1.15	1.15	1.15
PF	LO *Globigerinoides ruber* (pink)	0.120	1H-4, 21	4.71	1H-CC	4.95	4.83	0.13	0.13
CN	FO *Emiliania huxleyi*	0.26	1H-CC	4.87	2H-2, 80	7.30	6.09	1.22	1.22
CN	LO *Pseudoemiliania lacunosa*	0.46	2H-CC	14.52	3H-BCI	24.00	19.26	4.74	4.74
PF	LO *Globorotalia tosaensis*	0.65	5H-CC	43.38	6H-BCI	52.50	47.94	4.56	4.56
CN	LO *Calcidiscus macintyrei*	1.70	10H-CC	89.86	11H-CC	100.26	95.06	5.20	5.20
PF	LO *Globigerinoides fistulosus*	1.77	11H-CC	100.26	12H-CC	109.56	104.91	4.65	4.65
CN	LO *Discoaster brouweri*	2.00	13H-CC	119.32	14H-CC	128.78	124.05	4.73	4.73
PF	FO *Globorotalia truncatulinoides*	2.00	15H-3, 86	132.36	15H-CC	137.98	135.17	2.82	2.82
CN	LO *Discoaster pentaradiatus*	2.50	17H-CC	157.24	18H-CC	166.89	162.07	4.82	4.82
CN	LO *Discoaster surculus*	2.60	17H-CC	157.24	18H-CC	166.89	162.07	4.82	4.82
PF	LO *Dentoglobigerina altispira*	3.09	19H-CC	176.38	20H-CC	185.96	181.17	4.79	4.79
CN	LO *Sphaeroidinellopsis seminulina*	3.12	21H-CC	195.02	22H-3, 86	198.86	196.94	1.91	1.91
CN	LO *Reticulofenestra pseudoumbilicus*	3.70	21H-CC	195.02	22H-3, 86	198.86	196.94	1.91	1.91
			194-1198B-		194-1198B-				
PF	FO *Globigerinoides extremus*	8.3	3R-CC	214.80	6R-BCI	253.30	234.05	19.25	19.25
CN	LO *Reticulofenestra pseudoumbilicus* (>7 µm)	9.0	8R-CC	263.09	10R-BCI	291.80	277.45	14.36	14.36
PF	FO *Globorotalia plesiotumida*	10.9	11R-CC	292.73	13R-BCI	320.60	306.67	13.94	13.94
CN	LO *Cyclicargolithus floridanus*	11.9	13R-CC	311.00	16R-BCI	349.50	330.25	19.25	19.25
CN	LO *Sphenolithus heteromorphus*	13.6	18R-CC	363.57	19R-BCI	378.30	370.94	7.37	7.37
PF	FO *Orbulina* spp.	15.1	19R-CC	370.24	20R-BCI	388.00	379.12	8.88	8.88
CN	FO *Sphenolithus heteromorphus*	18.2	31R-CC	489.90	33R-BCI	513.00	501.45	11.55	11.55

Notes: Source: CN = calcareous nannoplankton, PF = planktonic foraminifers. Datum: LO = last occurrence, FO = first occurrence. Core, section, interval: BCI = bottom of cored interval.

Table T7. Interpolated ages of lithologic unit boundaries and seismic reflectors, Site 1198.

	Top of unit		
	Depth (mbsf)	Age (Ma)	Comments
Lithologic unit:			
IA	0.0	(0.06?)	Extrapolated
IB	62.0	1.0	
IIA	200.6	3.8 to 7.6	Hiatus
IIB	234.0	8.3	
IIC	330.3	12.0	
IIIA	397.6	15.5	
IIIB	455.2	17.1	
IV	503.6	18.5	
V	513.2	18.8	Extrapolated
Seismic sequences and reflectors:			
Megasequence D	0	(0.06?)	Extrapolated
D-black	Not present		
D-turquoise	175	2.9	
Megasequence C	203	3.8 to 7.7	Hiatus
Megasequence B	320	11.5	
Megasequence A	Not present		
Basement	514	18.8	Extrapolated

Table T8. Headspace gas composition, Site 1198.

Core, section	Depth (mbsf)	C_1 (ppmv)	C_2 (ppmv)
194-1198A-			
1H-3	3.00	2.20	0.0
2H-5	11.00	2.10	0.0
3H-5	20.50	1.80	0.0
4H-5	30.00	2.30	0.0
5H-5	39.50	1.90	0.0
7H-4	57.00	2.00	0.0
8H-5	68.00	1.90	0.0
9H-5	77.50	2.00	0.0
10H-5	87.00	1.90	0.0
11H-5	96.50	1.80	0.0
12H-5	106.00	2.00	0.0
13H-5	115.50	1.70	0.0
14H-5	125.00	2.00	0.0
15H-5	134.50	1.80	0.0
16H-5	144.00	2.20	0.0
17H-5	153.50	1.90	0.0
18H-5	163.00	1.90	0.0
19H-5	172.50	2.00	0.0
20H-5	182.00	2.10	0.0
21H-5	191.50	2.00	0.0
22H-4	199.50	2.00	0.0
194-1198B-			
1R-1	196.69	2.20	0.0
11R-1	291.80	1.80	0.0
17R-2	350.24	2.00	0.0
18R-3	361.92	2.20	0.0
19R-2	369.63	1.90	0.0
20R-2	379.67	1.90	0.0
21R-3	390.58	1.90	0.0
22R-5	403.60	2.80	0.0
23R-5	413.78	3.00	0.0
25R-5	432.40	2.60	0.0
26R-5	442.00	6.60	3.3
28R-5	461.15	2.60	0.0
31R-4	488.10	2.50	0.0
32R-5	499.25	2.30	0.0
33R-2	504.82	2.00	0.0

Note: C_1 = methane, C_2 = ethane.

Table T9. Interstitial water chemistry, Site 1198.

Core, section, interval (cm)	Depth (mbsf)	pH	Alk (mM)	Salinity	Cl^- (mM)	SO_4^{2-} (mM)	Na^+ (mM)	Mg^{2+} (mM)	Ca^{2+} (mM)	K^+ (mM)	NH_4^+ (μM)	Sr^{2+} (μM)	Li^+ (μM)	Mn^{2+} (μM)	Fe^{2+} (μM)
194-1198A-															
1H-2, 140–150	2.90	7.67	2.64	35.5	560	28.64	472	56.45	10.47	11.01	145	135	27.98	0.12	2.43
2H-4, 140–150	10.90	7.63	3.05	35.5	563	28.58	471	55.13	14.02	10.90	294	275	30.89	0.10	5.40
3H-4, 140–150	20.40	7.61	3.11	35.5	564	27.88	481	53.90	9.89	10.95	465	452	33.38	0.12	5.38
4H-4, 140–150	29.90	7.49	3.26	35.5	565	27.57	488	50.54	10.34	10.35	620	550	36.06	0.15	7.88
5H-4, 140–150	39.40	7.65	3.15	35.5	564	25.87	493	47.08	9.12	10.07	766	586	37.78	0.08	1.00
6H-4, 140–150	48.90	7.56	3.78	35.0	564	24.45	494	45.20	9.23	10.02	838	574	39.94	0.13	6.79
7H-4, 140–150	58.40	7.37	4.00	35.0	563	23.15	494	42.25	10.57	9.87	825	616	40.99	0.06	1.84
8H-4, 140–150	67.90	7.42	4.18	35.0	563	22.98	493	41.89	11.17	9.73	834	600	44.12	0.13	1.40
9H-4, 140–150	77.40	7.29	4.24	35.0	563	22.29	491	41.96	11.46	9.72	814	612	45.57	0.12	2.02
10H-4, 140–150	86.90	7.38	4.43	35.0	562	22.97	491	42.12	11.77	9.57	858	624	45.24	0.12	3.57
11H-4, 140–150	96.40	7.53	4.49	34.5	563	22.41	487	43.28	12.29	9.74	834	606	48.46	0.13	5.07
12H-4, 140–150	105.90	7.70	4.44	34.5	561	22.56	484	43.76	12.45	9.60	818	570	46.42	0.08	5.54
13H-4, 140–150	115.40	7.68	4.36	35.5	564	23.45	485	43.89	14.41	9.74	809	594	46.54	0.16	5.81
14H-4, 140–150	124.90	7.49	4.52	35.5	565	23.82	487	44.72	13.27	9.40	670	606	47.50	0.23	13.05
15H-4, 140–150	134.40	7.71	4.26	35.5	567	25.04	489	45.26	14.04	9.74	669	582	44.37	0.12	4.47
16H-4, 140–150	143.90	6.89	3.95	35.5	567	25.25	485	46.93	14.72	9.67	629	588	46.25	0.21	4.69
17H-4, 140–150	153.40	7.69	4.02	35.5	569	24.87	481	47.33	16.57	9.75	584	552	44.25	0.22	2.18
18H-4, 140–150	162.90	7.12	4.55	35.5	568	26.24	485	47.46	15.51	9.75	532	513	42.32	0.20	3.34
19H-4, 140–150	172.40	7.26	3.55	35.5	565	26.12	479	47.61	16.43	9.93	480	450	41.35	0.20	4.07
20H-4, 140–150	181.90	7.33	3.31	35.5	563	26.70	479	47.71	16.19	10.02	442	403	40.59	0.21	3.32
21H-4, 140–150	191.40	7.46	2.88	35.5	565	27.14	479	48.24	16.71	10.33	375	317	36.39	0.24	11.51
22H-3, 140–150	199.40	7.37	2.80	35.5	568	28.05	484	47.86	17.10	10.48	307	282	35.85	0.23	9.28
23X-1, 140–150	204.40	7.35	2.72	35.5	565	28.64	478	48.11	19.10	10.19	267	246	34.34	0.13	8.37
194-1198B-															
1R-2, 099–109	196.69	7.48	2.90	35.5	563	29.95	479	49.54	17.16	10.40	305	276	34.83	0.20	6.61
17R-1, 065–075	350.15	7.39	3.22	36.0	566	30.19	471	52.00	20.74	9.53	103	406	54.00	0.07	1.41
18R-2, 129–144	361.77	7.42	2.48	36.0	567	29.79	468	50.84	23.89	8.94	114	472	70.41	0.08	0.99
19R-1, 083–093	369.53	7.16	3.22	36.0	567	29.20	464	50.91	25.55	8.78	123	478	76.80	0.16	0.25
20R-1, 127–137	379.57	7.28	3.54	36.0	567	29.12	461	50.61	26.95	8.82	112	480	80.81	0.11	1.06
21R-2, 099–110	390.47	7.21	3.51	36.0	566	26.19	447	50.29	31.10	8.29	143	511	96.66	0.13	0.29
22R-4, 140–150	403.50	7.40	2.44	36.0	570	26.62	436	51.56	38.48	6.94	154	581	121.17	0.35	1.33
23R-4, 105–116	412.62	7.15	2.86	35.5	558	25.78	412	52.52	43.09	6.08	141	616	133.76	0.47	2.77
24R-4, 140–150	422.65	7.26	2.47	35.5	566	24.00	406	51.55	49.05	6.69	172	665	145.74	0.44	10.09
25R-4, 140–150	432.30	7.31	2.08	35.5	570	23.28	402	51.28	52.78	6.76	188	659	148.10	0.36	1.96
26R-4, 140–150	441.90	7.01	1.99	35.5	558	21.68	375	51.54	58.49	5.79	156	711	144.60	0.40	0.76
27R-4, 112–122	450.86	7.28	2.01	36.0	568	20.78	372	50.70	64.73	6.31	192	744	144.18	0.32	0.55
28R-4, 140–150	461.05			37.0	565	19.75	356	49.67	71.74	5.62	190	699	122.39	0.27	0.13
30R-4, 140–150	480.01			37.0	571	18.58	337	47.98	85.23	5.21	174				
31R-3, 140–150	488.00			37.5	573	17.16	311	43.53	102.18	4.66	210				
32R-4, 116–131	499.10			37.0	572	17.12	292	35.26	119.43	4.85	161				
33R-2, 016–025	504.98			39.0	570	16.42	270	29.47	135.35	3.58	152				

Note: Alk = alkalinity.

Table T10. Percentages of aragonite, calcite, dolomite, and noncarbonate minerals, Site 1198.

Core, section, interval (cm)	Depth (mbsf)	Aragonite (wt%)	Calcite (wt%)	Dolomite (wt%)	Non-carbonate (wt%)
194-1198A-					
1H-2, 62–63	2.12	31	60	0	9
2H-2, 62–63	7.12	28	56	0	16
2H-4, 62–63	10.12	29	59	0	12
2H-6, 62–63	13.12	22	68	0	10
3H-2, 62–63	16.62	29	57	0	14
3H-4, 62–63	19.62	24	63	0	12
3H-6, 62–63	22.62	29	60	0	11
4H-2, 62–63	26.12	32	54	0	14
4H-4, 62–63	29.12	35	57	0	7
4H-6, 62–63	32.12	33	60	0	7
5H-2, 62–63	35.62	29	61	0	11
5H-4, 62–63	38.62	22	59	0	19
5H-6, 62–63	41.62	27	65	0	8
6H-2, 62–63	45.12	23	66	0	12
6H-4, 62–63	48.12	24	57	0	19
6H-6, 62–63	51.12	23	53	0	24
7H-2, 62–63	54.62	22	60	0	18
7H-4, 62–63	57.62	22	65	0	13
7H-6, 62–63	60.62	23	67	0	9
8H-2, 62–63	64.12	21	58	0	21
8H-4, 62–63	67.12	18	64	0	19
8H-6, 62–63	70.12	13	71	0	17
9H-2, 62–63	73.62	12	65	0	23
9H-4, 62–63	76.62	13	67	0	21
9H-6, 62–63	79.62	12	65	0	22
10H-2, 62–63	83.12	10	65	0	25
10H-4, 62–63	86.12	11	60	0	29
10H-6, 76–77	89.26	13	76	0	11
11H-2, 62–63	92.62	9	77	0	14
11H-4, 62–63	95.62	9	71	0	20
11H-6, 62–63	98.62	8	81	0	11
12H-2, 62–63	102.12	10	74	0	16
12H-4, 62–63	105.12	8	74	0	18
12H-6, 62–63	108.12	9	70	0	21
13H-2, 62–63	111.62	7	63	0	30
13H-4, 62–63	114.62	7	74	3	16
13H-6, 62–63	117.62	6	80	0	14
14H-2, 62–63	121.12	0	77	2	21
14H-4, 62–63	124.12	0	62	0	38
14H-6, 62–63	127.12	0	81	5	14
15H-2, 62–63	130.62	0	77	0	23
15H-4, 62–63	133.62	0	81	0	19
15H-6, 62–63	136.62	0	83	0	17
16H-2, 62–63	140.12	0	72	3	25
16H-4, 62–63	143.12	0	77	0	23
16H-6, 62–63	146.12	0	65	0	35
17H-2, 62–63	149.62	0	80	0	20
17H-4, 62–63	152.62	0	80	0	20
17H-6, 62–63	155.53	0	80	0	20
18H-2, 62–63	159.12	0	81	0	19
18H-4, 62–63	162.12	0	76	0	24
18H-6, 62–63	165.12	0	64	0	36
19H-2, 62–63	168.62	0	77	3	20
19H-4, 62–63	171.62	0	81	0	19
19H-6, 62–63	174.62	0	86	0	14
20H-2, 62–63	178.13	0	84	0	16
20H-4, 62–63	181.13	0	75	0	25
20H-6, 62–63	184.13	0	81	0	19
21H-2, 62–63	187.62	0	76	0	24
21H-4, 62–63	190.62	0	76	0	24
21H-6, 62–63	193.62	0	71	0	29
22H-2, 62–63	197.12	0	73	2	24
22H-4, 62–63	200.12	0	77	0	23
23X-1, 62–63	203.62	0	83	15	3
194-1198B-					
2R-1, 36–37	205.56	0	90	6	4
4R-1, 48–50	224.88	0	95	4	0
5R-1, 13–14	234.13	0	77	22	1
6R-1, 4–5	243.64	0	96	2	2
7R-1, 55–56	253.85	0	96	3	1
8R-1, 1–2	262.91	0	95	3	3
10R-1, 49–50	282.69	0	94	4	2
11R-1, 74–75	292.54	0	94	3	2
12R-1, 9–10	301.49	0	96	0	4
15R-1, 22–23	330.52	0	97	0	3
16R-1, 3–4	339.93	0	97	0	3
17R-1, 23–24	349.73	0	93	3	5
18R-1, 81–82	359.91	0	94	3	4
19R-2, 38–39	370.01	0	91	0	9
20R-2, 67–68	380.34	0	92	0	8
21R-2, 57–57	390.05	0	95	0	5
22R-2, 70–71	399.80	0	82	0	18
22R-4, 70–71	402.80	0	69	2	29
22R-6, 70–71	405.80	0	47	0	53
23R-2, 73–74	409.28	0	70	1	29
23R-4, 69–70	412.26	0	48	5	47
23R-6, 66–67	414.89	0	59	19	23
24R-2, 71–72	418.96	0	53	1	46
24R-4, 48–49	421.73	0	76	3	21
24R-6, 61–62	424.86	0	69	2	30
25R-2, 67–68	428.57	0	53	1	46
25R-4, 77–78	431.67	0	69	9	22
25R-6, 78–79	434.68	0	58	3	39
26R-2, 72–73	438.22	0	58	11	32
26R-4, 72–74	441.22	0	57	6	37
27R–2, 73-74	447.89	0	68	6	26
27R-4, 72–73	450.46	0	82	3	15
27R-6, 77–78	453.23	0	82	3	15
28R-2, 72–73	457.37	0	63	10	27
28R-4, 72–73	460.37	0	74	5	21
28R-6, 74–75	463.18	0	85	2	13
29R-1, 70–71	465.60	0	78	2	20
30R-2, 64–65	476.50	0	79	5	16
30R-4, 41–42	479.02	0	82	4	14
30R-6, 61–62	482.22	0	77	2	21
31R-2, 64–65	485.74	0	91	0	9
31R-4, 43–44	488.53	0	82	0	18
32R-4, 62–63	498.56	0	95	0	5
32R-6, 23–24	500.77	0	98	0	2
34R-2, 22–23	514.66	0	1	0	99

Table T11. Carbon, nitrogen, sulfur, and hydrogen values and C/N and C/S ratios in sediments, Site 1198. (**See table note.** Continued on next page.)

Core, section	Depth (mbsf)	IC (wt%)	$CaCO_3$ (wt%)	TC (wt%)	TOC (wt%)	Total N (wt%)	Total S (wt%)	Total H (wt%)	C/N ratio	C/S ratio
194-1198A-										
1H-2	2.12	10.93	91.0	—	—	—	—	—	—	—
2H-2	7.12	10.13	84.4	10.20	0.07	0.06	0.10	0.23	1.18	0.71
2H-4	10.12	10.57	88.1	—	—	—	—	—	—	—
2H-6	13.12	10.80	89.9	—	—	—	—	—	—	—
3H-2	16.62	10.30	85.8	10.38	0.09	0.06	0.12	0.24	1.44	0.74
3H-4	19.62	10.50	87.5	—	—	—	—	—	—	—
3H-6	22.62	10.67	88.9	—	—	—	—	—	—	—
4H-2	26.12	10.30	85.8	10.43	0.12	0.07	0.11	0.22	1.70	1.11
4H-4	29.12	11.14	92.8	—	—	—	—	—	—	—
4H-6	32.12	11.11	92.5	—	—	—	—	—	—	—
5H-2	35.62	10.74	89.5	—	—	—	—	—	—	—
5H-4	38.62	9.56	79.6	9.66	0.11	0.06	0.12	0.26	1.77	0.88
5H-6	41.62	11.07	92.2	—	—	—	—	—	—	—
6H-2	45.12	10.61	88.3	—	—	—	—	—	—	—
6H-4	48.12	9.70	80.8	—	—	—	—	—	—	—
6H-6	51.12	9.14	76.2	9.17	0.03	0.04	0.17	0.30	0.69	0.16
7H-2	54.62	9.83	81.9	—	—	—	—	—	—	—
7H-4	57.62	10.44	87.0	—	—	—	—	—	—	—
7H-6	60.62	10.87	90.6	—	—	—	—	—	—	—
8H-2	64.12	9.45	78.8	9.67	0.22	0.04	0.16	0.26	5.68	1.38
8H-4	67.12	9.75	81.2	—	—	—	—	—	—	—
8H-6	70.12	10.01	83.4	—	—	—	—	—	—	—
9H-2	73.62	9.29	77.4	—	—	—	—	—	—	—
9H-4	76.62	9.54	79.5	—	—	—	—	—	—	—
9H-6	79.62	9.32	77.6	—	—	—	—	—	—	—
10H-2	83.12	9.03	75.2	—	—	—	—	—	—	—
10H-4	86.12	8.55	71.2	8.71	0.17	0.05	0.25	0.34	3.35	0.67
10H-6	89.26	10.67	88.9	—	—	—	—	—	—	—
11H-2	92.62	10.35	86.2	—	—	—	—	—	—	—
11H-4	95.62	9.59	79.9	9.74	0.14	0.05	0.26	0.25	2.86	0.56
11H-6	98.62	10.63	88.5	—	—	—	—	—	—	—
12H-2	102.12	10.09	84.1	—	—	—	—	—	—	—
12H-4	105.12	9.82	81.8	—	—	—	—	—	—	—
12H-6	108.12	9.46	78.8	—	—	—	—	—	—	—
13H-2	111.62	8.47	70.6	8.67	0.20	0.08	0.048	0.33	2.50	4.17
13H-4	114.62	10.05	83.7	—	—	—	—	—	—	—
13H-6	117.62	10.28	85.6	—	—	—	—	—	—	—
14H-2	121.12	9.52	79.3	—	—	—	—	—	—	—
14H-4	124.12	7.46	62.2	7.76	0.30	0.07	0.47	0.41	4.25	0.64
14H-6	127.12	10.28	85.7	—	—	—	—	—	—	—
15H-2	130.62	9.20	76.6	9.40	0.20	0.05	0.27	0.27	3.93	0.74
15H-4	133.62	9.69	80.7	—	—	—	—	—	—	—
15H-6	136.62	10.01	83.4	—	—	—	—	—	—	—
16H-2	140.12	8.97	74.7	9.20	0.23	0.07	0.34	0.28	3.26	0.68
16H-4	143.12	9.23	76.9	—	—	—	—	—	—	—
16H-6	146.12	7.81	65.1	8.18	0.37	0.09	0.56	0.39	3.97	0.67
17H-2	149.62	9.65	80.4	—	—	—	—	—	—	—
17H-4	152.62	9.62	80.1	—	—	—	—	—	—	—
17H-6	155.53	9.60	79.9	9.86	0.26	0.07	0.17	0.26	3.72	1.56
18H-2	159.12	9.72	80.9	—	—	—	—	—	—	—
18H-4	162.12	9.15	76.2	—	—	—	—	—	—	—
18H-6	165.12	7.72	64.3	8.11	0.39	0.09	0.52	0.42	4.31	0.74
19H-2	168.62	9.64	80.3	—	—	—	—	—	—	—
19H-4	171.62	9.67	80.6	—	—	—	—	—	—	—
19H-6	174.62	10.31	85.9	—	—	—	—	—	—	—
20H-2	178.13	10.03	83.5	—	—	—	—	—	—	—
20H-4	181.13	9.02	75.1	9.28	0.26	0.06	0.20	0.28	4.38	1.30
20H-6	184.13	9.69	80.7	—	—	—	—	—	—	—
21H-2	187.62	9.18	76.5	—	—	—	—	—	—	—
21H-4	190.62	9.15	76.2	—	—	—	—	—	—	—
21H-6	193.62	8.51	70.9	8.60	0.09	0.06	0.16	0.29	1.57	0.59
22H-2	197.12	9.10	75.8	—	—	—	—	—	—	—
22H-4	200.12	9.20	76.6	—	—	—	—	—	—	—
23X-1	203.62	11.70	97.5	—	—	—	—	—	—	—

Table T11 (continued).

Core, section	Depth (mbsf)	IC (wt%)	$CaCO_3$ (wt%)	TC (wt%)	TOC (wt%)	Total N (wt%)	Total S (wt%)	Total H (wt%)	C/N ratio	C/S ratio
194-1198B-										
2R-1	205.56	11.55	96.2	11.61	0.05	0.03	0.00	0.08	1.73	—
4R-1	224.88	11.96	99.6	—	—	—	—	—	—	—
5R-1	234.13	11.90	99.2	—	—	—	—	—	—	—
6R-1	243.64	11.78	98.1	—	—	—	—	—	—	—
7R-1	253.85	11.91	99.2	—	—	—	—	—	—	—
8R-1	262.91	11.67	97.2	—	—	—	—	—	—	—
10R-1	282.69	11.72	97.6	—	—	—	—	—	—	—
11R-1	292.54	11.71	97.6	—	—	—	—	—	—	—
12R-1	301.49	11.54	96.1	—	—	—	—	—	—	—
15R-1	330.52	11.62	96.8	—	—	—	—	—	—	—
16R-1	339.93	11.70	97.5	—	—	—	—	—	—	—
17R-1	349.73	11.42	95.2	—	—	—	—	—	—	—
17R-2	350.78	10.74	89.5	10.81	0.07	0.08	0.12	0.15	0.82	0.53
18R-1	359.91	11.58	96.5	—	—	—	—	—	—	—
18R-2	361.45	11.29	94.1	—	—	—	—	—	—	—
19R-2	370.01	11.00	91.6	11.03	0.03	0.03	0.04	0.11	1.03	0.78
20R-2	380.34	11.06	92.1	—	—	—	—	—	—	—
21R-2	390.04	11.39	94.9	—	—	—	—	—	—	—
22R-2	399.80	9.79	81.6	—	—	—	—	—	—	—
22R-4	402.80	8.57	71.4	—	—	—	—	—	—	—
22R-6	405.80	5.62	46.8	6.08	0.46	0.06	0.78	0.59	7.62	0.58
23R-2	409.28	8.57	71.4	—	—	—	—	—	—	—
23R-4	412.25	6.38	53.1	6.66	0.28	0.09	0.62	0.58	3.16	0.45
23R-6	414.88	9.30	77.5	—	—	—	—	—	—	—
24R-2	418.96	6.48	54.0	6.81	0.33	0.06	0.39	0.57	5.48	0.84
24R-4	421.73	9.45	78.7	—	—	—	—	—	—	—
24R-6	424.86	8.45	70.4	—	—	—	—	—	—	—
25R-2	428.57	6.46	53.8	6.90	0.43	0.06	0.45	0.52	7.24	0.98
25R-4	431.67	9.33	77.7	—	—	—	—	—	—	—
25R-6	434.68	7.33	61.1	7.65	0.33	0.04	0.42	0.47	8.13	0.78
26R-2	438.22	8.19	68.2	—	—	—	—	—	—	—
26R-4	441.22	7.56	63.0	7.87	0.30	0.07	0.27	0.43	4.33	1.12
27R-2	447.88	8.92	74.3	—	—	—	—	—	—	—
27R-4	450.46	10.19	84.9	—	—	—	—	—	—	—
27R-6	453.23	10.20	85.0	—	—	—	—	—	—	—
28R-2	457.37	8.72	72.7	9.01	0.29	0.05	0.30	0.33	5.80	0.97
28R-4	460.37	9.51	79.2	—	—	—	—	—	—	—
28R-6	463.18	10.39	86.6	—	—	—	—	—	—	—
29R-1	465.60	9.65	80.4	9.73	0.08	0.06	0.07	0.17	1.30	1.12
30R-2	476.50	10.14	84.5	—	—	—	—	—	—	—
30R-4	479.02	10.34	86.2	—	—	—	—	—	—	—
30R-6	482.22	9.46	78.8	—	—	—	—	—	—	—
31R-2	485.74	10.95	91.2	—	—	—	—	—	—	—
31R-4	488.53	9.86	82.2	10.01	0.15	0.04	0.16	0.21	3.77	0.93
32R-2	495.83	11.28	93.9	—	—	—	—	—	—	—
32R-4	498.56	11.35	94.5	—	—	—	—	—	—	—
32R-6	500.77	11.12	92.6	—	—	—	—	—	—	—
33R-1	503.93	10.93	91.1	10.84	0.00	0.00	0.00	0.09	—	—
33R-2	505.62	11.75	97.9	—	—	—	—	—	—	—
34R-1	513.21	11.79	98.2	—	—	—	—	—	—	—
34R-2	515.08	0.15	1.2	—	—	—	—	—	—	—
34R-4	517.40	0.05	0.4	—	—	—	—	—	—	—

Note: IC = inorganic carbon, TC = total carbon, TOC = total organic carbon.

Table T12. Results of Rock-Eval analyses on sediments, Site 1198.

Core, section	Depth (mbsf)	T_{max}	S_1	S_2	S_3	HI	OI	TOC (wt%)
194-1198A-								
1H-2	2.12	416	0.03	0.08	13.00	328	3,689	0.03
2H-2	7.12	402	0.04	0.08	15.50	253	36,133	0.04
2H-4	10.12	378	0.03	0.01	12.50	42	—	0.01
2H-6	13.12	408	0.03	0.04	20.27	100	—	0.01
3H-2	16.62	395	0.07	0.12	3.74	240	7,480	0.05
3H-4	19.62	400	0.05	0.10	30.81	166	51,350	0.06
3H-6	22.62	401	0.07	0.13	18.75	260	37,500	0.05
4H-2	26.12	410	0.02	0.05	5.64	150	18,633	0.03
4H-4	29.12	407	0.06	0.08	4.91	223	21,633	0.03
4H-6	32.12	392	0.04	0.07	2.69	175	6,725	0.04
5H-2	35.62	390	0.04	0.06	11.50	233	36,455	0.03
5H-4	38.62	378	0.08	0.09	20.57	225	51,425	0.04
5H-6	41.62	393	0.04	0.12	3.30	217	9,110	0.04
6H-2	45.12	396	0.06	0.09	14.31	233	39,783	0.03
6H-4	48.12	377	0.06	0.10	24.56	200	49,120	0.05
6H-6	51.12	379	0.06	0.10	3.69	142	5,271	0.07
7H-2	54.62	389	0.05	0.14	3.13	137	3,912	0.08
7H-4	57.62	387	0.03	0.08	20.07	266	—	0.03
7H-6	60.62	400	0.06	0.12	3.35	240	6,700	0.05
8H-2	64.12	381	0.11	0.13	25.53	216	42,550	0.06
8H-4	67.12	380	0.08	0.12	27.84	200	46,400	0.06
8H-6	70.12	395	0.07	0.19	4.44	211	4,933	0.09
9H-2	73.62	382	0.10	0.24	30.73	200	25,608	0.12
9H-4	76.62	383	0.06	0.12	3.57	150	4,462	0.08
9H-6	79.62	385	0.06	0.16	20.29	145	18,445	0.11
10H-2	83.12	385	0.10	0.24	38.60	184	29,692	0.13
10H-4	86.12	384	0.06	0.16	6.39	133	5,325	0.12
10H-6	89.26	388	0.09	0.12	26.27	171	37,528	0.07
11H-2	92.62	395	0.08	0.14	28.35	200	40,500	0.07
11H-4	95.62	377	0.08	0.13	5.11	162	6,387	0.08
11H-6	98.62	383	0.08	0.11	16.44	275	41,100	0.04
12H-2	102.12	389	0.10	0.22	14.98	220	14,980	0.10
12H-4	105.12	379	0.08	0.11	4.85	157	6,928	0.07
12H-6	108.12	386	0.10	0.15	19.35	150	19,350	0.10
13H-2	111.62	379	0.09	0.17	26.49	170	26,490	0.10
13H-4	114.62	399	0.13	0.21	6.03	175	5,025	0.12
13H-6	117.62	384	0.11	0.15	17.39	166	19,322	0.09
14H-2	121.12	388	0.12	0.20	18.44	133	12,293	0.15
14H-4	124.12	382	0.07	0.23	6.45	100	2,804	0.23
14H-6	127.12	381	0.11	0.13	18.76	185	26,800	0.07
15H-2	130.62	381	0.13	0.26	23.00	173	15,333	0.15
15H-4	133.62	385	0.11	0.22	24.30	220	24,300	0.10
15H-6	136.62	396	0.05	0.21	29.57	233	32,855	0.09
16H-2	140.12	395	0.08	0.25	32.64	138	18,133	0.18
16H-4	143.12	388	0.09	0.28	10.53	140	5,265	0.20
16H-6	146.12	390	0.09	0.38	41.96	126	13,986	0.30
17H-2	149.62	394	0.30	0.33	38.93	183	21,627	0.18
17H-4	152.62	390	0.14	0.32	10.42	177	5,788	0.18
17H-6	155.53	406	0.13	0.47	35.13	235	17,565	0.20
18H-2	159.12	388	0.15	0.23	31.96	191	26,633	0.12
18H-4	162.12	392	0.12	0.44	10.24	183	4,266	0.24
18H-6	165.12	395	0.13	0.50	42.25	151	12,803	0.33
19H-2	168.62	400	0.24	0.45	34.81	225	17,405	0.20
19H-4	171.62	401	0.18	0.62	36.43	229	13,492	0.27
19H-6	174.62	402	0.10	0.38	6.93	200	3,647	0.19
20H-2	178.13	400	0.07	0.32	42.56	177	23,644	0.18
20H-4	181.13	387	0.11	0.31	38.73	182	22,782	0.17
20H-6	184.13	403	0.13	0.39	36.52	243	22,825	0.16
21H-2	187.62	395	0.17	0.52	9.84	200	3,784	0.26
21H-4	190.62	405	0.14	0.41	46.20	205	23,100	0.20
21H-6	193.62	400	0.14	0.37	37.34	231	23,337	0.16
22H-2	197.12	396	0.13	0.29	36.47	207	26,050	0.14
22H-4	200.12	393	0.15	0.26	7.49	185	5,350	0.14
23X-1	203.62	408	0.00	0.00	1.31	—	—	0.00
194-1198B-								
2R-1	205.56	353	0.03	0.02	12.19	—	—	0.00
4R-1	224.88	—	0.02	0.01	4.39	—	—	0.00
5R-1	234.13	—	0.01	0.01	11.12	—	—	0.00
6R-1	243.64	316	0.03	0.02	1.20	—	—	0.00
7R-1	253.85	319	0.01	0.01	0.00	—	—	0.00
8R-1	262.91	400	0.01	0.01	1.85	100	18,100	0.01
10R-1	282.69	351	0.03	0.02	4.44	150	—	0.01
11R-1	292.54	409	0.04	0.08	4.35	275	20,641	0.03
12R-1	301.49	318	0.01	0.01	1.01	—	—	0.00
12R-1	302.36	318	0.01	0.01	5.32	50	—	0.01
13R-1	311.00	342	0.01	0.01	7.35	100	3,925	0.02
15R-1	330.52	408	0.05	0.08	0.00	—	—	0.00
16R-1	339.93	401	0.02	0.02	3.40	150	25,850	0.01
17R-1	349.73	414	0.10	0.13	2.01	225	3,954	0.05
17R-2	350.78	406	0.19	0.20	3.32	210	3,947	0.09
18R-1	359.91	402	0.08	0.08	1.17	225	7,675	0.03
18R-2	361.45	400	0.11	0.12	4.40	240	9,342	0.05
19R-2	370.01	400	0.06	0.10	6.91	250	17,275	0.04
20R-2	380.34	404	0.04	0.12	2.36	116	3,503	0.08
21R-2	390.04	410	0.02	0.04	1.61	88	4,013	0.04
22R-2	399.80	407	0.12	0.37	12.94	205	7,188	0.18
22R-4	402.80	403	0.13	0.42	13.37	161	5,142	0.26
22R-6	405.80	391	0.04	0.11	6.28	28	1,630	0.39
23R-2	409.28	402	0.04	0.12	5.12	36	1,528	0.35
23R-4	412.25	397	0.09	0.41	25.91	113	7,197	0.36
23R-6	414.88	415	0.04	0.21	7.17	125	4,258	0.17
24R-2	418.96	400	0.18	0.52	28.11	136	7,397	0.38
24R-4	421.73	408	0.09	0.27	6.06	153	3,503	0.17
24R-6	424.86	402	0.15	0.43	15.88	159	5,881	0.27
25R-2	428.57	402	0.14	0.61	25.50	164	6,891	0.37
25R-4	431.67	407	0.19	0.12	6.58	187	3,031	0.20
25R-6	434.68	401	0.18	0.50	22.60	166	7,533	0.30
26R-2	438.22	394	0.16	0.35	16.16	159	7,345	0.22
26R-4	441.22	403	0.18	0.42	21.58	161	8,300	0.26
27R-2	447.88	398	0.23	0.38	12.15	180	5,785	0.21
27R-4	450.46	407	0.08	0.30	1.85	214	1,321	0.14
27R-6	453.23	405	0.09	0.29	7.90	148	7,231	0.11
28R-2	457.37	407	0.14	0.50	15.26	166	5,086	0.30
28R-4	460.37	411	0.09	0.46	10.88	209	4,945	0.22
28R-6	463.18	409	0.07	0.26	4.86	216	4,050	0.12
29R-1	465.60	410	0.17	0.44	14.75	176	5,900	0.25
30R-2	476.50	407	0.09	0.24	9.65	240	9,650	0.10
30R-4	479.02	411	0.08	0.33	6.50	183	3,611	0.18
30R-6	482.22	405	0.08	0.31	9.28	193	5,800	0.16
31R-2	485.74	415	0.06	0.12	3.72	156	4,990	0.07
31R-4	488.53	406	0.13	0.26	9.54	200	7,338	0.13
32R-2	495.83	404	0.08	0.12	4.89	240	9,780	0.05
32R-4	498.56	399	0.09	0.08	2.19	200	5,475	0.04
32R-6	500.77	409	0.06	0.21	1.62	146	1,214	0.14
33R-1	503.93	433	0.06	0.02	2.85	200	28,500	0.01
33R-2	505.62	—	0.07	0.01	0.00	—	—	0.00
34R-1	513.21	346	0.06	0.02	1.71	—	—	0.00

Notes: T_{max} = temperature of maximum hydrocarbon generation during pyrolysis in °C, S_1 = milligram of free hydrocarbons per gram of rock, S_2 = milligram of pyrolyzed hydrocarbons per gram of rock, S_3 = milligram of carbon dioxide per gram of rock, HI = hydrogen index in milligram of hydrocarbon per gram of TOC, OI = milligram of carbon dioxide per gram of TOC, TOC = total organic carbon. — = not available.

Table T13. Logging operations, Hole 1198B.

Date (Feb 2001)	Time (local)	Comments
10	2020	Hole preparation complete; rig up wireline.
	2140	RIH with HNGS-APS-HLDS-DITE.
	2240	Uplog with triple combo at 900 ft/hr from tight spot at 235.5 mbsf to seafloor.
11	0130	Pull tools out of hole and rig down.
	0145	End of logging operations.

Notes: RIH = run in hole, HNGS = hostile environment natural gamma ray sonde, APS = accelerator porosity sonde, DITE = dual induction tool, HLDS = high-temperature lithodensity sonde. Drillers total depth = 522.5 mbsf, water depth = 331.5 mbrf, end of pipe = 74 mbsf.